0-315-03687-7

National Library of Canada | Bibliothèque nationale du Canada

Canadian Theses Division | Division des thèses canadiennes

Ottawa, Canada
K1A 0N4

51582

PERMISSION TO MICROFILM — AUTORISATION DE MICROFILMER

• Please print or type — Écrire en lettres moulées ou dactylographier

Full Name of Author — Nom complet de l'auteur

Donald William John Sargent

Date of Birth — Date de naissance	Country of Birth — Lieu de naissance
May 23, 1951	Canada

Permanent Address — Résidence fixe

Box 839 Sub 11 U of A Edmonton T6G 2E0

Title of Thesis — Titre de la thèse

A Process Simulation Test on a Small Unlined Tunnel in Jointed Coal

University — Université

University of Alberta

Degree for which thesis was presented — Grade pour lequel cette thèse fut présentée

MSc

Year this degree conferred — Année d'obtention de ce grade	Name of Supervisor — Nom du directeur de thèse
1981	Dr. N.R. Morgenstern

Permission is hereby granted to the NATIONAL LIBRARY OF CANADA to microfilm this thesis and to lend or sell copies of the film.

The author reserves other publication rights, and neither the thesis nor extensive extracts from it may be printed or otherwise reproduced without the author's written permission.

L'autorisation est, par la présente, accordée à la BIBLIOTHÈQUE NATIONALE DU CANADA de microfilmer cette thèse et de prêter ou de vendre des exemplaires du film.

L'auteur se réserve les autres droits de publication; ni la thèse ni de longs extraits de celle-ci ne doivent être imprimés ou autrement reproduits sans l'autorisation écrite de l'auteur.

Date	Signature
April 24, 1981	

NL-91 (4/77)

National Library of Canada
Collections Development Branch

Canadian Theses on
Microfiche Service

Bibliothèque nationale du Canada
Direction du développement des collections

Service des thèses canadiennes
sur microfiche

NOTICE

The quality of this microfiche is heavily dependent upon the quality of the original thesis submitted for microfilming. Every effort has been made to ensure the highest quality of reproduction possible.

If pages are missing, contact the university which granted the degree.

Some pages may have indistinct print especially if the original pages were typed with a poor typewriter ribbon or if the university sent us a poor photocopy.

Previously copyrighted materials (journal articles, published tests, etc.) are not filmed.

Reproduction in full or in part of this film is governed by the Canadian Copyright Act, R.S.C. 1970, c. C-30. Please read the authorization forms which accompany this thesis.

THIS DISSERTATION
HAS BEEN MICROFILMED
EXACTLY AS RECEIVED

AVIS

La qualité de cette microfiche dépend grandement de la qualité de la thèse soumise au microfilmage. Nous avons tout fait pour assurer une qualité supérieure de reproduction.

S'il manque des pages, veuillez communiquer avec l'université qui a conféré le grade.

La qualité d'impression de certaines pages peut laisser à désirer, surtout si les pages originales ont été dactylographiées à l'aide d'un ruban usé ou si l'université nous a fait parvenir une photocopie de mauvaise qualité.

Les documents qui font déjà l'objet d'un droit d'auteur (articles de revue, examens publiés, etc.) ne sont pas microfilmés.

La reproduction, même partielle, de ce microfilm est soumise à la Loi canadienne sur le droit d'auteur, SRC 1970, c. C-30. Veuillez prendre connaissance des formules d'autorisation qui accompagnent cette thèse.

LA THÈSE A ÉTÉ
MICROFILMÉE TELLE QUE
NOUS L'AVONS REÇUE

Ottawa, Canada
K1A 0N4

NL-339 (Rev. 8/80)

THE UNIVERSITY OF ALBERTA

A PROCESS SIMULATION TEST ON A SMALL UNLINED TUNNEL IN JOINTED COAL

by

© DONALD WILLIAM JOHN SARGENT

A THESIS

SUBMITTED TO THE FACULTY OF GRADUATE STUDIES AND RESEARCH

IN PARTIAL FULFILMENT OF THE REQUIREMENTS FOR THE DEGREE

OF MASTER OF SCIENCE

DEPARTMENT OF CIVIL ENGINEERING

EDMONTON, ALBERTA

SPRING, 1981

THE UNIVERSITY OF ALBERTA

RELEASE FORM

NAME OF AUTHOR DONALD WILLIAM JOHN SARGENT

TITLE OF THESIS A PROCESS SIMULATION TEST ON A SMALL UNLINED TUNNEL IN JOINTED COAL

DEGREE FOR WHICH THESIS WAS PRESENTED MASTER OF SCIENCE

YEAR THIS DEGREE GRANTED SPRING, 1981

Permission is hereby granted to THE UNIVERSITY OF ALBERTA LIBRARY to reproduce single copies of this thesis and to lend or sell such copies for private, scholarly or scientific research purposes only.

The author reserves other publication rights, and neither the thesis nor extensive extracts from it may be printed or otherwise reproduced without the author's written permission.

(SIGNED) .....

PERMANENT ADDRESS:

Box 839, sub 11

University of Alberta

Edmonton, Alberta T6G 2E0

DATED April 21, 1981 19

THE UNIVERSITY OF ALBERTA

FACULTY OF GRADUATE STUDIES AND RESEARCH

The undersigned certify that they have read, and recommend to the Faculty of Graduate Studies and Research, for acceptance, a thesis entitled A PROCESS SIMULATION TEST ON A SMALL UNLINED TUNNEL IN JOINTED COAL submitted by DONALD WILLIAM JOHN SARGENT in partial fulfilment of the requirements for the degree of MASTER OF SCIENCE.

Dr. N.R. Morgenstern .....
Supervisor

Dr. J.G. MacGregor .....

Dr. B. Stimpson .....

Dr. P.K. Kaiser .....

Date..April 8,1981.....

Abstract

This thesis uses a Process Simulation Test (PST) facility to study the pre-failure process and some associated rate effects around a small diameter unlined tunnel in a naturally jointed coal specimen. This is a continuation of a laboratory study to investigate the time-dependent behavior of a tunnels in strain-weakening rock masses with time-dependent strength and deformation properties.

Thirteen individual tests have been carried out on one test specimen. Tunnel closure, average specimen strain and average radial strain measurements as well as visual inspections of the tunnel have been recorded. Time-independent and time-dependent deformations have been examined.

The deformation response of this test specimen was dependent on loading history. Hence, loading or stress history have been considered in comparisons of deformation results.

Scale effects have been discussed since enlarging the tunnel size by 25% caused about 10% higher immediate and delayed tunnel closures.

Local "yielding" and "weakening" processes have been associated with stress redistribution and alteration of the immediate and delayed tunnel deformation behavior of this specimen. In particular, stress concentrations near the tunnel lead to 25% greater tunnel closures and a 10% lower propensity for delayed closures. Still, the tunnel remained

self-supporting with total closures of about 3.5 to 4.0%. Moreover, greater extension radial strains and strain-rates developed further away from the tunnel wall. Thus the radial extensometers responded to these local deformation processes.

Homogeneous and non-homogeneous linear elastic analyses have been used to predict deformations that are consistent with the observed time-independent deformation behavior of the specimen. In particular, assumption of an annular region of reduced stiffness around the tunnel was found to predict deformations that are consistent with the observed alteration of the specimen deformation behavior. Analysis of the deformation process has been carried out by considering of radial strain measurements.

Acknowledgements

I wish to sincerely thank Dr. N.R. Morgenstern for his patient guidance, financial support and enthusiastic encouragement during all phases of this research. Also, I would like to thank Dr. P.K. Kaiser for his generous advice on many phases of the laboratory testing, data evaluation and presentation of test results. I have felt like a team member while working on this research, and this has truly been an enlightening experience.

I wish to thank the members of the examining committee for their patience and valuable comments which I have endeavoured to include in this thesis.

I would like to thank the Department of Civil Engineering for finanical support and opportunities afforded me. In particular, I wish to thank the professors in this department for their efforts toward my education and their hospitality to me while I have been a graduate student.

I also wish to thank the non-acedemic staff in the Department of Civil Engineering. In particular, I wish to acknowledge the assistance of Messrs. G. Cyre, O. Wood and A. Muir and his machinists. Also I wish to acknowlegde Messrs. B. Billey, D. Fushtey, D. Gagnon, S. Gamble and R. Gitzel for their assistance in the lab. I wish to thank Mr.H. Soderberg for assistance in instrumenting the test specimen Mr. R. Howells for assistance with the computer. I wish to especially thank Mr. Scotty Rogers for assistance on graphics. You have all contributed much to this research.

I wish to extend a special thanks to all my fellow graduate students. I wish to thank Mr. Alain Guenot for his guidance in the very initial testing. I would like to thank Mr. John Simmons for his guidance in applying his finite element program for this analysis. I wish to thank Messrs. Alan Gale, Sean Maloney and Kevin Sterne for their comments on parts of the text of this thesis. I wish to especially thank Mr. John Sobkowicz for his review of many drafts and valuable comments toward improving the grammar, forewhich I must bear final responsibility. I owe a very special thanks to Mr. Kevin Sterne with whom many hours have been spent in exhaustive and most fruitful discussions centering on theoretical aspects related to tunnelling. Indeed, my association with the many talented graduate students of this department has been a truly rewarding experience for realizing many meaningful insights into the theory and practice of engineering.

I wish to thank my family for their constant interest during this study. It is through my parents foresight that I have what I have today, a most insatiable desire for learning.

Finally, I wish to extend my deepest appreciation to Leah, my very dearest companion. Without her constant love and overwhelmingly enthusiastic support during even the earliest stages of my studies, it would not have been possible.

Table of Contents

Chapter Page

1. CHAPTER I
INTRODUCTION 1

1.1 AIM OF THIS THESIS 1

1.2 BACKGROUND ON THE PROCESS SIMULATION TEST 2

1.3 ROCK MASS BEHAVIOR AROUND REAL TUNNELS 3

1.4 SCOPE OF THIS THESIS 6

2. CHAPTER II
PROCESS SIMULATION TEST (PST) SPECIMEN AND TEST PROCEDURE 10

2.1 INTRODUCTION 10

2.2 DESCRIPTION OF THE COAL 11

2.2.1 SUMMARY OF THE COAL PROPERTIES 12

2.2.2 SUMMARY OF DEFORMATION PROPERTIES MEASURED IN THE PROCESS SIMULATION TEST 14

2.3 DESCRIPTION OF THE MC1 SPECIMEN 14

2.3.1 INTRODUCTION 14

2.3.2 STRUCTURAL CONDITION OF MC1 15

2.3.3 DISPLACEMENT MEASUREMENT 16

2.3.3.1 TUNNEL CLOSURE 16

2.3.3.2 AVERAGE RADIAL STRAIN 17

2.3.3.3 BOUNDARY DISPLACEMENTS 18

2.3.4 SPECIMEN CONDITION AFTER TESTING 19

2.4 DESCRIPTION OF THE TEST PROCEDURE 20

2.4.1 INTRODUCTION 20

2.4.2 PREPARATION OF A TEST SPECIMEN 21

2.4.3 STEP BY STEP DESCRIPTION OF THE TEST PROCEDURE 23

2.4.4 TEST EQUIPMENT 25

2.4.4.1 COMPRESSION MACHINE 25

2.4.4.2 LOAD AND DISPLACEMENT MONITORING DEVICES 26

2.4.5 CALCULATION PROCEDURES AND GRAPHICS DISPLAYS 27

2.5 LIMITATIONS OF TESTING 31

3. CHAPTER III
DISCUSSION OF PROCESS SIMULATION TEST (PST) RESULTS ...43

3.1 INTRODUCTION 43

3.2 SUMMARY OF ANTICIPATED BEHAVIOR 45

3.2.1 LINEAR SYSTEM BEHAVIOR 47

3.2.2 STRESS REDISTRIBUTION PROCESSES 49

3.3 SUMMARY OF THE TESTING PROGRAM 50

3.4 DESCRIPTION OF THE PRESENTATION OF TEST RESULTS ...55

3.5 PRELIMINARY TESTS, MC1.7 and MC1.8 57

3.5.1 INCREASING FIELD STRESS RESPONSE 58

3.5.2 CONSTANT FIELD STRESS RESPONSE 60

3.5.3 COMPARISON OF TUNNEL CLOSURE AND RADIAL STRAIN RESPONSE 62

3.6 NON-HYDROSTATIC EPISODES, MC1.10-11-12 AND MC1.15-16-17 63

3.6.1 INCREASING FIELD STRESS RESPONSE 64

3.6.2 CONSTANT FIELD STRESS RESPONSE 68

3.6.3 COMPARISON OF THE TUNNEL CLOSURE AND RADIAL STRAIN 70

3.7 BIMODAL LOADING RATE TESTS, MC1.9 AND MC1.14 72

3.7.1 INCREASING FIELD STRESS RESPONSE 73

3.7.2 CONSTANT FIELD STRESS RESPONSE 76

3.7.3 COMPARISON OF TUNNEL CLOSURE AND RADIAL

STRAIN 80

3.8 BREAKING THE SPECIMEN 83

3.8.1 DEFORMATION RESPONSE 83

3.8.2 PHYSICAL OBSERVATIONS 85

3.9 CONCLUSIONS 87

4. CHAPTER IV
ANALYSIS OF TEST RESULTS 110

4.1 INTRODUCTION 110

4.2 HOMOGENEOUS LINEAR ELASTIC SIMULATION 111

4.3 NON-HOMOGENEOUS LINEAR ELASTIC SIMULATION 114

4.3.1 FINITE ELEMENT CALCULATION 114

4.3.2 SIMULATION OF PST MEASUREMENTS ASSUMING NON-HOMOGENEOUS ELASTIC BEHAVIOR 115

4.3.2.1 SIMULATION OF TEST MC1.12 116

4.3.2.2 SIMULATION OF TESTS MC1.11 AND MC1.16 118

4.3.2.3 CALCULATED STRESS DISTRIBUTION 120

4.4 PHYSICAL BEHAVIOR OF COAL 121

4.5 PHENOMENOLOGICAL BEHAVIOR AND THE PST BEHAVIOR ...122

4.5.1 TIME-INDEPENDENT YIELDING AND PROPERTY ALTERATION 123

4.5.2 TIME-DEPENDENT YIELDING AND PROPERTY ALTERATION 124

4.5.3 SCALE EFFECTS 125

4.6 CONCLUSIONS 126

5. CHAPTER V
CONCLUSIONS 137

5.1 STATEMENT OF THE TEST STUDY 137

5.2 SIMULATION OF THE SPECIMEN BEHAVIOR 139

5.3 MODES OF DEFORMATION 139

5.4 PRACTICAL IMPLICATIONS 143
REFERENCES 146
APPENDIX A1 151
APPENDIX A2 154
APPENDIX B1 156
APPENDIX C1 161

List of Tables

Table		Page
C1-1	Details of the Test Program	162
C4-1	Definition of Graphics Symbols	165

List of Figures

Figure		Page
1.1	Modes of Ground Behavior (da Fontoura, 1980)	8
1.2	Types of Rock Mass Behavior (Kaiser and Morgenstern, 1981)	9
2.1	Schematic Sketch of MC 1 Prepared for Testing	34
2.2	Developed Section, 15 cm Diameter Tunnel, After Test MC 1.7	35
2.3	Schematic View of Radial Extensometer Locations	36
2.4	Photo Reduced Sketch of the Top of Specimen MC1 After Testing	37
2.5	Developed Section, 15 cm Diameter Tunnel, After Test MC 1.19	38
2.6	Flow Diagram : Increasing Load Procedure	39
3.1	a. Linear Elastic Stress, Strain and Displacement for the PST; N=1.0 b. Linear Elastic Stress; N=0.25(Terzaghi and Richter, 1952)	93
3.2	Linear Visco-elastic Creep for Binary (Isotropic and Deviatoric) Formulation (Kaiser, 1979)	94
3.3	Summary of the Test Sequence	95
3.4	Average Deformation Modulus for Each Test Normalized to Test MC1.10	96
3.5	Average Deformation Moduli for Test MC1.14 Normalized to Test MC1.9	97
3.6	Average Closure Rate Parameters for Each Test Normalized to Test MC1.10 at 15(MPa) Field Stress	98
3.7	Average Closure Rate Parameters for Test MC1.14 Normalized to the 10(MPa) Field Stress	99
3.8	Closure Rate Parameters for Test MC1.14 Normalized to Test MC1.9	100
3.9	Field Stress Versus Tunnel Closure	101
3.10	Summary of Field Stress Versus Strain	102

Figure Page

3.11 Field Stress Versus Average Radial Strain; Zone A, Principal Axes Extensometers 103

3.12 Field Stress Versus Average Radial Strain; Zone A, Diagonal Extensometers 104

3.13 Field Stress Versus Average Radial Strain; Zone B, Principal Axes Extensometers 105

3.14 Field Stress Versus Average Radial Strain; Zone B, Diagonal Extensometers 106

3.15 Summary of Strain Rate Versus Time for Test MC1.10 and Test MC1.12 107

3.16 Summary of Strain Rate Versus Time for Test MC1.9 .108

3.17 Summary of Strain Rate Versus Time for Test MC1.14 109

4.1 Tunnel Closure and Average Radial Strain Assuming a Homogeneous Linear Elastic PST Specimen 129

4.2 Finite Element Mesh 130

4.3 Tunnel Closure and Average Specimen Strain Assuming a Non-Homogeneous Linear Elastic PST Specimen 131

4.4 Average Radial Strain Assuming a Non-Homogeneous Linear Elastic PST Specimen 132

4.5 Average Radial Strain for a Homogeneous Case and a Non-Homogeneous Case; With a Field Stress Ratio of 0.6 133

4.6 a. Homogeneous and Non-Homogeneous Linear Elastic Maximum and Minimum Principal Stress Distribution
b. Homogeneous and Non-Homogeneous Linear Elastic Deviatoric Stress Distribution 134

4.7 Schematic Stress-Strain Diagram of Rock (Kaiser and Morgenstern, 1978) 135

4.8 Schematic Diagram of Phenomenological Model and a Simple Version of the Model With Mechanical Elements (Kaiser and Morgenstern, 1981a) 136

Figure Page

C2-1 Range of Boundary Normal Stress 163

C3-1 a. Determination of Apparent Deformation Modulus .164

C3-1 b. Determination of Closure Rate Parameters 164

C4-1 Field Stress Versus Strain Curves for Some Locations for Test MC1.7 166

C4-2 Field Stress Versus Strain Curves for Some Locations for Test MC1.8 167

C4-3 Strain Versus Time Curves for Some Locations for Test MC1.7 168

C4-4 Strain Versus Time Curves for Some Locations for Test MC1.8 169

C4-5 Strain Rate Versus Time Curves for Some Locations for Test MC1.8 170

C5-1 Deformation Modulus Along the Four Tunnel Diameters in Each Test Normalized to Test MC1.10 ..171

C5-2 Average Specimen Deformation Modulus for Each Test Normalized to Test MC1.10 172

C5-3 Tunnel Closure Along the Four Tunnel Diameters in Each Test Normalized to Test MC1.10 173

C5-4 Deformation Modulus and Tunnel Closure for Tests MC1.7 to MC1.10 Normalized to the 0-180 Diameter ..174

C5-5 Deformation Modulus and Tunnel Closure for Tests MC1.11 to MC1.14 Normalized to the 0-180 Diameter .175

C5-6 Deformation Modulus and Tunnel Closure for Tests MC1.15 to MC1.19 Normalized to the 0-180 Diameter .176

C5-7 Closure Rate Parameters for Tests MC1.7 to MC1.10 Normalized to the 0-180 Diameter 177

C5-8 Closure Rate Parameters for Tests MC1.12 to MC1.17 Normalized to the 0-180 Diameter 178

C6-1 Strain Versus Time Curves for Some Locations for Tests MC1.9 and MC1.14 179

List of Plates

Plate		Page
2.1	Top and Bottom View of Test Specimen after Testing	40
2.2	Test Machine	41
2.3	Lateral Load Distribution by Set of Triangles	42

1. CHAPTER I

INTRODUCTION

The design and construction of tunnels is classified under the following catagories (Kaiser and Morgenstern, 1981):

1. empirical, based on past experience;
2. theoretical, based on prediction and analysis using physical laws;
3. physical modelling, using specific prototypes or a model to illustrate mechanisms.

The Process Simulation Test (PST) is a physical modelling facility to illustrate mechanisms. Its purpose is to study "the time-dependent processes related to excavation of a tunnel in a strain-weakening rock mass with time-dependent strength and deformation properties" (Kaiser and Morgenstern, 1981).

1.1 AIM OF THIS THESIS

The prime objective is to use the PST apparatus to study the failure process and some associated rate effects around a small unlined tunnel in a naturally jointed coal specimen.

Thus, tests were carried out on a specimen of jointed coal containing a small unlined tunnel, MC1. They were based on previous testing done with the PST facility. Over the period of the 10 month test program, test results were examined to aid as a guide for setting the course of the

test program. Then, with testing complete, they were studied in detail to determine trends and correlations. In view of the test results, a simple theoretical formulation was used to simulate some test observations.

These results should give insights into the deformational mechanisms controlling rock mass behavior around real tunnels.

1.2 BACKGROUND ON THE PROCESS SIMULATION TEST

The test specimen is located in a testing machine such that normal surface stress (field stress) may be applied to the specimen surfaces. The state of stress inside the specimen depends on the magnitude of the field stress and varies with location. At the tunnel wall, the radial stress approaches zero and, assuming a hydrostatic field stress and linear elastic behavior, the tangential stress exceeds the field stress by a factor of two. Displacement of the tunnel wall and specimen surfaces as well as the average radial strains may be monitored with time.

The test apparatus was built and used by Kaiser (1979) to study the pre-failure time-dependent deformation process for one specimen, MC2. Kaiser (1979) interpreted deformation measurements using linear elastic and linear visco-elastic formulations. Guenot (1979) studied the tunnel deformation behavior by testing two specimens, MC3 and MC4, and showed that a conventional elasto-plastic formulation inadequately explained details of behavior near

failure. Using some of Guenot's data to check the accuracy and validity of a boundary value problem solution for axi-symmetric creep around a tunnel in coal, da Fontoura (1980) demonstrated that an empirical non-linear creep law for this coal showed good agreement between prediction and observation at low to moderate field stress.

1.3 ROCK MASS BEHAVIOR AROUND REAL TUNNELS

Studying the time-dependent processes associated with underground openings in rock, da Fontoura (1980) defines causes, factors and characteristic modes of ground behavior. The time-dependent change in boundary conditions (.eg., advances of the tunnel face) and the time-dependent character of the rock mass cause the time-dependent deformation of an underground opening. Figure 1.1 (da Fontoura, 1980) shows four characteristic modes of ground behavior and three categories of factors which control the behavior of an underground opening. However, Figure 1.1 does not include a category for self-supporting tunnels. According to da Fontoura (1980), the combination of the factors shown in Figure 1.1 govern the performance of a rock tunnel.

The four characteristic modes of ground behavior shown in Figure 1.1 overlap slightly, and a simple classification distinguishes between gravity controlled and ground reaction induced mechanisms. Loosening, according to da Fontoura (1980), relates to gravity aspects of deformation (.ie.,

large displacements occur as rock blocks separate from the rock mass and move into the opening). Fracturing, squeezing and swelling dominate when large stress concentrations occur around an underground opening.

The term loosening has been used in discussion of tunnels in rock that exhibit either 'self-supporting' or 'support-requiring' behavior. Terzaghi (1946) introduces the loosening mechanism for a discussion of 'bridge action' and 'overbreak' in self-supporting sections of tunnels in unweathered stratified rock. For moderately jointed, massive rock, failure of block contacts due to excessive deformation leads to loosening and deterioration of the rock mass (Terzaghi,1946). This would be inhibited by support designed for loosening pressure. Loosening depends on a combination of mechanical defects and size, shape and orientation of the opening. Thus, strength reduction and deformations vary in a wide range depending on rock type and the scale effect.

According to da Fontoura (1980), the fracturing mode occurs due to stress concentrations in brittle rock and corresponds with fracture growth due to tensile or shear failure. The squeezing mode corresponds to the delayed response due to the rheological behavior and/or due to overstressing (strength failure) and post failure behavior of the rock. The swelling mode corresponds to delayed volumetric increase due to stress relief, water migration and alteration of physical properties(.eg., strength loss

due to increased water content). Squeezing and swelling modes are characteristically time-dependent.

Terzaghi (1946) used the concept of a 'ground cylinder' to describe the deformation behavior that occurs with construction of a tunnel. In particular, a rock element at the tunnel wall would experience a tangential shortening and radial extension as it moves into the tunnel under hydrostatic field stress. Thus, a rock element is compressed by neighbouring rock elements.

For analytical purposes, rock mass behavior may be characterized according to time-independent and time-dependent behavior, as shown in Figure 1.2 (Kaiser and Morgenstern, 1981). Deformations occur due to changes in the stress conditions and accordingly, the following deformation processes may occur (Kaiser and Morgenstern, 1981):

1. deformation due to time-dependent deformation properties (viscous or general creep behavior);
2. stress redistribution due to non-linear creep properties;
3. stress redistribution due to anisotropic or non-homogeneous creep properties;
4. stress redistribution due to local yielding;
5. stress redistribution due to global yielding;
6. stress redistribution and stabilization of failure propagation due to time-dependent post failure resistance.

1.4 SCOPE OF THIS THESIS

Descriptions of the coal test specimen used in this study, MC1, and the test procedures are presented in Chapter 2. A summary of the characteristics of the jointed coal material is given in addition to the deformation properties measured in the PST. The test procedures used in this testing program are defined and the test apparatus, calculation procedures and data processing procedures are described. Finally, in Chapter 2 some limitations are discussed with reference to interpretation of test results.

A summary of the test program is given in Chapter 3. In thirteen individual tests, field stress was applied to the test specimen with a plane strain boundary condition to produce either:

1. an axially symmetric stress condition, referred to as a "hydrostatic" field stress, or
2. a radially symmetric stress concentration, referred to as a "non-hydrostatic" field stress.

Alteration of the deformation behavior due to radially symmetric stress concentrations was evaluated by conducting tests with a hydrostatic field stress. In addition, some aspects of loading rate dependent deformation behavior were studied in tests with a "Bimodal Loading Rate" in which the loading rate was reduced at the middle of the load range.

The test results and significant observations are described in four sections of Chapter 3, categorized according to the test type. A "size effect" was discovered

upon enlarging the tunnel size in preliminary tests. Alteration the deformational behavior was observed due to tests with an non-hydrostatic field stress. Stress redistribution processes are required to explain alteration of the deformation behavior. In the last test, the deformation behavior changed insignificantly even though the specimen had been ruptured along jointing in the previous test with a non-hydrostatic field stress. Finally in Chapter 3 conclusions are given based on test observations.

Analytical formulations to simulate the deformation behavior of the PST specimen are presented in Chapter 4. The time-independent deformation behavior prior to the initial "Non-hydrostatic Episode" is simulated by a linear elastic formulation. However, a non-homogeneous linear elastic formulation is required to simulate deformation behaviour after the initial test with a non-hydrostatic field stress. In Chapter 4 the phenomenological model for rock with time-dependent strength and deformation properties, developed by Kaiser and Morgenstern (1981), is used as a basis for a qualitative discussion of the PST behavior.

Conclusions, deformation modes and some practical implications based on test observations and analytical results are presented in Chapter 5.

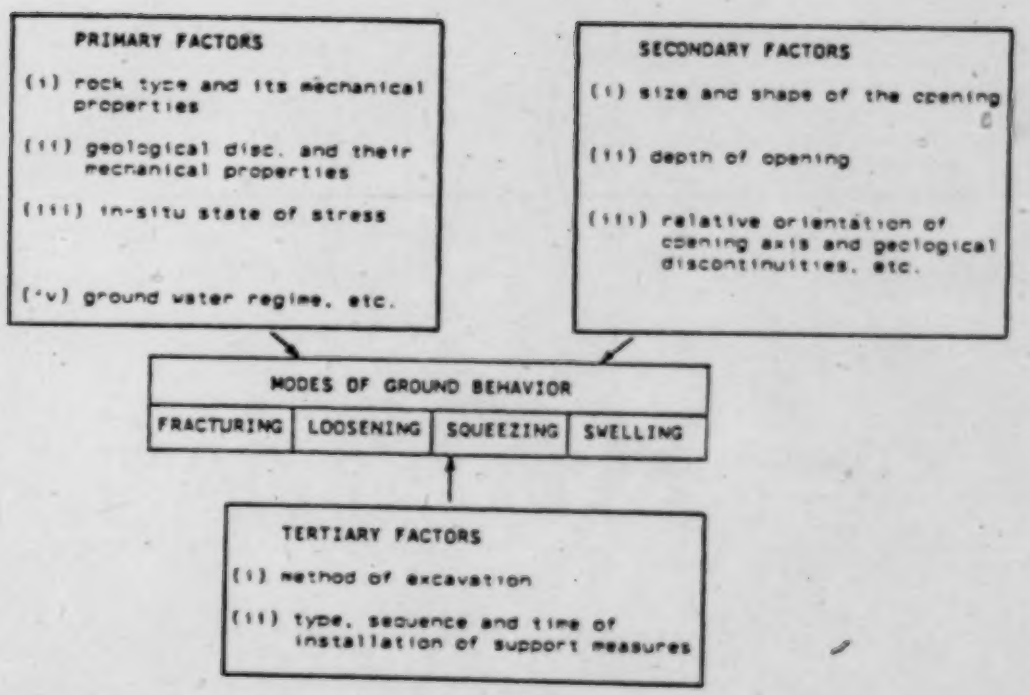
PRIMARY FACTORS
(i) rock type and its mechanical properties
(ii) geological disc. and their mechanical properties
(iii) in-situ state of stress
(iv) ground water regime, etc.
SECONDARY FACTORS
(i) size and shape of the opening
(ii) depth of opening
(iii) relative orientation of opening axis and geological discontinuities, etc.
MODES OF GROUND BEHAVIOR
FRACTURING
LOOSENING
SQUEEZING
SWELLING
TERTIARY FACTORS
(i) method of excavation
(ii) type, sequence and time of installation of support measures

Figure 1.1 Modes of Ground Behavior (da Fontoura, 1980)

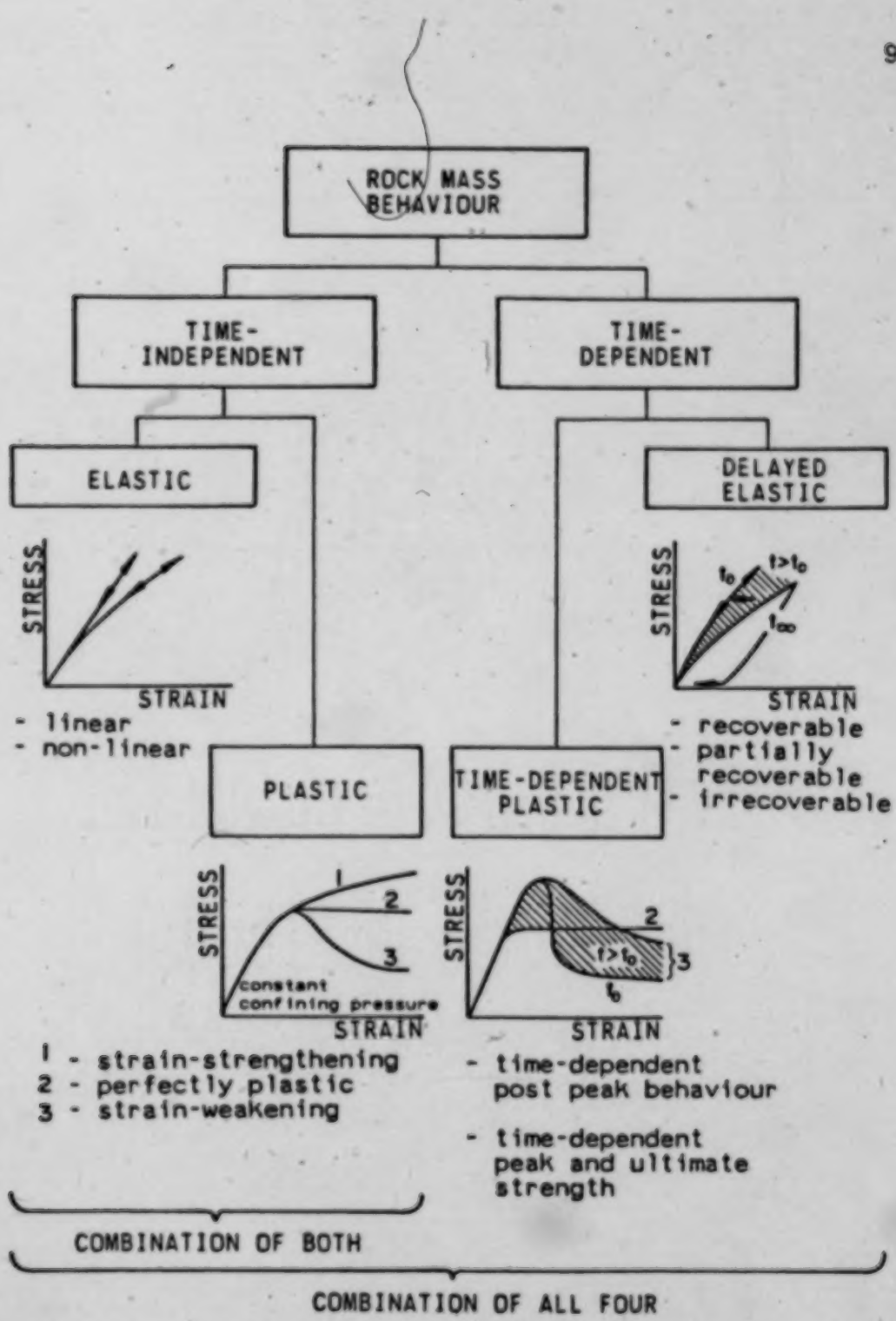

Figure 1.2 Types of Rock Mass Behavior (Kaiser and Morgenstern, 1981

2. CHAPTER II

PROCESS SIMULATION TEST (PST) SPECIMEN AND TEST PROCEDURE

2.1 INTRODUCTION

This chapter describes the coal material and test specimen characteristics, as well as, the PST procedures and facilities. This provides desirable information to assist interpretation of the PST test results.

Typically, the specimen is tested in two physical configurations, before and after drilling a circular tunnel at the center of the block. Prior to the test program reported in this thesis, a 12 cm diameter tunnel had been drilled into this specimen. After test MC 1.7, the first test in this test program, the tunnel was enlarged to a 15 cm diameter.

The PST is carried out by applying and maintaining prescribed boundary normal stresses (field stress) to the surfaces of the tabular shaped, jointed coal specimen (60x60x20 cm) ;and by monitoring the specimen and tunnel displacements with time. The test specimen functions as a laboratory scale geologic medium and exhibits a time-independent and delayed deformation behavior.

The test procedure was carried out based on experience gained during previous test series done by Kaiser (1979) and Guenot (1979). The adopted test procedures and test facilities have been only slightly modified for the test series reported here.

The next two sections describe the physical character of the specimen and the location of displacement monitoring devices.

The fourth section describes the procedures, equipment and facilities used to carry out the Process Simulation Test as relates to interpretation of the specimen behavior.

The last section reviews some testing limitations that influence interpretation of specimen behavior.

2.2 DESCRIPTION OF THE COAL

The coal used for the PST was taken from the Highvale Mine located 75 km west of Edmonton, Alberta. This strip mine provides coal for the nearby Sundance power plant operated by Calgary Power Ltd.

The coal possesses the following characteristics, desirable for Process Simulation Testing (Kaiser and Morgenstern, 1981):

1. discontinuities;
2. cohesive and frictional strength components;
3. time-dependent strength and deformation behavior; and
4. a strain-weakening stress-strain relationship.

The specimen material has rock mass characteristics comparable to many natural materials. It exhibits a satisfactory degree of similitude in model laws but caution is necessary if results of inelastic deformation measurements and failure modes are compared to the behavior of actual tunnels (Kaiser and Morgenstern, 1981).

The coal properties have been investigated by Noonan and Morgenstern (1974), Kaiser and Morgenstern (1978, 1981), Guenot (1979), Kaiser (1979) and da Fontoura (1980).

2.2.1 SUMMARY OF THE COAL PROPERTIES

The coal, classified as sub-bituminous B, is bright and banded. Classification testing yielded an average moisture content of 24% and a specific gravity of 1.58.

The coal is horizontally bedded with two orthogonal cleat systems oriented perpendicular to bedding. The predominant cleat system is called a major joint system, the other, a minor joint system. The bedding is thinly banded. The major joints are closely spaced, approximately 2 cm on average. The major joints, typically planar, are not continuous across major bedding planes. Thus the coal is described as heterogeneous and orthotropic.

The deformation and strength properties for the coal differ slightly depending on the test method. In general, the properties depend on the orientation and continuity of the defects, confinement and loading rate. The variation of the mechanisms prevailing in the various test methods causes some variation in the property parameters.

The unconfined compressive strength for the coal varies between 8 to 12 MPa. The ultimate friction angle is 30 degrees, obtained from direct shear tests on pre-cut surfaces (Morgenstern and Noonan, 1974).

Direct shear test results, on jointed specimens, show

strength anisotropy. In addition, if the joints are discontinuous, very little movement occurs along the discontinuity prior to peak strength (Morgenstern and Noonan, 1974).

Constant strain-rate (0.3-0.8 %/hr) triaxial test results on jointed coal specimens obey a bi-linear Coulomb failure criterion (Kaiser and Morgenstern, 1980). At confinement pressures below 1 MPa, the failure stress plot exhibits little cohesion and a high internal friction angle, 60 to 70 degrees. Yielding occurs between 0.1% to 0.3% axial strain and peak strength occurs around 0.5% to 1.6 % axial strain. For confinement pressures up to 12 MPa, the failure stress plot exhibits more cohesion, 2-3 MPa, and a lower internal friction angle, 30 degrees. Moreover, yielding and peak strengths occur at greater axial strains of 0.5% to 3.75%.

Relaxation triaxial tests, on jointed coal specimens, exhibit loading history dependent long-term and short-term strength (Kaiser and Morgenstern,1978). In the pre-failure range, the strain rate during single and multiple stage creep tests obeys a power law relationship as a function of time and stress level (da Fontoura, 1980). Above the long-term peak strength, the available shearing resistance depends on a rate-dependent micro-structural weakening process and declines to ultimate resistance with increasing plastic strain.

2.2.2 SUMMARY OF DEFORMATION PROPERTIES MEASURED IN THE PROCESS SIMULATION TEST

Apparent deformation properties for the PST may be calculated by using tunnel closure and specimen boundary displacement measurements in the linear elastic formulation shown in Appendix A1. In general, linear elastic parameters obtained in previous testing correlate with that for MC1.

Kaiser (1979) notes the loading rate dependency of linear elastic parameters and reports Young's Modulus, E, varied between 1900 and 2050 MPa for fast loading without a tunnel and 1500 MPa for slow loading of the same specimen with a tunnel. Young's Modulus during slow loading varied between 1100 MPa perpendicular to jointing to 1450 MPa parallel to jointing. Poisson's Ratio varied between 0.2 parallel to bedding and 0.1 perpendicular to bedding (Kaiser,1979). Guenot (1979) reports a significant variation of Young's Modulus, between 1300 and 2300 MPa, and Poissons Ratio of 0.2 parallel to bedding.

2.3 DESCRIPTION OF THE MC1 SPECIMEN

2.3.1 INTRODUCTION

Specimen MC1 was trimmed from a jointed coal sample such that the specimen thickness equals one-third of the specimen length. The specimen reference system is shown in Figure 2.1, a schematic sketch of MC1. The tunnel axis corresponds with the polar coordinate axis and the top surface of the specimen represents Station 0 on the tunnel

axis.

Prior to this testing program, an old extensometer system had been installed into specimen MC1. For this test program, some of these extensometers were reclaimed to accommodate the new improved extensometers and some were left inside the specimen. No results are available for previous testing.

2.3.2 STRUCTURAL CONDITION OF MC1

The bedding and jointing structure was clearly visible on the specimen surface. Bedding planes were oriented perpendicular to the tunnel axis. Major joint planes were oriented at 45 degrees to the horizontal and vertical axes. An indication of the orientation of the geologic structure is shown in Figure 2.2.

A fracture in MC1, oriented approximately perpendicular to bedding and to the major joint set, crossed the model outside the perimeter of the circular tunnel as shown in Figure 2.1. After testing, no evidence of displacement along the fracture surface (i.e.slickensides) was observed. The fracture surface was generally dull or shiny black and slightly curved, irregular and rough (1-2 cm relief).

Small diameter holes (9 mm diameter), for the old extensometer system, interupted the continuity of the specimen. The small diameter holes were located as follows:

1. for radial strain measurement; one hole was collared on each lateral face (except face 3) and on the two edges

of face 4, and oriented radially around the tunnel axis to within 10 mm of the large diameter tunnel wall,

2. for tangential strain measurement; three holes were collared on the edges of face 2 and oriented to one side of the tunnel wall to within 80 to 110 mm of the tunnel axis.

It is assumed that these small diameter holes insignificantly affect the deformational behavior of the test specimen.

2.3.3 DISPLACEMENT MEASUREMENT

The displacements were monitored by electrical monitoring devices, displacement transducers (LVDT). The displacement transducers were located to measure the tunnel wall and specimen boundary displacements as well as the relative movement of extensometer anchors.

2.3.3.1 TUNNEL CLOSURE

Tunnel closure is defined as the ratio of the diametral displacement to the original diameter. Tunnel closures were measured with eight LVDT's, two located along each of four tunnel diameters spaced 45 degrees apart and at four stations along the tunnel axis spaced 25 mm apart as shown in Figure 2.3. The tunnel closure measurement is designated by the diametral location relative to the reference radius shown in Figure 2.1 (eg. 0-180 diameter closure).

The LVDT's were mounted inside the tunnel on a stand

fixed to the steel plate below the specimen block. The two LVDT's along each tunnel diameter were mounted coaxially and the LVDT cores were forced by a spring to bear directly on the tunnel wall.

Translation and rotation of the specimen plus penetration of the LVDT core into cracks and broken zones on the tunnel wall occasionally influenced tunnel closure measurements. During the later part of the test program, broken, bulging zones on the tunnel wall also interfered with closure measurement. Although assessing closure measurement interference is difficult, in general the LVDT cores were rested against a smooth, latex coated tunnel surface.

2.3.3.2 AVERAGE RADIAL STRAIN

The relative displacement of extensometer anchors was measured by sixteen LVDT's, each connected to an extensometer located in a small diameter drill hole adjacent to the tunnel (Figure 2.1). The average radial strain for each extensometer was calculated by dividing the measured displacement difference by the distance between anchor center points.

Each extensometer was located at one of four stations along the tunnel axis and in one of two zones, Zone A or Zone B, as shown in Figure 2.3. The gauge lengths of Zone A and B extensometers were calculated as the distance between anchor centerlines, about 3 cm and 5 cm respectively. Gauge

length was calculated as the distance between anchor centerlines. The extensometer location is designated by the radial location relative to the tunnel axis and reference radius shown in Figure 2.1, (eg., radial strain along the 180 radius).

An extensometer, consisting of a coaxial rod and tube, was grouted inside a small diameter drill hole inside the test specimen. The rod was free to move inside of the tube. The rod anchor, about 1 cm long, was located at the end of a 6 mm diameter drill hole. The tube anchor, about 1.5 cm long, was located inside a 9 mm diameter drill hole, back from the rod anchor. The anchor length, on average, was about equal to 1 to 1/3 of the extensometer gauge length.

The present extensometers seem to give satisfactory results. However, a quantitative evaluation of the extensometer calibration has not been done. Reducing the anchor size, to decrease the ratio of anchor size to gauge length, should increase the extensometer sensitivity. At least further evaluation of extensometer performance would clarify the significance of anchors size. Perhaps modified prototypes with small size anchors could be installed inside the specimen and evaluated during future testing.

2.3.3.3 BOUNDARY DISPLACEMENTS

The boundary displacements, along the three principal loading directions, were measured with eight LVDT's. One LVDT was located at each corner of the longitudinal loading

head to measure longitudinal displacement and one was located on each face at station 165 to measure the average specimen strain. The LVDT's were mounted on metal stands fixed to the steel plate below the specimen. On the lateral faces, the LVDT cores were forced by a spring to bear on teflon discs fixed to steel pins grouted into the specimen at a depth of 30 to 40 mm (Figure 2.1). Occasionally, boundary displacement measurements were unreliable since the loading machine interfered with the steel pins.

2.3.4 SPECIMEN CONDITION AFTER TESTING

A shear zone developed during the last low confinement test, MC1.18, as shown in a photo reduced sketch of the top of the specimen, in Figure 2.4. This shear zone is also visible in Plate 2.1, photos showing the top and bottom surfaces of the test specimen after testing. The crack pattern that developed during the testing program is also shown together with jointing in Figure 2.4. A broken zone is shown in Figure 2.4. It is also shown in Figure 2.5, a sketch of the tunnel surface after testing, and it is visible in the top view of the specimen in Plate 2.1. The change in the tunnel surface due to the test program is illustrated by comparing Figure 2.5 to Figure 2.2, a sketch of the tunnel wall at the beginning of the test program.

Differential displacements occurred along the shear zone and at the specimen boundary (Plate 2.1). Part of the shear zone consisted of a 1 to 4 cm wide broken zone

corresponding with a regularly thin bedded zone, from Station 0 to 90. The other part of the shear zone occurred along a planar joint from Station 90 to 200. Some slickensides were visible on the planar joint surfaces.

Inspection of the extensometers after testing revealed the following:

1. For the 270 radius, Zone A extensometer, one anchor was located in the broken zone and other further from the tunnel in a more intact rock mass.
2. For the 270 radius, Zone B extensometer, one anchor was located in intact rock mass and the other further from the tunnel near the fracture.
3. For the 225 radius, the Zone B extensometer straddled the fracture, and the anchor furthest from the tunnel was near the shear zone.

All other extensometer anchors were located in the intact rock mass.

2.4 DESCRIPTION OF THE TEST PROCEDURE

2.4.1 INTRODUCTION

The process simulation test is carried out with a compression machine, consisting of an air-hydraulic loading system and three reaction frames for each of three independent loading axes. Plate 2.2 shows a view of the compression machine. The specimen is situated inside the reaction frames with the tunnel axis oriented vertically. The air-hydraulic system applies pressure to hydraulic rams

located around the specimen and inside the reaction frame. An automatic data acquisition unit records output from electrical load and displacement transducers. A computer program package uses test measurements to speedily calculate graphics displays of test results.

The next subsection reviews the preparation of the specimen for testing. The last two subsections describe the test procedures and test apparatus. A brief explanation of th computer calculations and graphics displays is also given. Kaiser (1979), Guenot (1979) and Kaiser and Morgenstern (1981) cover the test apparatus in more detail.

2.4.2 PREPARATION OF A TEST SPECIMEN

During sampling, large intact jointed coal samples (1 m^3) are carefully excavated from the coal seam and transported to the laboratory. The samples are sealed with two coats of latex and stored in a humidified room.

During construction of a test specimen, the surfaces of the specimen are made planar and small diameter drill holes are drilled into the specimen to accommodate the extensometers. Small depressions on the specimen surfaces are filled with thin grout layers and each side of the specimen is sanded to make the surface planar and parallel to the opposite side. Then, the specimen is sealed in a thin wax paper and plaster-of-paris coating. Two small diameter (6,9 mm diameter) drill holes are advanced from the center of each side and each corner of the specimen toward

the proposed tunnel axis. Reclaimed small diameter holes, drilled for previous testing, are cleaned out to minimize damage to the drill hole surfaces. Records are kept of the drilling rate and difficulty together with the colour of drill returns. An extensometer is located and grouted inside each drill hole. A small diameter probe is used inside the drill hole to determine the location and size of the extensometer anchors.

In preparation for testing, the specimen, situated in the compression machine, is centered on two lubricated teflon sheets over the top of a passive concrete reaction block in the longitudinal reaction frame. The longitudinal rigid loading head is placed on two lubricated teflon sheets over top of the specimen then, the lateral loading platens are placed against teflon sheets at the four lateral faces. The teflon sheets reduce friction forces between the specimen and the compression apparatus. The loading and monitoring systems are set-up to begin testing. Initially, the specimen is preloaded to close cracks in preparation for future high pressure testing. Preloading of MC1 was completed prior to this test series.

During the drilling of the circular tunnel, the specimen is positioned in the test apparatus so that a concrete drill may be located over the proposed tunnel location. No test loads are applied during this drilling. The circular tunnel is drilled in approximately ten minutes using a diamond coring shell. The tunnel wall is coated

with a latex sealant and the drill core is retained for geologic mapping purposes. The specimen, with a circular tunnel, is returned to its proper location in the compression machine and the loading and monitoring systems are set up for future testing.

2.4.3 STEP BY STEP DESCRIPTION OF THE TEST PROCEDURE

Four phases of testing are carried out during a typical test:

1. Increasing Boundary Load Phase;
2. Reducing Boundary Load Phase;
3. Constant Elevated Boundary Load Phase or Stage; and
4. Recovery Phase or Stage.

A test plan, incorporating these procedures, is prepared prior to testing, however occasionally the test plan is altered during a test to accommodate any unexpected response. Typically, a test is planned for a duration of one to several days or weeks.

The specimen is loaded in an incremental manner, by increasing the lateral boundary stress while nulling the longitudinal displacement (plane strain boundary condition). During a test with a hydrostatic field stress, the boundary stress along the horizontal and vertical axes are approximately equal. During a test with a non-hydrostatic field stress, the ratio of the boundary stress for the two lateral load axes, N, differs from unity.

The increasing load phase is continued according to the

test plan, barring interruptions, and then either the load is reduced or held constant for a specified time. A detailed description of the increasing load procedure is shown in Figure 2.6. The average loading rate is controlled by changing the time interval between 0.5 MPa boundary stress increments; or else, by maintaining constant pressure for a one day interval at each 1 MPa stress increment (slow loading). During a fast increasing load phase, each 0.5 MPa stress increment is usually maintained for a constant time interval, between 4 to 8 minutes.

The reducing load phase is carried out more rapidly than the increasing load phase and without visually monitoring load cell readings. Thus, the specimen is unloaded by reducing the lateral pressure, in approximate 0.5 MPa decrements, while nulling the longitudinal displacement.

The constant elevated load and recovery (zero load) phases or stages are carried out using automatic test equipment, thereby allowing testing to continue for extended time intervals. Typically, electrical monitoring device readings are recorded at increasing time intervals after the beginning of a constant load level (one minute interval for the first 5 minutes; 2 minutes interval for the next 10 minutes; 5 minute interval for 45 minutes; 15 for 2-3 hours; 30 for 5-8 hours; 60 for 16-24 hours; and 120 minute intervals thereafter.) The operator is freed to observe the specimen condition and to process test measurements using

specially designed computer software.

Typically, the plots of test results are reviewed throughout the test and are updated with new information as it becomes available. Thus, the specimen behavior is interactively assessed during a test and the testing program may be continued according to the plan or altered to accommodate changes in anticipated behavior.

2.4.4 TEST EQUIPMENT

The geomechanical model test equipment was designed and built by Kaiser (1979) based on equipment developed and tested by Heuer and Hendron (1969, 1971). The major factors considered in the design are described by Kaiser and Morgenstern (1981).

2.4.4.1 COMPRESSION MACHINE

The compression machine consists of three large reaction frames, a specially designed air-hydraulic system with a safety system (Plate 2.2). The air-hydraulic system maintains hydraulic pressure during long term testing with small fluctuations (less than 1%) (Kaiser and Morgenstern, 1981). The safety system is designed to prevent damage to the test equipment during specimen collapse, specimen rotation or power failure.

Plane strain is actively controlled by a rigid longitudinal loading head located on top of the specimen. The longitudinal displacement of the top of the rigid

loading head is measured relative to the passive steel plate located below the specimen. The longitudinal displacement of the rigid loading head is nulled by load application through four hydraulic rams located to react against the upper reaction head of the longitudinal reaction frame. Load cells are located between the rams and reaction head to measure the load. A window is located in the rigid loading head to make the tunnel accessible during a test.

Lateral loading is applied by load application through eight hydraulic rams, two on each of four sides of the specimen, located in each of the two cantilevered lateral reaction frames. The load from each ram is transferred through a load cell and a set of triangles (flexible load platens) onto the lateral surfaces of the specimen (Plate 2.3). The loading system is designed to apply a maximum of 16 MPa normal stress onto the surfaces of the specimen.

2.4.4.2 LOAD AND DISPLACEMENT MONITORING DEVICES

The loads and displacements of the specimen are monitored by two types of electrical monitoring transducers, load cells and LVDT's. Each transducer is measured against a known standard and a calibration equation is determined. Appendix B1 describes the transducers and calibration procedures.

Evaluation of the lateral load cell calibration showed that the combination of 3 or 4 load cell readings, taken along one load axis, provides a reasonable load measurement

for evaluation of the test results (Appendix B1). Some load cells have a lower degree of uncertainty than others. All load cells should be calibrated over the range of interest, that is, increasing, decreasing or constant load phase and above 25% of their maximum load. Study of the specimen behavior in the low pressure range would be augmented by specifically designed load monitoring devices. The degree of uncertainty associated with the load cell calibrations could explain the large load variations shown by test results in Appendix C2.

The LVDT's are very accurate and provide good results for the PST. Strain sensitivity is at least 0.001% for the tunnel and extensometer measurements and 0.03% for two of the four LVDT's used for boundary displacement measurements.

2.4.5 CALCULATION PROCEDURES AND GRAPHICS DISPLAYS

Stress and strain are calculated using load and displacement transducer readings. Tunnel closure for each tunnel diameter is calculated by combining two LVDT displacement measurements, each normalized to the tunnel radius. Average radial strain is obtained directly from the LVDT displacement measurement for an extensometer, normalized to the extensometer gauge length. Average specimen strain for the lateral loading axes is calculated by combining two LVDT displacement measurements, each normalized to one-half of the specimen length. Average longitudinal strain is calculated by combining four LVDT

measurements, each normalized to the specimen thickness.

More than 10,000 data points may be taken during a typical test. Thus, automatic data acquisition and computer data processing are required for the PST.

Two computation procedures are carried out for presentation of test results. The initial computation procedure uses load and displacement measurements to produce stress-strain and strain-time graphical plots. The second computation procedure statistically evaluates the strain-time measurements to produce strain-rate versus time graphical plots. Guenot (1979) reported that the procedure for calculating the time-dependent deformation seems correct. The following list chronologically outlines the computation procedures.

Stress-strain and strain-time computational procedure:

1. Initialize all transducer and time readings (i.e. substract zero readings from all readings);
2. Interpret transducer readings using the calibration equations to obtain force and displacement;
3. Normalize force and displacement values, as follows:
   a. Boundary stress equals force per loaded area;
   b. Normalized displacement equals displacement per length eg. extensometer gauge length, tunnel radius (units of strain);
4. Combine normalized values (eg. the average of 3 or 4 load cell readings gives the axial stress);
5. Plot pairs of measurements on orthogonal axes, (eg.

strain versus time).

Strain-rate versus time computational procedure:

1. Initialize all measurements to the beginning of a constant load interval;
2. Fit a linear line (least squares method) to three pairs of strain-time values. The pairs are selected relative to time after the start of constant load (uses consecutive pairs for first hour, use every second pair for 1 to 20 hours, use every third pair after 20 hours);
3. Repeat the previous step using every tenth pair to obtain the trend (neglect the first 30 pairs);
4. Plot the calculated line slopes (strain-rate) at the middle of each respective time interval on double log orthogonal axes.

Examples of the computation results are shown in Figures C4-1 to C4-5 and the graphical symbols are explained on Table C4-1 in Appendix C4.

The stress versus strain and strain versus time plots are produced by joining test measurements with straight lines. All pairs of stress-strain measurements taken during increasing and decreasing loading phases plus the last measurement taken during the recovery phase are shown on orthogonal, linear axes and joined by straight lines. The average vertical stress, shown along the ordinate axis, is calculated by taking the average stress for 3 or 4 load cells located long the vertical lateral loading axis, that is along the 0-180 diameter. Three types of strain,

in particular, tunnel closure, average radial strain and average specimen strain, shown along the abscissa axis, are calculated by combining the three types of normalized displacements. All pairs of strain-time measurements taken during a constant load phase are shown on orthogonal, linear axes and joined by straight lines. For these plots, strain is shown along the ordinate axis and time along the abscissa axis.

The strain-rate versus time plot is produced by plotting different symbols for positive and negative strain-rates on double log coordinate axes. The symbols used in strain-rate plots are shown on Table C4-1 in Appendix C4.

In each of the stress-strain and strain-time plots, the location plan for strain measurements is shown on a schematic, plan view diagram of the specimen. In the schematic diagram, the solid circle represents the tunnel, the dashed circles indicate each of two radial extensometer zones, A and B, on the diagonal lines indicate the joint orientation. A symbol identifies the strain measurement location for each test curve shown. In the strain-rate-time plots, the test curve, one per plot, is labelled to correspond with the respective strain-time curve.

2.5 LIMITATIONS OF TESTING

Variations in both the loading conditions and the deformation measurement are discussed as relates to the interpretation of the mechanisms of deformational behavior. Practical requirements for the PST have been outlined by Kaiser (1979) and Kaiser and Morgenstern (1981).

The boundary normal stress during a test varies non-uniformly on the lateral surfaces of the specimen. The indicated load varies between adjacent load cells by a maximum of about 20% to 25% of the maximum field stress (Figure C2-1). In the low field stress range, even larger non-uniform stresses exist (Figure C2-1). Figure C2-1 shows the variation of boundary normal stress according to the load cell measurements. However, a 10% degree of uncertainty for the load cell calibration equations complicates assessment of the non-uniform boundary normal stress (Appendix B1).

Constant hydraulic pressure supply to all rams located along a loading axis precludes a 25% variation between adjacent load cells. The friction force perpendicular to the longitudinal axis due to longitudinal loading is approximately 5% of the field stress. Therefore, a conservative estimate of non-uniform stress variation would be perhaps 10%. Hence, the non-uniform boundary stress conditions at low field stresses are assumed to insignificantly affect test results.

The relative position of the tunnel and the

extensometers, the radial alignment and mechanical operation of the extensometers infuence the interpretation of the radial strain measurements. The two distinct zones of extensometers, Zone A and Zone B, exhibit substantially different results depending on location relative to the tunnel. To a lesser degree, the relative position of extensometers within either zone may also differ. Therefore, comparisons of extensometer measurements within a zone may be slightly affected by variations in location. Also, the nature of the grout-rock bond at the anchor; and the rod and tube friction likely varies between extensometers and may influence performance to some degree. The detailed differences between extensometers are assumed to insignificantly affect results discussed in Chapter 3.

The loading rate during the increasing load phase varies slightly, perhaps by 15%; and particularly during the earlier portion of the test program. The loading procedure was improved during later testing based on experience gained earlier in the testing program.

The effect of the latex sealant was neglected in the analysis of results. However, the sealant provided sufficient confinement to generally prevent material from falling from the tunnel wall.

The influence of boundary conditions on theoretical formulation was addressed by Guenot (1979). In particular, Guenot (1979) showed that the influence of longitudinal stress and the proximity of the specimen boundary may be

neglected. However, a plane strain boundary condition must be maintained in a test.

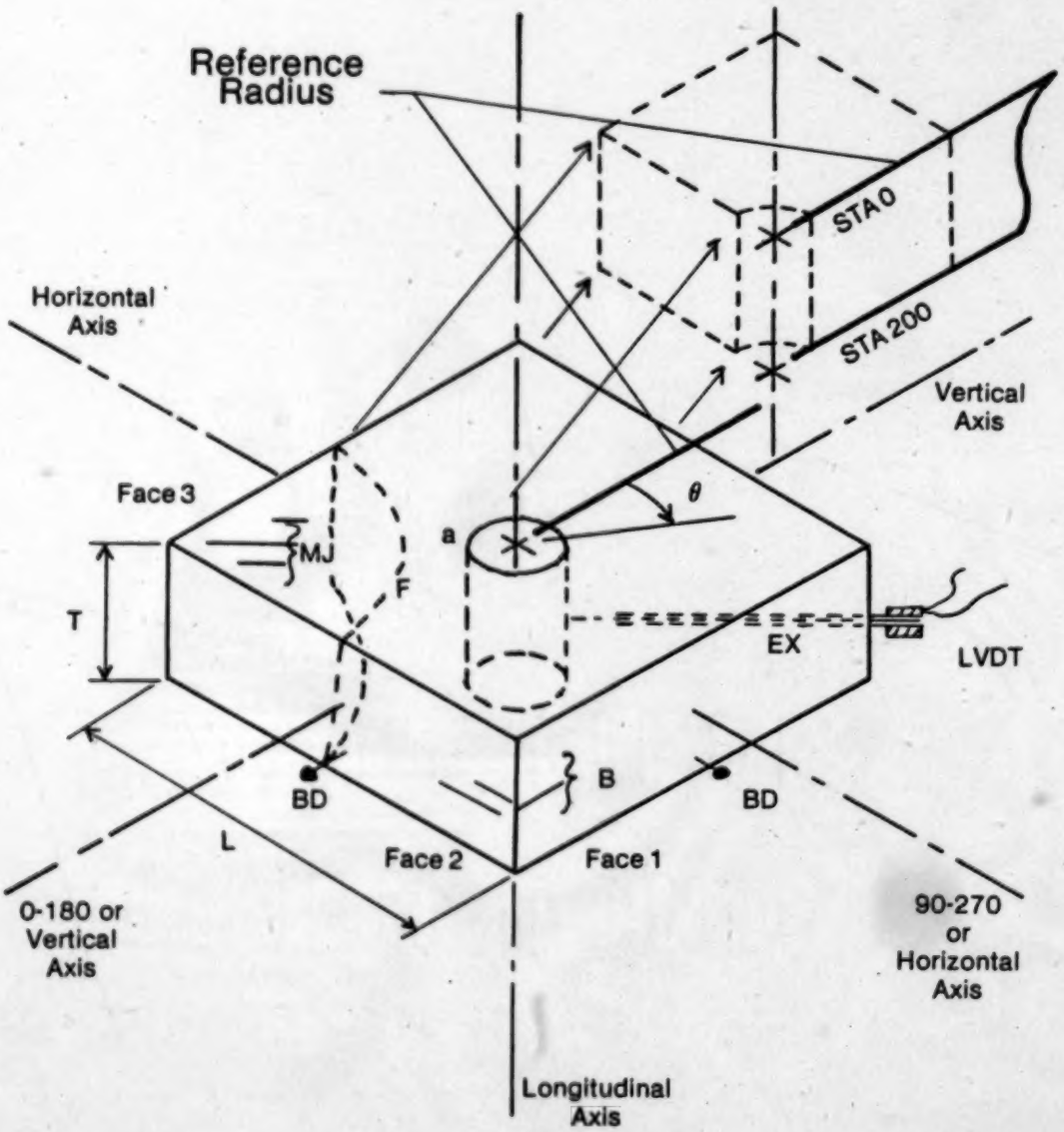

B	Bedding	EX	Extensometer
MJ	Major Joint Set	BD	Boundary Displacement
F	Major Fracture	T	Thickness (200 mm)
a	Tunnel Radius	L	Length (600 mm)

Scale 1:10

Figure 2.1 Schematic Sketch of MC 1 Prepared for Testing.

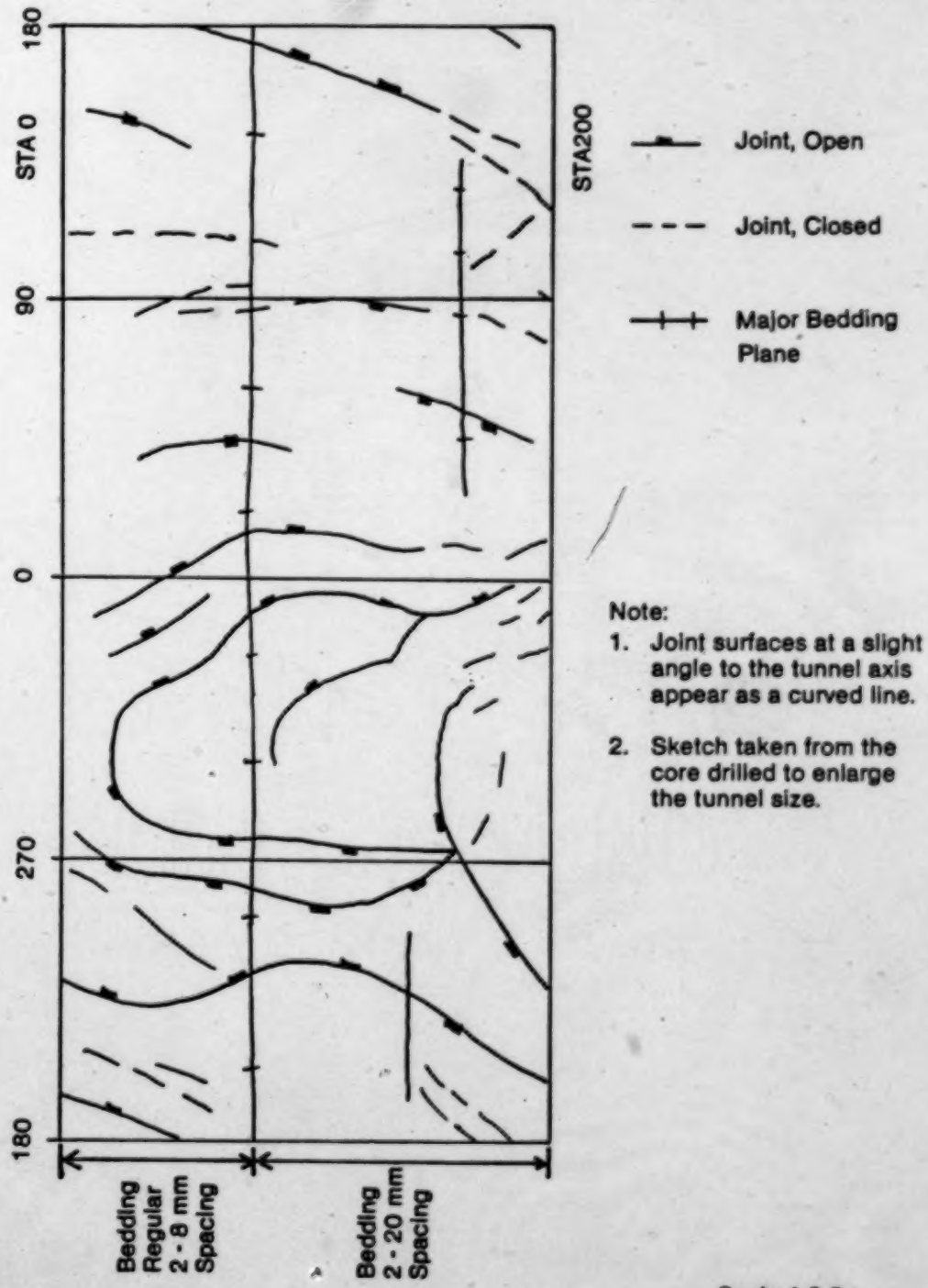

Figure 2.2 Developed Section, 15 cm Diameter Tunnel, After MC 1.7

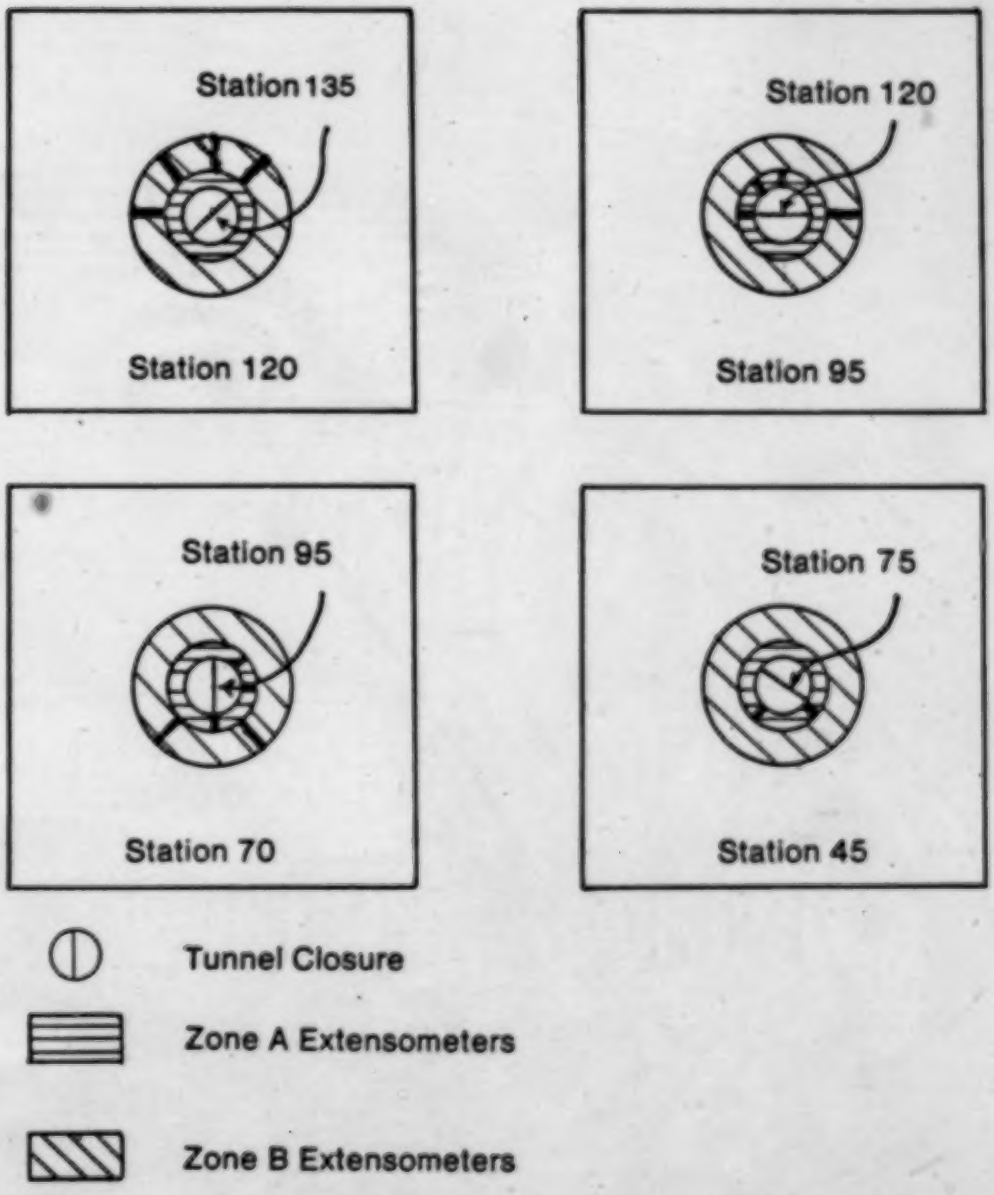

Figure 2.3 Schematic View of Radial Extensometer And Tunnel Closure Locations.

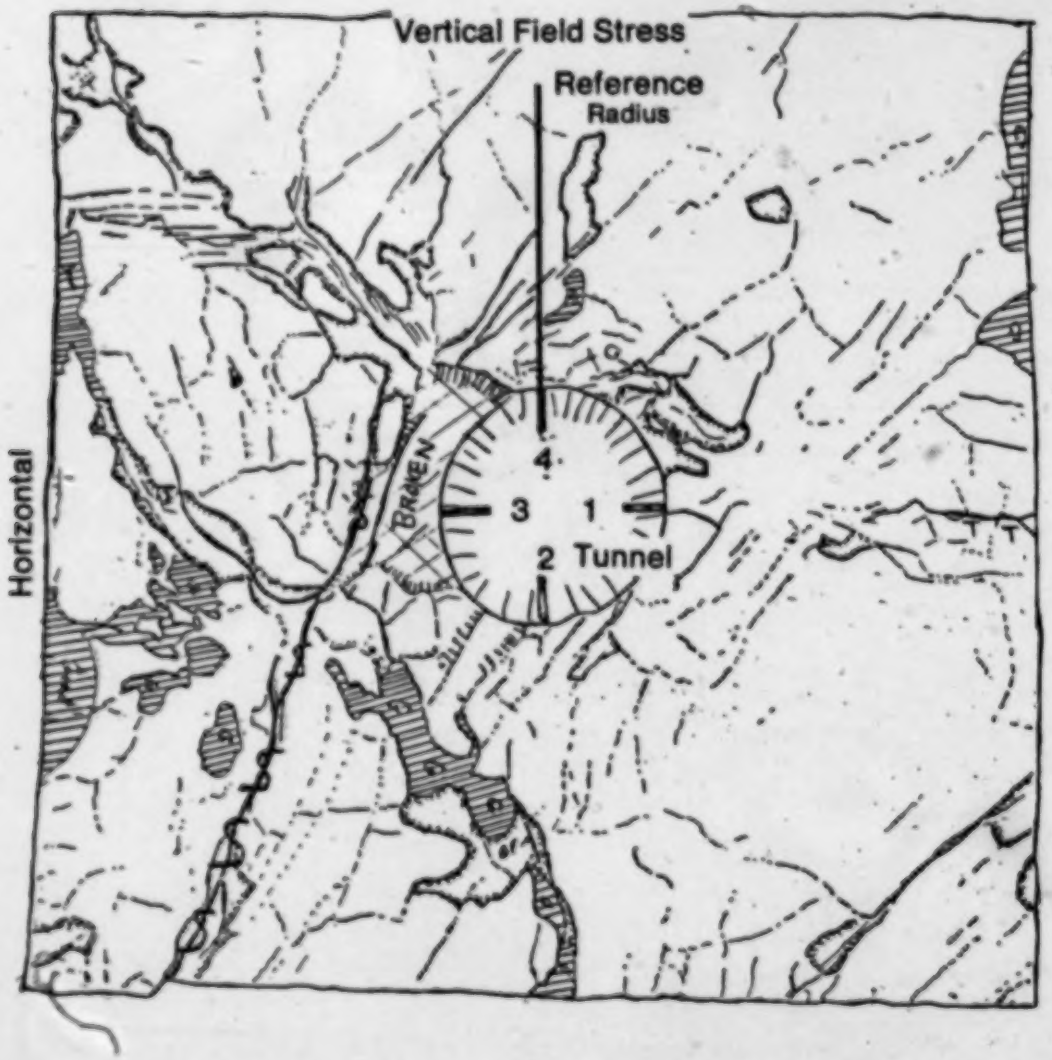

Figure 2.4 Photo Reduced Sketch of the Top of Specimen MC1 After Testing.

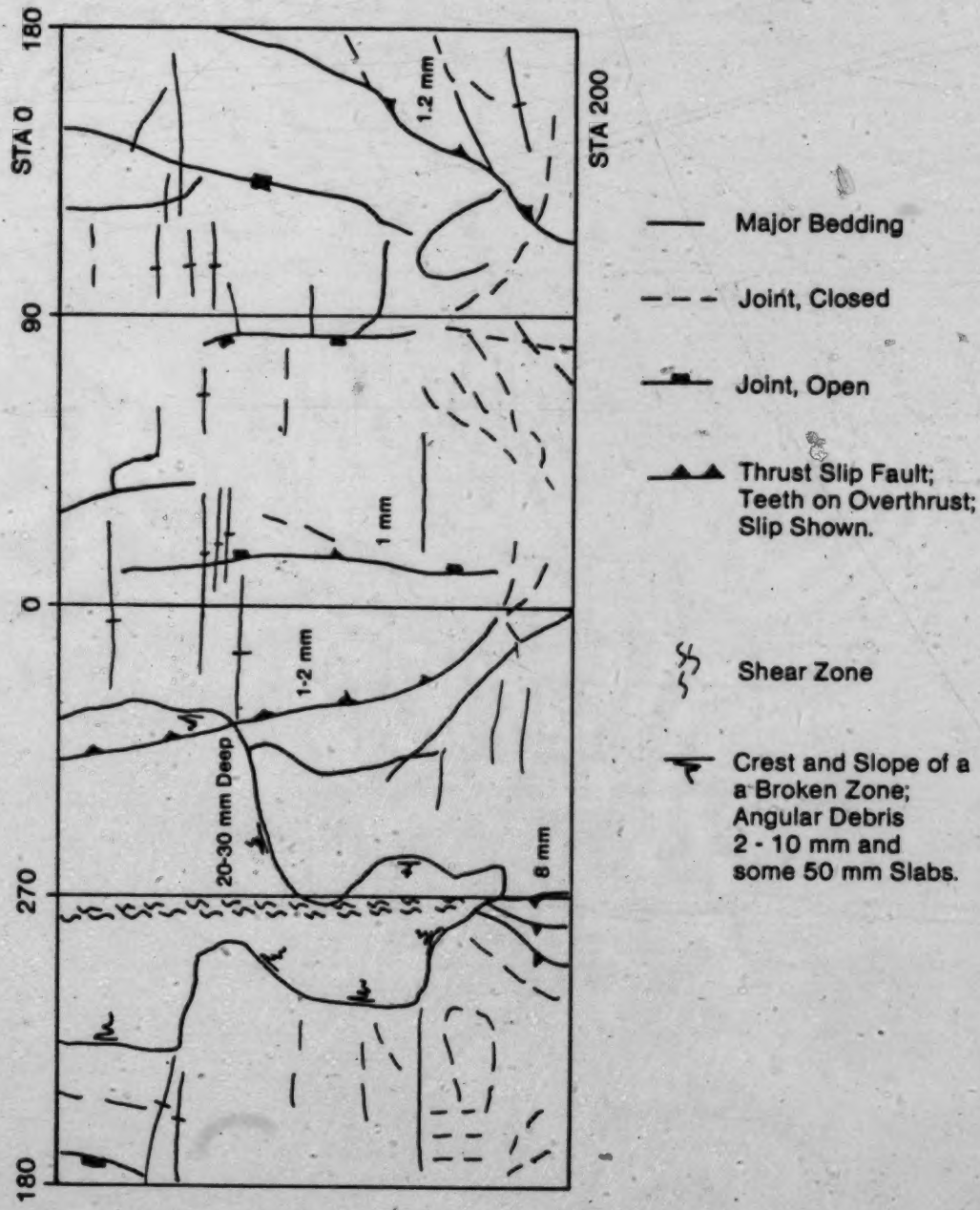

Figure 2.5 Developed Section, 15 cm Diameter Tunnel, After MC 1.19

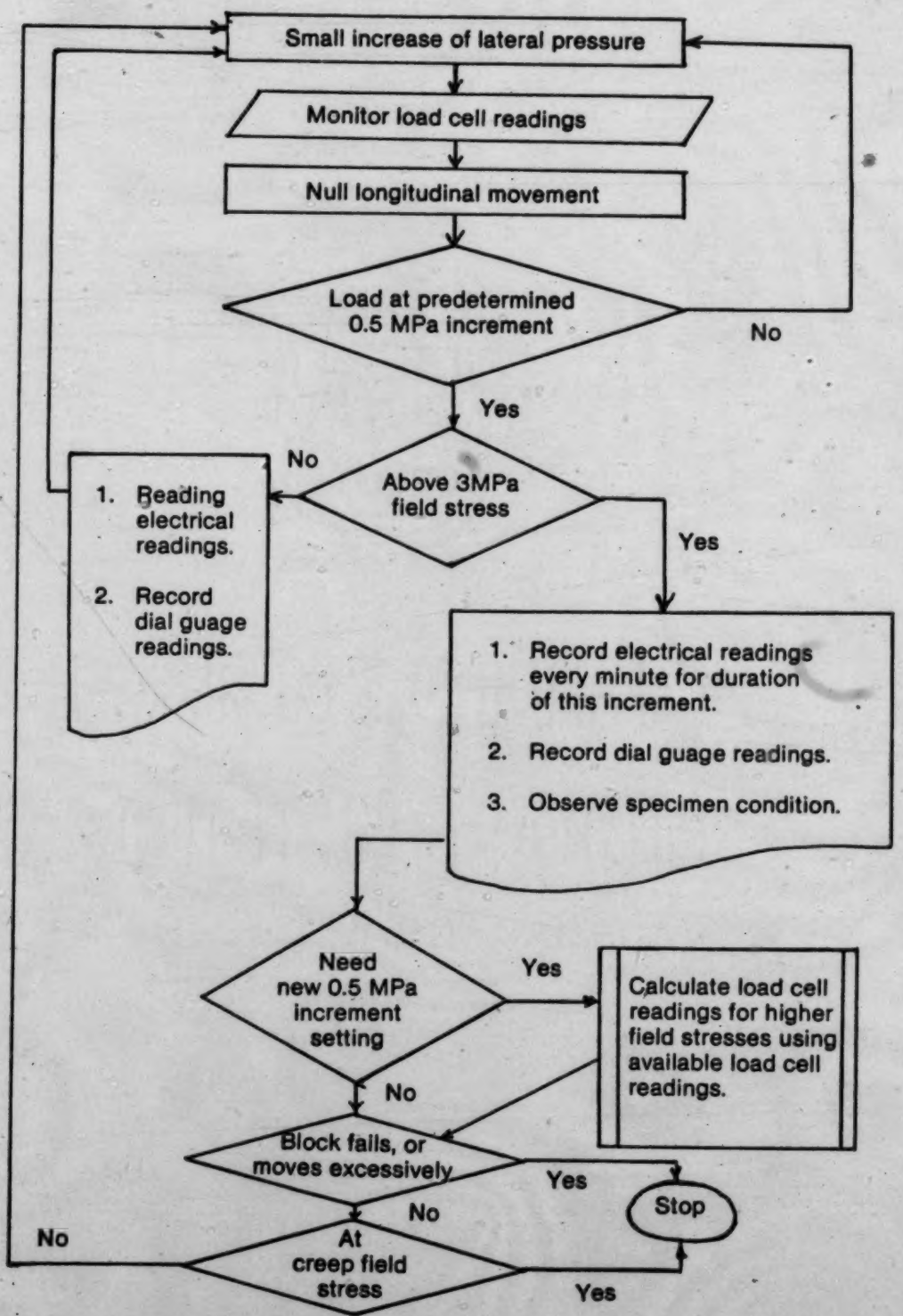

Figure 2.6 Flow Diagram : Increasing Load Procedure.

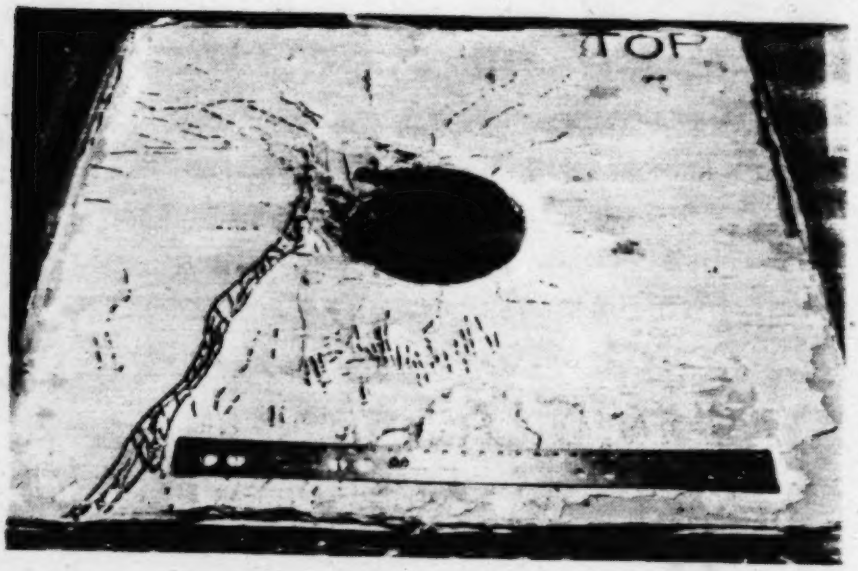

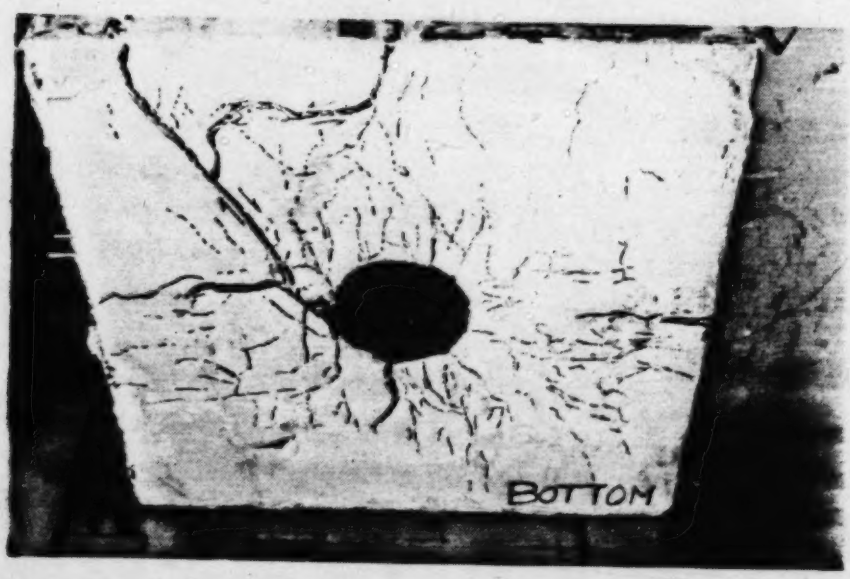

Plate 2.1 Top And Bottom View Of Test Specimen After Testing

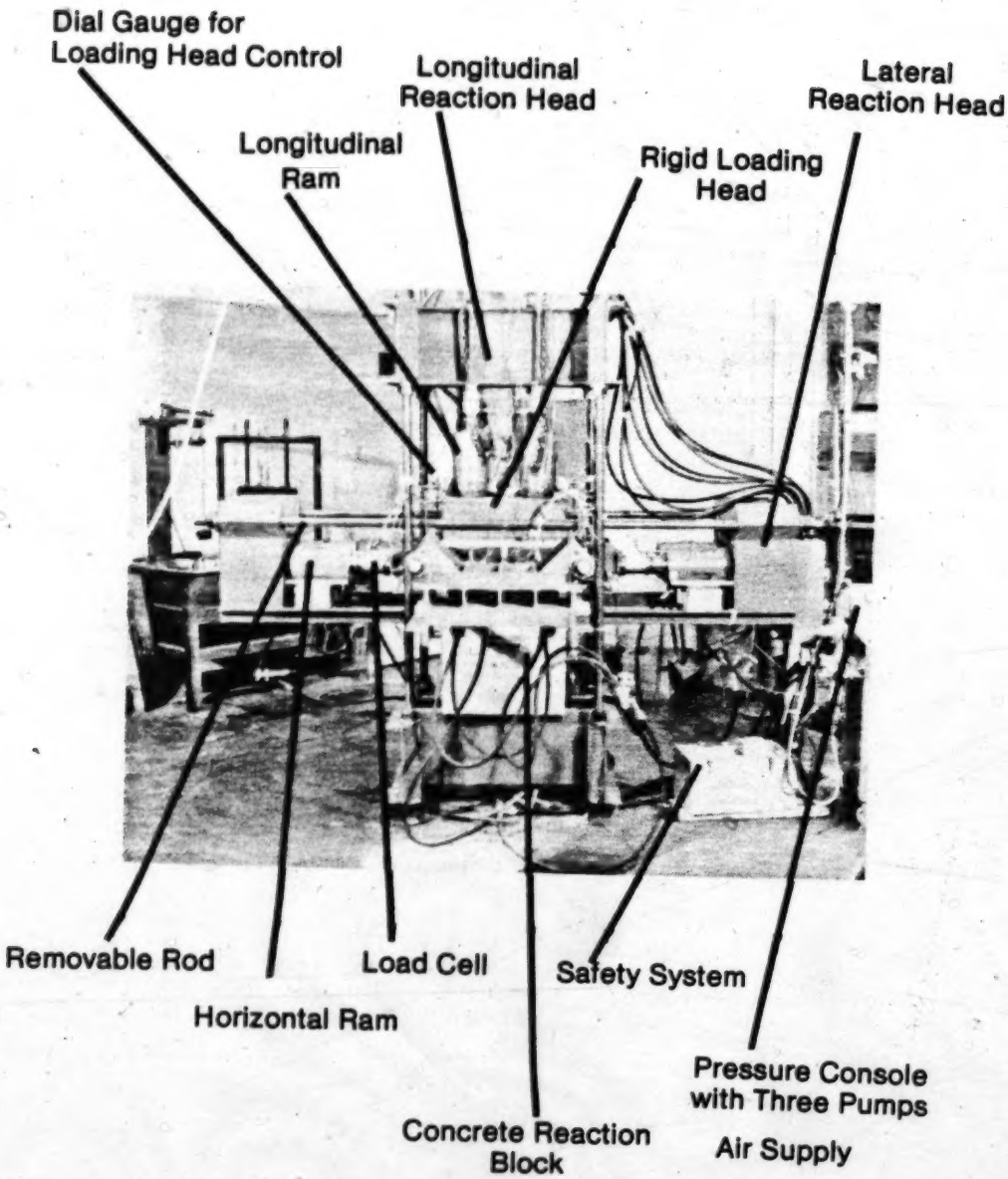

Plate 2.2 Test Machine

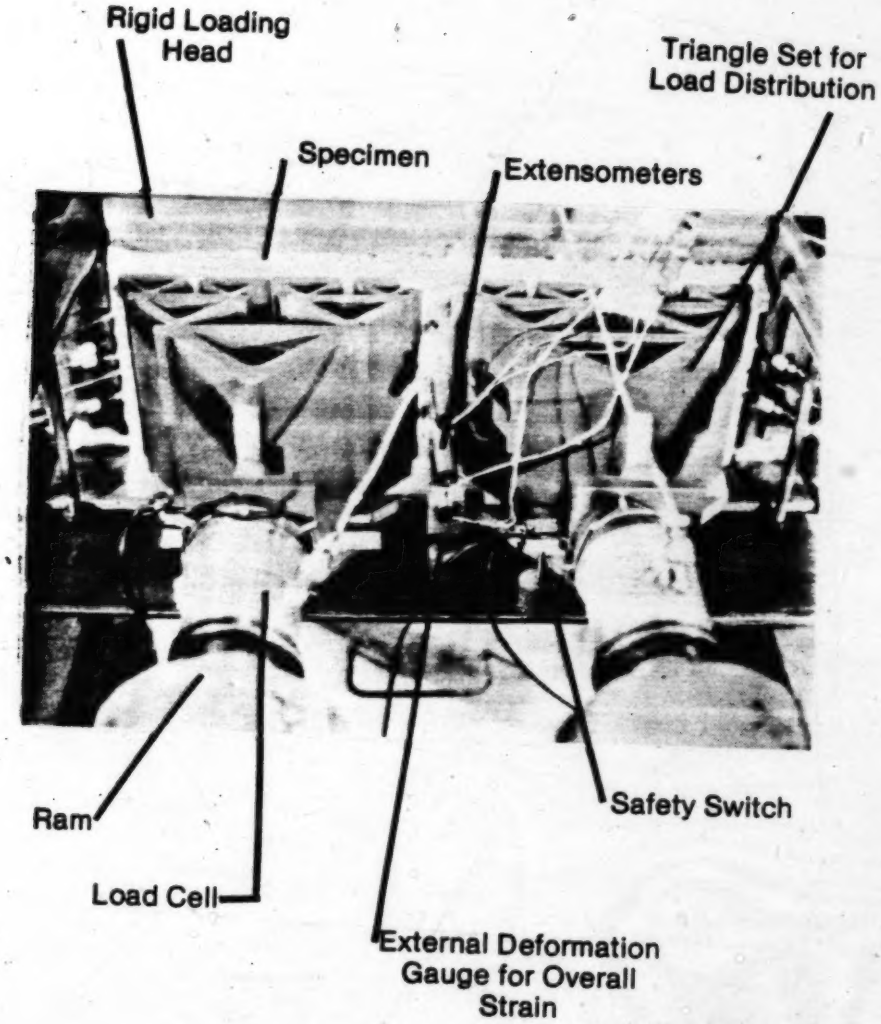

Plate 2.3 Lateral load distribution by set of triangles

3. CHAPTER III

DISCUSSION OF PROCESS SIMULATION TEST (PST) RESULTS

3.1 INTRODUCTION

This testing program was designed to study two aspects, the yielding or failure process and some associated rate effects. Hence, three test objectives were defined,as follows:

1. study the effect of enlarging the tunnel size;
2. study the effect of weakening the rock adjacent to the tunnel, in particular, by creating an "Equivalent Opening" by applying a non-hydrostatic field stress onto the specimen (low confinement test); and
3. study the effect of decreasing the loading rate at the middle of the loading range.

A series of thirteen repeated loading tests have been carried out on one specimen, MC1. The tunnel size was enlarged by 25% during the preliminary tests. Tests with a hydrostatic field stress were carried out before and after each of three tests with a non-hydrostatic field stress to assess the effects of each of the three low confinement tests. Tests with a "Bimodal Loading Rate" were carried out to evaluate loading rate dependency and to further assess the initial low confinement episode. The last test was carried out, after the specimen ruptured during a low confinement test, to provide results for an entirely altered rock mass.

Test observations are described and compared to anticipated behavior, predicted from theoretical formulations and conceptual aspects. Deformational response is predicted assuming linear elasticity and linear visco-elasticity. Stress redistribution is discussed qualitatively. For a specified loading history, the deformation character of a segment of one test may be compared with that in another test, or perhaps, with another segment within the same test. Physical observations of the specimen condition during testing are used to augment interpretations. The observed and theoretical deformation behavior are assumed to be insignificantly affected by the proximity of the specimen boundary to the tunnel. Conclusions are based on test observations.

Section 3.2 establishes some theoretical concepts and terminology needed for discussion of the test results. The effect of the loading history is discussed assuming linear elastic and linear visco-elastic behavior. Stress redistribution mechanisms are reviewed.

Section 3.3 describes the loading history during the test program. The testing procedure and general deformation behavior are characterized. Section 3.4 describes the method of presenting the test results and explains the terminology used.

Sections 3.5 to 3.7 describe the test results in detail; prior to breaking the specimen. Initially, significant observations are summarized. In three

sub-sections, the increasing field stress response and constant field stress response are desribed, then the tunnel closure and radial strain behavior are compared. Physical observations are given to augment understanding of the deformational behavior. Results obtained by Kaiser (1979) and Guenot (1979) are given, when possible, for comparative purposes.

Section 3.8 describes the breaking of the specimen and compares test observations for two different rock masses.

The last section presents conclusions evident from the "Process Simulation Test" (PST) observations.

Tables and figures showing test results are located at the end of the chapter. Details and examples of test results are located in Appendix C. The figures provide an invaluable reference to the description of the test results. A complete record of test curves are summarized in an internal report for this research program at the Department of Civil Engineering, University of Alberta.

3.2 SUMMARY OF ANTICIPATED BEHAVIOR

The PST specimen may be viewed, for purposes of discussion, as a specified, spatial arrangement of small size rock elements. Each rock element responds to the movement of adjacent elements. Moreover, the stress level and stress path vary for each element between the tunnel wall and specimen boundary. Thus, various types of element behavior mechanisms and modes, with time-independent and

time-dependent behavior, combine under given loading conditions to produce a characteristic behavior.

Considering two types of boundary loading conditions, incremental increasing loading and constant load (elevated and zero constant load), simplifies loading path considerations for test interpretation. Specifying the incremental loading procedure with two loading rates, fast and slow, with intervals of constant load between each step, facilitates comparative analysis between tests, albeit, the physical condition of the specimen may differ for each test.

The PST loading path, deviatoric plus isotropic loading, differs substantially from the general field loading path of deviatoric unloading. For a linear system, deviatoric and isotropic components are directly additive. In particular for the PST, the loading path consists of loading a plate and unloading a hole in a prestressed medium (real case). Specifying linearity over limited ranges may approximate non-linearity. For example, several short straight line segments with different slopes approximates a curved line. However, the loading history is assumed not to affect the mechanisms of behavior (Kaiser and Morgenstern, 1981).

The PST rock mass behavior may be characterized according to a classification of types of rock mass behavior that distinguishes between time-independent and time-dependent behavior (Kaiser and Morgenstern, 1981). Evaluation of radial strain results is necessary to identify

the deformation mechanisms (Kaiser, 1979).

3.2.1 LINEAR SYSTEM BEHAVIOR

Linear elastic and linear visco-elastic formulations exhibit time-independent and time-dependent deformational behavior respectively. The closed form solution in terms of the Airy stress function by Kirsch for boundary loading of an infinite isotropic elastic plate with a hole provides the basis for calculating the parameters of interest. The elastic visco-elastic correspondence principle provides a simple procedure for solving the time-dependent formulation (Findlay, 1976). The equations for these formulations are shown in Appendices A1 and A2. The stress distribution as well as the displacement and strain distributions for a homogeneous linear elastic formulation are shown in Figure 3.1. Both formulations predict instantaneous initial behaviour and the linear visco-elastic formulation predicts delayed deformations as a function of the constitutive relations and loading history.

Assuming homogeneous behavior, enlarging the tunnel diameter by 25% changes the stress distribution. The instantaneous and delayed tunnel wall displacements increase by 25%, but tunnel closure remains unchanged since, by definition, it is normalized by tunnel size. In addition, negative radial strain increases by about twice as much in Zone A as compared to Zone B. Tunnel closure exceeds the average specimen strain by about 3 or 4 times.

Assuming linear elastic behavior, tests carried out with a non-hydrostatic field stress create radially symmetric distributions of deviatoric stress level (Figure 3.1b). The loading rate is lower for elements located along the maximum load axis. In addition, the average confinement level is lower since less field stress is applied in the minimum load direction.

Assuming instantaneously fast loading simplifies time-dependent interpretation, and an incremental loading procedure complicates interpretation. Assuming incremental loading of a linear visco-elastic specimen, tests carried out with a "Bimodal Loading Rate" exhibit loading rate and loading history dependent deformation. For example, fast incremental loading produces less tunnel closure than slow loading. According to the Boltzman Superposition Principle, the strain output depends on the incremental stress input. For a Kelvin element, a spring in parallel with a dashpot, the strain is independent of loading history in the long term.

For comparison with test results, Kaiser (1979) used the three parameter linear solid, a spring in series with a Kelvin element, in a linear visco-elastic formulation with different material properties for deviatoric and isotropic stresses. Short retardation time for the deviatoric component and longer retardation time for the isotropic component predicts strain-rate reversals. Some strain-rate results obtained by Kaiser (1979) for a uniform 1 MPa

instantaneous field stress increment are shown in Figure 3.2. Hereafter, this formulation is called a binary visco-elastic formulation. The material properties were selected to produce results comparable with PST observations. The deformation magnitude depends directly on stress increment magnitude and most deformations occur within the first day and tend toward the same compression rate controlled by the isotropic creep parameters (Kaiser, 1979). The strain-rate and rate of decrease of the strain-rate depend on the relative nature of the deviatoric and isotropic creep properties, or conversely, changing the material properties affects the strain behaviour.

3.2.2 STRESS REDISTRIBUTION PROCESSES

Kaiser (1979) used a non-linear, stress dependent bulk modulus and deviatoric creep of a three parameter linear solid in a binary visco-elastic formulation to predict the change in the slope of the average radial strain curve in the low field stress range. Assuming the bulk modulus increases with stress, the strain distribution changes from compression at low field stress toward extension at higher field stresses.

Kaiser (1979) developed the "Equivalent Opening Approach" (EOA) to describe PST results and to qualitatively evaluate practical implications of stress redistribution. The equivalent opening is an opening in a linear elastic medium whose wall displacements correspond at a particular

instant to the wall displacement pattern observed in the real opening (Kaiser, 1979). Hence, the "EOA" represents an approximation of a non-linear system by assuming a linear system, and provides a method for practical interpretation of the deformation mechanism, .eg., to develop appropriate instrumentation systems, excavation layouts and support systems.

Several factors may control stress redistribution in the PST, as follows (Kaiser, 1979):

1. Non-linear, stress dependent creep properties;
2. Anisotropic creep properties;
3. Asymmetric creep property distributions;
4. Yielding, local and global;
5. Strength loss and strain-weakening.

Analysing some of Guenot's (1979) test data, da Foutoura (1980) illustrated quite clearly the mechanism of stress transfer due to creep. Kaiser (1979) used an EOA to illustrate the time-dependent stress redistribution. In particular, as the EO expands the radial strain rate changes toward more extension. This change is comparable to the difference between a strain rate curve for R=2a as compared to R=1.5a for example, as shown in Figure 3.2.

3.3 SUMMARY OF THE TESTING PROGRAM

For purposes of detailed discussion, the testing program is described in four sections, sections 3.5 to 3.8, defined according to the loading history during a test.

Details of testing, including testing difficulties, are shown on Table C1-1 in Appendix C1. The deformational response during a test depends on the loading history, hence specifying the loading history for the specimen facilitates comparison of deformational behavior.

A summary of the boundary loading and tunnel closure history is shown in Figure 3.3. The lower part of Figure 3.3 shows accumulated tunnel closure with time, beginning with test MC1.8. The upper part of Figure 3.3 shows the vertical field stress or boundary normal stress, the field stress ratio "N" and the field stress loading rate for each test. Field stress ratio "N" is defined as the ratio of the field stress for the 90-270 diameter axis, the horizontal direction, to that for the 0-180 diameter axis, the vertical direction. A numerical field stress ratio is shown for tests differing substantially from unity, .eg., tests with a "non-hydrostatic" field stress. Test numbers increase sequentially with time, for example MC1.9 then MC1.10; and "MC" stands for coal specimen, "1" for specimen number and ".10" for test number. The testing history reported herein begins with test MC1.7 and finishes with test MC1.19.

In summary, the loading procedures for a test include incremental increasing, decremental reducing and constant field stress (elevated or zero). Each test finishes by reducing the field stress to zero and allowing most delayed deformations to terminate.

Preliminary tests MC1.7 and MC1.8 were carried out in a

similar manner. Test MC1.7 is not shown in Figure 3.3 because the tunnel diameter differs from all other tests. To study the effect of increasing the tunnel diameter by 25%, the specimen was tested on each occasion by rapidly increasing the field stress to 10 MPa; reducing to approximately 5 MPa and increasing to 10 MPa again; and then maintaining constant field stress for one day before finishing the test. However, the field stress ratio differed from unity during test MC1.7, N=1.3. The average increasing loading rate was 6 to 10 MPa per hour for test MC1.7 and 9.5 MPa per hour for test MC1.8.

A "Non-hydrostatic Episode" consists of three consecutive tests, the first and last test being conducted under hydrostatic field stress, the second test being conducted under a short-term non-hydrostatic field stress. The tests with non-hydrostatic field stress were carried out by rapidly increasing the field stress to machine capacity with a field stress ratio considerably less than unity, then quickly unloading to zero field stress. To evaluate the effect of the short-term test, a test with hydrostatic field stress were carried out, before and after each short-term test, by rapidly increasing field stress to machine capacity; and maintaining constant field stress for two to four days before finishing the test. For these tests, the field stress ratio was typically 5-10% greater than unity (Figure 3.3).

Three "Non-hydrostatic Episodes" were carried out. The

earliest episode, MC1.10-.11-.12, and the second episode, MC1.15-.16-.17, were done on the specimen prior to excessive failure. During the third episode, MC1.17-.18-.19, the specimen broke considerably under non-hydrostatic field stress. The field stress ratio and loading rate for each test is shown in Figure 3.3.

Two tests with a "Bimodal Loading Rate", MC1.9 and MC1.14, were carried out before and after the earliest "Non-hydrostatic Episode". This test was conducted by rapidly increasing field stress to 10 MPa and maintaining constant load for one day; then rapidly increasing the field stress by 1 MPa increments and maintaining constant load for one day intervals at 11, 12, and 13 MPa respectively. Thus, after the 10 MPa field stress, the average incremental loading rate was decreased by two orders of magnitude. Then, after one day at 13 MPa, the field stress was quickly reduced to 10 MPa and held for one day before rapidly increasing it again to 13 MPa and maintaining constant field stress for one day. Thus, a cycled loading sequence is included in the loading history. Thereafter, the field stress was rapidly increased to 14 MPa and maintained for one day; then increased to machine capacity, 14.5 - 15 MPa, and held for four of five days before finishing the test. The field stress ratio for MC1.9, approximately 0.95 during the initial loading to 10 MPa, was adjusted toward unity during the 10 MPa constant field stress interval. Between each test, the average field stress ratio differed by

approximately 10% and the average loading rate differed by about 2 MPa per hour (Figure 3.3).

Routine visual inspection of the specimen during the testing program served to locate specific phenomena which were then followed during subsequent tests. Thourough inspection was difficult since the specimen was nearly closed in by the testing machine but a large portion of the tunnel wall was visible during testing. Physical change of the specimen seemed to be more pronounced during the latter part of testing, if only because more emphasis was placed on recording physical change in the latter part of the testing program.

Although changes in deformational behavior occur during the testing program, some typical deformations recur. For example, stress-strain curves are generally non-linear over the full range of field stress, particularly at low values, and frequently linear over specified ranges. Delayed tunnel closure and boundary displacement rates decrease with time, however radial strain rates typically change from extension to compression with time. The tunnel closure and radial strain pattern is asymmetric during hydrostatic field stress tests and radially symmetric during non-hydrostatic field stress tests. The radial strain measurements are plotted at a scale approximately one order of magnitude smaller than that for tunnel closures. Partly irrecoverable tunnel closure and radial strain persist after finishing a test (Figure 3.3).

3.4 DESCRIPTION OF THE PRESENTATION OF TEST RESULTS

Discussion of the testing results is presented with reference to three types of figures showing test results. "Apparent deformation moduli" are calculated using selected tunnel closure measurements and some average specimen strain measurements in the closed form linear elastic formulation shown in Appendix A1. They are presented in a normalized fashion to provide quantified results for discussion of tunnel behavior and rock mass behavior in general. Secondly, selected tunnel closure measurements, taken from stress closure curves and closure-rate-time curves, are also presented in a normalized fashion for discussion purposes. Finally, plots of tunnel closure, average specimen strain and average radial strain are presented in summary diagrams to provide a reference for qualitative discussion of rock mass behavior.

The tunnel closure measurements and average specimen strain mesurements, used in the linear elastic formulation and in normalized comparisons, were obtained by approximating test results with a straight line. On the stress closure curves, four types of straight line slope segments were specified for increasing loading paths as follows:

1. Average - average slope between 4 and 10 MPa;
2. Tangent - tangent slope at 10 MPa;
3. Fast Reload - average slope for increasing loading portion of the cycled loading history at elevated field

pressure during one test;

4. Slow - average slope for slow loading through the 11 to 13 MPa field stress range, "Bimodal Loading Rate" tests only.

On the double logarithmic closure rate versus time curves, closure rate parameters are defined for a straight line approximation of the test curves. The geometric straight line slope is defined as parameter "n". It represents the rate of decrease of closure-rate with time. The logarithmic value of closure-rate at one hour is defined as parameter "b". It represents the potential for closure. For the purposes of discussion, it is important to realize that a decrease in the value of the "b" parameter actually represents an increase in the potential for closure, since closure rates reported here are less than unity. Sample calculations of the linearization technique and the apparent deformation modulus are shown in Figure C3-1.

Significant relationships and trends are discussed with reference to summary plots of stress-strain and strain-rate-time. Quantitative evaluation of radial strain trends is complicated by variations in measurements, hence radial strain trends are discussed qualitatively only. For brevity, strain-time plots are seldom presented. However, strain-rate-time plots, statistically evaluated using strain-time data, represent the character of the strain-time plot and facilitate comparison between various constant load intervals. Working drawings showing both stress-strain and

strain-rate-time curves were studied and then some test results were selected for presentation.

Figures 3.9 to 3.14 summarize the stress-strain results for specimen MC1. In these figures, field stress is shown along the ordinate, at one scale, and either tunnel closure, average specimen strain or average radial strain is shown along the abscissa, at various scales. The initial strain for each test is marked by a vertical line and the test number together with field stress ratio are shown above the curves for each test (test MC1.7 not shown). The displacement or strain monitor location is schematically shown in an inset sketch. Stress-strain curves are shown for Zone A extensometers in Figures 3.11 and 3.12 and for Zone B extensometers in Figures 3.13 and 3.14.

Figures 3.15 to 3.17 summarize the selected strain-rate-time results. Voluminous results were obtained at constant field stresses but they are not included here. All summary figures have been traced by hand from computer generated plots, examples of which are shown in Appendix C4.

3.5 PRELIMINARY TESTS, MC1.7 and MC1.8

Increasing the tunnel diameter by 25% creates greater short-term delayed tunnel closure and a correspondingly reduced apparent deformation modulus. Moreover, linear theoretical formulations fail to predict the observed tunnel closure response. Thus, the delayed tunnel closure behavior depends on the tunnel size.

As anticipated, radial strain measurements, during both incremental increasing and constant field stress, exhibit greater extension behavior after increasing the tunnel size since now the extensometers are located nearer the tunnel wall. However, radial strain depends on location (Figure 3.1a). The rock mass changes with location, therefore inappropriately complex analysis would be necessary to evaluate the radial strain results in detail.

3.5.1 INCREASING FIELD STRESS RESPONSE

The average apparent deformation modulus for test MC1.7 predicts only 90% of the tunnel closure for test MC1.8. Thus, the average apparent deformation modulus decreases after enlarging the tunnel (Figure 3.4). Figure 3.4 shows a plot of the average apparent deformation moduli derived by averaging the apparent deformation moduli calculated for the four tunnel diameters, and normalizing the average to one test, MC1.10. Figures C5-1 to C5-8 in Appendix C5 show the apparent deformation moduli and the tunnel closure for each diameter on two types of normalized plots. In one type of plot, moduli and tunnel closure measurements are normalized to one test, test MC1.10. In the other type of plot, moduli and tunnel closure measurements are normalized to one diameter, the 0-180 diameter. Comparing the apparent deformation moduli for tests MC1.7 and MC1.8, the least change occurs along the 45-225 diameter (Figure C5-1).

Apparent deformation moduli differ significantly

between each diameter, especially for test MC1.7, as shown in Figure C5-4. Actually, in this figure, two of the moduli are off scale. The tunnel closure measurements vary only slightly between each diameter. Thus, the linear elastic formulation inconsistently represents tunnel closure response. The non-hydrostatic field stress ratio in test MC1.7, N=1.3, complicates direct comparison of preliminary test results. However, the less field stress dependent diagonal diameter tunnel closures increase by 10%-30% after enlarging the tunnel size (Figure C5-3).

The stress versus closure plots are similar for the preliminary tests. Appendix C4 contains the field stress versus tunnel closure results and some of the field stress versus radial strain results for these tests. For test MC1.8, the stress-closure curves for the 0-180 and 135-315 diameters exhibit very slight yielding at elevated field stress. Both tests exhibit a greater fast reload stiffness as compared to the initial loading stiffness. After unloading, tunnel closure recovers incompletely, however due to difficulties during test MC1.8, not all of the recovery results are available.

Comparing average radial strain results for both tests, test MC1.8 exhibits more extension at low field stress and especially at elevated field stress (Appendix C4). Comparing average radial strain in both Zones A and B for test MC1.8, zone A exhibits a greater change than predicted by a linear elastic formulation. Generally, the observed

radial strain response is consistent with linear predictions, however, stress dependent material properties preclude quantitative evaluation.

The average radial strain response varies asymmetrically around the tunnel due to defects inside the specimen. For example, the fracture, straddled by the 225 radius extensometer in Zone B, causes substantially more crack closure radial strain as compared to other locations (Figures C4-1 and C4-2). Superposition of fracture and continuum deformation modes contributes to the asymmetric radial strain distribution. Thus, knowledge of the rock mass condition in the vicinity of the extensometer is necessary for accurate interpretation of the strain results.

The average specimen strain, approximately one-quarter of the tunnel closure, increases after enlarging the tunnel. This is consistent with the linear elastic prediction.

Boundary effects insignificantly influence the results. Assuming linear elastic behavior, increasing the hypothetical specimen size in proportion to the change in the tunnel size affects boundary displacement by less than 1%.

3.5.2 CONSTANT FIELD STRESS RESPONSE

The closure rate parameters, b and n, together with the total delayed closure change by 15-20% after enlarging the tunnel (Figure 3.6). The "b" parameter decreases and the "n" parameter increases together with the total delayed

closure. Figure 3.6 shows the average closure rate parameters for each test normalized to one test, MC1.10. Comparison of the delayed tunnel closure shown in Figures C4-3 and C4-4 illustrates the increase in total delayed tunnel closure for the larger tunnel. The change in the closure rate parameters suggests delayed tunnel closure occurs more rapidly and also terminates more rapidly, thus effectively becoming a short-term phenomenon. Thus, an increased amount of short-term delayed tunnel closure corresponds with a lower apparent deformation modulus. However, linear visco-elasticity predicts no change in tunnel closure response after increasing the tunnel size.

Comparison of the radial strain time plots for both tests, shown in Figures C4-3 and C4-4, shows the increase in the amount of extension strain after increasing the tunnel size. This change is consistent with the anticipated variation of delayed radial strain for different distances from the tunnel, as illustrated in Figure 3.2 for the binary visco-elastic formulation.

During delayed recovery of test MC1.7, extension strains occur in zone A and zone B, changing to compression in zone A after 50 to 70 hours. No recovery results are available for test MC1.8.

The delayed tunnel closure rate parameter "b" exceeds the comparable boundary displacement parameter by approximately one-half order of magnitude. Non-hydrostatic field stress during test MC1.7 and testing problems during

test MC1.8 complicate comparisons, however the observed behavior is consistent with predictions assuming linear visco-elasticity.

3.5.3 COMPARISON OF TUNNEL CLOSURE AND RADIAL STRAIN RESPONSE

Increased tunnel closure and extension radial strain occur after enlarging the tunnel size, for both incremental increasing and constant field stress. Although ambiguity exists about radial strain interpretation, to a first approximation, linear theoretical formulations predict the observed radial strain observations. However, linear theoretical formulations fail to predict the increased tunnel closure.

The coal material exhibits a non-linear, stress dependent creep response (da Fontoura,1980). The effect of increasing the tunnel diameter in this type of material is not readily apparent.

The difference in loading rates between each test inconsistently explains increased tunnel closure. Assuming linear material properties,for a faster loading rate, greater delayed tunnel closure would occur, perhaps comparable to results for test MC1.8. However, a greater closure stiffness would be expected, contrary to test observations.

Local rupture of the tunnel wall and the associated stress redistribution insignificantly affect response in

either test. Local rupture initially occurred during test MC1.9, at 12 MPa field stress.

Testing prior to enlarging the tunnel size complicates interpretation. If an EO were created prior to test MC1.8; the change in tunnel closure after enlarging the tunnel size may conservatively represent this "size effect". As will be discussed next, development of an EO creates a "softened" or "weakened" zone adjacent to the tunnel. Increasing the tunnel size removes some of this zone and exposes a larger volume of rock to deviatoric stress. Then, due to stress concentrations near the tunnel, time-dependent deformation would increase, perhaps comparable to test results.

3.6 NON-HYDROSTATIC EPISODES, MC1.10-11-12 AND MC1.15-16-17

The deformation response changes significantly during the earlier "Non-hydrostatic Episode", MC1.10-11-12, more so than during the later episode. In particular, during incremental loading, tunnel closure increases and coincidently, during constant field stress, tunnel closure rate parameter n decreases and parameter b increases. Also, more extension radial strain occurs further away from the tunnel, inside the rock mass. However, linear elastic formulations predict comparable response for both hydrostatic field stress tests, MC1.10 and MC1.12.

Stress redistribution mechanisms are required to explain test observations. In particular, an EO, of about 125% to 135% of the initial tunnel size, is created under

the short-term non-hydrostatic field stress. Thus the size of the time-independent EO increases. The propensity for delayed closure and the rate of decrease of the delayed closure decrease slightly. Thereafter, proportionally greater tunnel closure occurs together with correspondingly greater extension strain away from the tunnel wall.

3.6.1 INCREASING FIELD STRESS RESPONSE

Average apparent elastic deformation moduli, derived from tests prior to test MC1.11, exceed those for subsequent tests by approximately 25%-35% (Figure 3.4). Also, tunnel closure measurements differ for each diameter, especially after the initial low confinement episode. However, during the latter part of testing, they correspond between diameters (Figures C5-1 and C5-3). Figure 3.4 also illustrates the insignificant change in apparent deformation properties during tests MC1.15-.16-.17. So, the first test with non-hydrostatic field stress creates an increased amount of tunnel closure during subsequent tests, plus to a lesser degree, influences the closure symmetry. Therefore, test MC1.11 evidently creates a non-circular shaped EO, about 125-135% larger than the initial tunnel size. The second episode inappreciably influences tunnel response. The mechanisms altering tunnel response during the first episode do not prevail during the second episode.

Stress redistribution occurring after test MC1.11 and a comparatively larger confinement reduction between tests

MC1.10 and MC1.11, as compared to between tests MC1.11 and MC1.16, may explain the relatively insignificant response alteration during the later episode. The "Equivalent Opening" created during test MC1.11 redistributes stress into higher confinement zones, away from the tunnel. Yielding would be anticipated only after stress concentrations exceed values previously experienced by the specimen. Although, the field stress ratio "N" in test MC1.11 is nearer unity than in test MC1.16, the magnitude of the change of "N" between tests MC1.10 and MC1.11 exceeds that between tests MC1.11 and MC1.16 by approximately twice (.ie., 1 to 0.6 as compared to 0.6 to 0.4). Also, proximity of the specimen boundaries may subdue the strain response in test MC1.16 as more extension strain occurs further from the tunnel. Finally, higher confinement away from the tunnel may inhibit expansion of an equivalent opening.

Apparent deformation moduli exhibit radial symmetry during tests with a non-hydrostatic field stress. In test MC1.11, apparent deformation moduli, obtained from measurements in test MC1.10, under-estimate tunnel closure by 10% for the maximum load axis and by 25% for the diagonal diameters; and over-estimate tunnel closure by 60% for the minimum load axis.

The radial strain distribution also exhibits radial symmetry during non-hydrostatic field stress tests. Radial strains respond primarily along principal axes with more compression along the 0-180 axis and more extension along

the 90-270 axis (Figures 3.11 to 3.14). Radial strains respond moreso in zone A than in zone B and, in zone B, moreso along the 90-270 diameter than the 0-180 diameter. Thus, the observed radial strain pattern is consistent with the anticipated behavior assuming a linear elastic material, however discrepancies exist. For example, the magnitude of response varies between comparable diagonal locations. These results illustrate the influence of the local rock mass conditions on the radial strain behavior.

The tunnel closure pattern changes slightly after test MC1.12 (Figure C5-1). An elliptical closure pattern occurs during test MC1.11, and upon hydrostatic loading during test MC1.12, greater tunnel closures occur along the 90-270 diameter. During the first "Non-hydrostatic Episode", the apparent deformation modulus changes by approximately 10% for the 0-180 diameter as compared to 25% for the 90-270 diameter (Figure C5-1). Subsequently, in tests after test MC1.12, the apparent deformation modulus for the 0-180 diameter continually decreases, while remaining approximately constant for the 90-270 diameter (Figure C5-1). Indeed, a field stress ratio of 5-10% above unity could cause the radially symmetric closure pattern, particularly since the rock mass exhibits stress dependent deformation properties. Non-uniform field stress during the earlier tests, shown in plots of boundary stress variation in Appendix C2, precludes detailed study of the variation of closure patterns. However, field stress varies

non-uniformily during the later tests, but tunnel closures vary only slightly. Thus, the tunnel closure pattern becomes more axi-symmetric.

During the test program, the radial strain distribution indicates that stress transfer occurs as more compression strain occurs in zone A and more extension strain occurs in zone B. However, the magnitude of this alteration is greatest after a test with a non-hydrostatic field stress. Comparison of the average stress-strain curves for each test, shown in Figure 3.10, illustrates the change in average radial strain behavior during the test program. Stress-strain curves for tests during a "Non-hydrostatic Episode" differ significantly (Figures 3.11 to 3.14). In particular, note the change in the shape of the stress-strain curves for zone A and zone B during tests MC1.10-1.11-1.12. Comparing curves for tests MC1.10 and MC1.12, generally more compression occurs in zone A and more extension in zone B in test MC1.12. This behavior is not so evident for tests MC1.15-16-17. In particular, no change or slight compression occurs in zone A, and either more compression or more extension occurs in zone B (Figures 3.11 to 3.14). This alteration of radial strain is consistent with stress redistribution away from the tunnel.

After unloading, irrecoverable tunnel closure and radial strain remain after tests with either hydrostatic or non-hydrostatic field stress. Less than 0.4% irrecoverable tunnel closure remains after tests during the initial

"Non-hydrostatic Episode" (Figure 3.3). During the later episode, irrecoverable tunnel closure varies between zero and 1%. However, irrecoverable closure for specimen MC4 near failure, given by Guenot (1979), exceeds that for specimen MC1. Comparing curves presented in Figures 3.11 to 3.14, the magnitude of irrecoverable strain varies, but it is usually less than 0.05%. Irrecoverable strain for specimen MC4 near failure, given by Guenot (1979),exceeds that for specimen MC1 by approximately one-half order of magnitude. Thus, comparatively minor inelastic behavior occurs in the MC1 specimen.

3.6.2 CONSTANT FIELD STRESS RESPONSE

Tunnel closure rate parameters, b and n, increase and decrease respectively by 5-10% while radial strain rate exhibits slightly more extension after a test with non-hydrostatic field stress, especially in zone B during the first episode. Figure 3.6, a normalized comparison of the average closure rate parameters, illustrates the change in closure rate parameters. Closure rate parameters are not shown for test MC1.11 since no constant elevated field stress was not applied. Figure 3.15, showing the tunnel closure rate and radial strain rate curves for tests MC1.10 and MC1.12, qualitatively illustrates the change in strain rate behavior. In particular, the curve shape differs after test MC1.11. Also, the closure-rate curves for test MC1.12 are slightly non-linear as compared to those for test

MC1.10. Radial strain rate behavior differs slightly prior to each low confinement test, that is,more compression strain rates occur during test MC1.15 as compared to test MC1.10. However, after both low confinement tests, radial strain rate behavior changes slightly toward more extension, especially in zone B.

The time dependent behavior of a low confinement episode is different from the effect of enlarging the tunnel size. Compared to the preliminary tests, the delayed tunnel closure apparently tends toward a more long-term, lower potential behavior.

Assuming a binary visco-elastic specimen, the difference in loading rates for tests MC1.10 and MC1.12, 6 as compared to 4 MPa per hour, could cause greater tunnel closure for slower incremental loading with a corresponding decrease of the closure rate parameters, perhaps comparable with test observations. However, as will be explained later with reference to test results, more compression radial strain occurs after faster incremental loading, contrary to observations for zone B shown in Figure 3.15. Thus, a loading rate difference inconclusively explains delayed deformation behavior.

Also, after test MC1.11, the recovery closure rate parameters, b and n, respectively increase and decrease slightly and radial strain rate behavior exhibits slightly greater compression. No response changes occur during tests MC1.15-16-17. This behavior indicates that a response

alteration occurs after test MC1.11, comparable with the elevated field stress response alteration. However, interpretation of the recovery results is complicated since delayed response depends on the unloading procedure, and unloading procedures vary between tests moreso than the loading procedure.

3.6.3 COMPARISON OF THE TUNNEL CLOSURE AND RADIAL STRAIN

Generally lower confinement together with radially symmetric stress and loading rate concentrations combine to produce an alteration of the apparent deformation properties during test MC1.11. Also, the radial strain behavior changes, Zone A exhibits more compression and Zone B exhibits more extension. However, the delayed tunnel closure and radial strain behavior change only slightly during the "Non-hydrostatic Episode". Thus, a "softened" or "weakened" zone is created adjacent to the tunnel which tansfers stress further inside the rock mass.

A radially symmetric tunnel closure pattern during test MC1.12 indicates that an elliptical Equivalent Opening is developed during test MC1.11. The major axis of this EO is orientated parallel to the 0-180 diameter, the minimum closure diameter. Assuming linear elastic properties and $N<1$, maximum tangential stress and loading rate occur along the 90-270 axis, the minimum load (horizontal) axis (Figure 3.1b). Further, if higher stress causes yielding of elements along the 90-270 axis, an elliptical EO oriented

opposite to the observed behavior would be anticipated (.ie., the major axis orientated parallel to the 90-180 diameter). Hence, upon reloading during test MC1.12, maximum closure of this elliptical opening would occur along the 0-180 diameter, contrary to the observed behavior. Therefore, an elliptical EO is apparently developed due to lower stress levels which leads to "softening" or "weakening" of the rock mass near the tunnel and along the 0-180 diameter.

Several radial strain measurements and physical observations indicate that considering only tunnel closure in analysis of PST results leads to a misinterpretation of the mechanisms of behavior. Firstly, comparison of radial strain curves for the 45 and 225 radii, shown in Figures 3.5 and 3.7, illustrates the variation in radial strain along one diameter during different tests. However, the tunnel closure curves are comparable in both tests for the 45-225 diameter, shown in Figure 3.12. Secondly, after test MC1.11, the radial strain response along the 270 radius in zone A, shown in Figure 3.11, differs from other measurements along the horizontal axis. During rupture of the specimen, a broken zone was created at this location in zone A (Figures 2.4 & 2.5). Indeed, comparatively higher deformations in zone A along the 270 radius, may have caused larger tunnel closures, thus indicating an elliptical shaped EO as previously discussed. As well, the fracture, located as shown in Figure 2.1 concentrates stresses between the

tunnel wall and the fracture plane, thereby excessively loading these rock elements. Thus, the radial strain distribution varies between different locations around the tunnel.

Moreover, local variations in the radial strain measurements indicates local "softening" or "weakening" of the rock mass. Therefore, development of an asymmetrical EO seems most likely.

Examination of PST results brought Kaiser (1979) to postulate that tunnel closure represents an overall rock mass response and radial strain responds to local creep and yield (.ie., to the processes of deformation). Also, anisotropic tunnel closure may be due to an asymmetric creep property distribution, and, moreover, this asymmetry causes radial strain in other locations (Kaiser, 1979).

Comparison of tunnel closure and radial strain for MC1 indicates that tunnel closure represents an average response. Also, the local rock mass conditions, particularily an asymmetric property distribution, influence the PST performance.

3.7 BIMODAL LOADING RATE TESTS, MC1.9 AND MC1.14

The PST specimen exhibits loading rate dependent tunnel closure and radial strain behavior. As the loading rate decreases, larger tunnel closures occur, thus the size of this EO increases. This change in the EO size is called a delayed EO. In detail, time-dependent tunnel closure

results generally depend on loading history, in particular, on the magnitude of the field stress increment, field stress magnitude and stress path. Radial strain rate behavior may also exhibit stress path and field stress magnitude dependency. Therefore, when evaluating deformation behavior, loading history must be considered. A binary visco-elastic formulation could predict loading rate dependent behavior, but would fail to predict field stress magnitude and stress path dependency.

Time-dependent behavior differs between tests MC1.9 and MC1.14, due to the "Non-hydrostatic Episode" carried out between these tests. In particular, upon reducing the loading rate in test MC1.14, the change in the size of the delayed EO is smaller than in test MC1.9. A binary visco-elastic formulation fails to predict this alteration of time-dependent behavior.

3.7.1 INCREASING FIELD STRESS RESPONSE

Slow loading allows greater time-dependent tunnel closure thus the apparent deformation modulus is lower for slow loading as compared to fast loading. Tunnel closure curves for tests MC1.9 and MC1.14, presented in Figure 3.9, and the slope calculation procedure, presented in Figure C3-1a, illustrate the effect of reducing the loading rate at 10 MPa field stress. In terms of the EOA, reducing the loading rate allows the size of the delayed EO to increase.

Typically, slightly greater total compressive radial

strain occurs during the slow loading procedure as compared to the fast loading procedure. Radial strain curves presented in Figures 3.11 to 3.14 show an increased amount of compression for tests with a "Bimodal Loading Rate" as compared to rapid loading to machine capacity. For example, compare curves for tests MC1.9 and MC1.14; in particular, note the trend change at 10 MPa. Also, approximately two times more irrecoverable compressive radial strain persists after a test with a "Bimodal Loading Rate" as compared to rapid loading to machine capacity. A binary visco-elastic formulation could approximate the increased compressive strain during slow loading. However, the increased total compression strain at elevated field stress together with proportionally larger irrecoverable strain indicates that the specimen compacts slightly under sustained and variable elevated field stress, thus violating elastic theory.

The apparent deformation modulus differs for the two tests with a "Bimodal Loading Rate" due to the non-hydrostatic field stress episode. Figure 3.5, showing the ratio of the apparent deformation moduli of each diameter for test MC1.14 to that for test MC1.9, illustrates the difference between the tests. The fast reloading moduli show the greatest mean alteration, about 35%, while the slow loading moduli show the least mean alteration, about 25% (Figure 3.5). The tunnel closure and apparent deformation moduli vary for each diameter (Figures C5-4 and C5-6). The least alteration of apparent deformation moduli occurs along

the 90-270 diameter (Figure 3.5). Comparing the two tests, a smaller difference exists between the fast and slow moduli in test MC1.14 (Figure 3.5). Therefore, the effect of the loading rate change is less significant after the low confinement episode. In particular, the delayed EO expands by 24% in test MC1.9 as compared to only 14% in test MC1.14. Thus, the delayed EO depends on loading history.

The average radial strain behavior differs significantly between test MC1.9 and test MC1.14, particularly in zone B. Comparison of strain curves for tests MC1.9 and MC1.14, presented in Figures 3.11 to 3.14, illustrates this difference. The largest amount of compressive strain at elevated field stress occurs during test MC1.9, in particular, in zone B. The least compressive strain response due to loading rate change occurs in zone A during test MC1.14. Thus, the least delayed radial strains occur in Zone A after the low confinement test.

In general, the asymmetrical radial strain distribution around the tunnel may be attributed to the superposition of non-linear response due to the crack closure at low field stress; and the deformation mechanism causing alteration of deformation behavior. The radial strain curve for the 225 radius in zone B, shown in Figure 3.14, illustrates the significance of crack closure at low field stress. Alteration of the apparent deformation properties during test MC1.11 causes the different radial strain pattern between tests MC1.9 and MC1.14.

3.7.2 CONSTANT FIELD STRESS RESPONSE

The time-dependent tunnel closure parameters, b and n, increase and decrease respectively by about 15% after reducing the loading rate. Figure 3.7 shows the average normalized tunnel closure rate parameters, b and n, for each elevated field stress increment during test MC1.14. The change of b and n for the 11, 12, and 13 MPa field stresses seems reasonable, assuming a binary visco-elastic material. In particular, the magnitude of stress input differs by a ratio of 10:1 between the initial 10 MPa field stress and 1 MPa increments for 11, 12 and 13 MPa field stress, therefore the potential for delayed straining should decrease. Thus, the delayed tunnel closure depends on stress history.

After unloading to 10 MPa field stress and reloading to 13 MPa field stress, closure rate parameters are about equal to the initial values for the 13 MPa field stress (Figure 3.7). Assuming a binary visco-elastic formulation, slightly higher b and n values would be anticipated for a 3 MPa stress input as compared to a 1 MPa stress imput, provided full deformations occur at 10 MPa field stress. Also, upon loading to 14 MPa field stress, b and n increase slightly, thus indicating field stress dependency. However, stress path effects, after unloading and reloading at 13 MPa field stress, complicate interpretation of the field stress dependency. Finally, significantly lower values for b and n at 14.5 MPa further illustrates the field stress increment dependency (Figure 3.7).

Superposition of isotropic and deviatoric components of deformation complicates evaluation of tunnel closure rate. Variation in the magnitude of field stress increments, ±15% during slow loading increments, also complicates comparison of deformation response for various field stresses.

Excluding these complications, comparison of tunnel closure rate parameters for different field stresses in Figure 3.8 illustrates their loading history dependence. Suitable testing is required to evaluate isotropic creep behavior and to separate stress path and field stress magnitude effects. Nevertheless, these results illustrate the necessity for specifying loading history for comparisons of deformation behavior.

Examination of the radial strain rate results further illustrates the loading history dependent deformation behavior. Comparison of radial strain rate results for slow loading in test MC1.9 to that for fast loading in test MC1.10 shows that slightly more extension occurs in both zones during slow loading, except in zone A during test MC1.9. The loading history differs between slow loading in test MC1.9 and fast loading in test MC1.10 (.ie., a 1 MPa load increment takes 15 minutes whereas a 15 MPa load increment takes 3 hours). Thus, assuming a binary visco-elastic formulation together with incremental loading, more extension would occur after a shorter loading interval since mobilization of the isotropic deformation component takes longer.

Radial strain rate response differs between zone A and zone B as shown in Figures 3.16 and 3.17. After loading to 10 MPa, zone A exhibits a greater amount of extension than zone B. Subsequently, during slow loading increments, no change or slightly more compression occurs in zone A while more extension occurs in zone B, especially during test MC1.14. This qualitative analysis of radial strain is based on summary analysis of results for each field stress magnitude. The individual curves are shown in the internal report.

Indeed, this alteration of radial strain rate behavior correlates with expansion of the delayed EO after reducing the loading rate. However, as previously shown, superposition of isotropic and deviatoric deformations and non-linear, stress-dependent deformation properties complicates evaluation of radial strain rate behavior.

Delayed deformation behavior for tests with a "Bimodal Loading Rate" differ slightly due to the "Non-hydrostatic Episode" carried out between tests. For test MC1.9, tunnel closure rate parameters, b and n, slightly exceed those for test MC1.14, particularly along the 90-270 diameter. Figure 3.8, showing the ratio of closure rate parameters of test MC1.14 to that of test MC1.9, illustrates the closure rate difference between tests. The reduction of the parameters for the 90-270 diameter corresponds with alteration of the apparent deformation modulus. However, other diameters do not exhibit this type of behavior. In addition, comparison

of Zone B radial strain rate curves shown in Figures 3.16 and 3.17 shows the greater amount of extension in test MC1.14 as compared to test MC1.9. In Zone B in test MC1.14, increased delayed extension radial strain corresponds with greater extension strain observed during incremental loading. Thus, alteration of the closure rate and radial strain rate is consistent with the time-independent behavior.

Delayed compressive radial strain recovery continues at some extensometer locations long after removing the field stress. For example, during test MC1.9 in Zone B, compressive radial strain continues at some locations and one gauge exhibits increased compressive strain after 160 hours, while in zone B, smaller magnitude delayed recovery strains occur. During test MC1.14, comparable recovery behavior occurs except some locations in zone B also exhibit slightly increased compressive radial strain after several hours at zero field stress. Appendix C6 shows the strain-time curves for tests, MC1.9 and MC1.14 at recovery. The delayed recovery further exemplifies a superposed deformation behavior. A binary visco-elastic formulation may predict creep rate change. However, comparable behavior would be expected at all Zone B locations. Local yield effects could account for this asymmetric response, and indeed, some extensometers exhibiting response changes are located near local yield zones. In particular, the Zone A 270 radius extensometer was located in the section that

broke up during test MC1.18 (Figure 2.5).

3.7.3 COMPARISON OF TUNNEL CLOSURE AND RADIAL STRAIN

Local deterioration of the tunnel wall affects tunnel closure measurements and slightly influences the radial strain distribution. For example, alteration of the apparent deformation modulus for the 135-315 diameter exceeds the mean value for the tunnel by 10% (Figure 3.6). Local rupture at the tunnel wall along the 315 radius exaggerates the alteration of this apparent deformation modulus. Moreover, the local rupture creates a radially symmetric EO.

During the initial 12 and 13 MPa field stresses in test MC1.9, coal dust collected on the LVDT located along the 315 radius, plus at 13 MPa field stress, an open tension crack (about 2mm wide) was identified on the tunnel wall adjacent to the 315 radius. The open crack did not interfere with the LVDT operation. Relative to other parts of the tunnel, the 270-315 section of the tunnel wall exhibited a broken texture. This section of the tunnel also broke up during test MC1.18 (Figure 2.5). During test MC1.14, the tension crack opened at elevated load and closed during recovery. This rupture mechanism may correspond with the buckling mode described by Guenot (1979).

The deformation behavior changes along the 135-315 diameter during the initial slow loading in test MC1.9. The apparent deformation modulus exceeds that for other

diameters by about 15% (Figure C5-4). Also, the closure rate parameter "b" is about 15-25% greater than the average for all diameters at 11 and 12 MPa field stress. Thus the propensity for immediate and delayed closure is less than other diameters. Then, at 13 MPa field stress increased tunnel wall displacements occur coincident with a more short-term closure rate behavior and the appearance of the tension crack. Figure C3-1a shows the increased closure for the 135-315 diameter at 13 MPa field stress. Figure C5-7 shows the "n" and "b" parameters for the 135-315 diameter at 13 MPa field stress. The potential for delayed closure and the rate of decrease of delayed closure increase. The apparent deformation moduli and closure rate parameters are comparable with other diameters during the latter part of the test program (Figures C5-5 and C5-8). Thus, for the 135-315 diameter, local rupture causes the 10% deviation from the mean value as shown in Figure 3.5. This alteration of the closure rate is generally consistent with behavior seen in the preliminary tests.

The radial strain behavior along the 315 radius also changes. Radial strain measurements along the 315 radius indicate no abnormality due to the local rupture at 13 MPa during test MC1.9 (Figures 3.13 and 3.15). However, radial strain results differ significantly between tests MC1.9 and MC1.14, at least moreso along the 315 radius than along the 135 radius. In particular, for the 315 radius, zone A exhibits more compression and zone B exhibits more extension

during test MC1.14 (Figures 3.13 and 3.15). Thus, the tunnel closure measures an average response whereas the radial strain responds to local conditions.

Moreover, local deterioration of the tunnel wall, comparable to reduced load carrying capacity for local rock elements, promotes local deformations comparable to that observed during the "Non-hydrostatic Episode". For the apparent deformation moduli to decrease and extension radial strain to increase in zone B, a zone of "weakened" or else "softened" rock elements must exist adjacent to the tunnel. However, in the "non-hydrostatic episode", the delayed closure potential and the rate of the decrease of the delayed closure decrease, opposite to the behavior at the local rupture.

Generally, tunnel closure and radial strain behavior indicate compaction of the specimen during the test program. Irrecoverable tunnel closures (typically about 0.4% and slightly higher after tests with a "Bimodal Loading Rate") exist for each diameter, except the 90-220 diameter (Figure 3.3). Although incomplete results are available, irrecoverable average specimen strain is about 25% of the irrecoverable tunnel closure (.ie. about 0.1%). Radial strains exhibit history dependent total strain, as previously discussed. Irrecoverable compressive radial strains (typically less than 0.1% and about 0.2% after tests with a "Bimodal Loading Rate") exist at most locations, except if large extension strains occur whence irrecoverable

strain is less (Figures 3.11 to 3.14). Irrecoverable radial strains indicate that the specimen compacts only slightly during the testing history. The specimen compacts slightly between each test however this is insignificant in comparison with aspects studied during this test program. For example, compare the radial strain curves for the test sequence MC1.12-13-15, conducted with hydrostatic field stress, to that for the initial "Non-hydrostatic Episode" (Figures 3.11 to 3.14). Typically, in tests MC1.12-13-15, the radial strain curve shapes change insignificantly. However, in the "Non-hydrostatic Episode", the trends of the radial strain curves at elevated field stress change markedly.

3.8 BREAKING THE SPECIMEN

The specimen ruptured along jointing at 10 MPa field stress during test MC1.18. Large displacements occurred during loading to 10 MPa field stress and remained after unloading. One final hydrostatic field stress test, MC1.19, was carried out on the broken specimen to evaluate the behavior of a structurally different rock mass.

3.8.1 DEFORMATION RESPONSE

The deformation behavior during the non-hydrostatic field stress test, MC1.18, prior to failure, generally corresponds with previous results for specimen MC1. The apparent deformation moduli obtained for test MC1.17

under-estimate the tunnel closure along the 0-180 diameter and over-estimate tunnel closure along the 90-270 diameter for test MC1.18. Also, radial strain is generally consistent with previous tests. After failure, large irrecoverable strains exist, contrary to previous results. About 2% irrecoverable tunnel closures exist for the 0-180 diameter (Figure 3.3). However, other displacement monitors went off scale when the specimen broke, therefore irrecoverable displacements could not be measured.

The physical condition of the specimen for test MC1.19 differed markedly from that for test MC1.17. In particular, a shear zone was created as shown in Figure 2.4.

Comparing tests MC1.17 and MC1.19, shows that the tunnel closures differ insignificantly however the radial strain distributions differ significantly, especially in and adjacent to the broken regions in the specimen. The apparent deformation moduli correspond between tests (Figure 3.4). The radial strain distribution differ, for example, along the 315 radius (Figures 3.12 and 3.14). Also, general deterioration of the tunnel wall corresponding with the broken zone shown in Figure 2.5 corresponds with more extension strains in Zone B (Figures 3.13 and 3.14).

The delayed deformations apparently change insignificantly between tests MC1.17 and MC1.19. Tunnel closure rate parameters correspond between tests (Figure 3.6). Radial strain rate results differ slightly (located in the internal report). For example, zone A generally

exhibits slightly more compression, however, broken zones exhibit variable response. Finally, the difference in constant load values for test MC1.17, 15 MPa field stress, and test MC1.19, 12 MPa field stress, precludes elaborate comparisons.

The tunnel closure behavior apparently does not change significantly. Therefore, "softening" or "weakening" processes evidently were not reactivated at 10MPa field stress in test MC1.18.

3.8.2 PHYSICAL OBSERVATIONS

The general condition of the tunnel wall deteriorated significantly during test MC1.18. The shear zone, shown in Figure 2.4, developed during the low confinement test, MC1.18. Deterioration of the tunnel wall was evident at quite low field stress. For example, at 2 MPa, in test MC1.18, a 2 cm^3 block of coal fell from near the top of the tunnel at the 245 radius; and at 4.5 MPa, a wedge of coal intruded about 2-4 mm into the tunnel along the tunnel axis at the 245 radius and interfered with the LVDT at this location. In general, the condition of the specimen deteriorated at higher field stresses. For example, at 8 MPa, the tension crack on the tunnel wall at the 315 radius was open about 5 mm; and rock noise was quite distinctive. Incidently, minor increase in confinement stress, or else, incrementing the field stress for the minimum load axis prior to that for the maximum load axis prevented excessive

rock noise. The specimen moved excessively during the last load increment to 10 MPa maximum field stress and the field stress was quickly reduced to avoid rotation or translation of the specimen. During recovery, the tunnel wall was remarkably intact except for material bulging into the tunnel near the 315 radius (the latex seal on the tunnel surface prevented debris from falling off the wall). Also, the specimen boundaries exposed to maximum loading were concave in toward the tunnel.

The shear zone was clearly identified during test MC1.19, hence loading was stopped at 12 MPa to avoid excessive differential displacement between loading platens on either side of the shear zone.

Tunnel wall deterioration continued at the tunnel wall during test MC1.19, thus interfering with some tunnel closure meassurements. The intruding wedge, at the 245 radius, interfered with tunnel closure measurement. The 315 radius LVDT core penetrated the loose, broken material bulging into the tunnel. During constant elevated load, local bulging occured along the 135 radius, perpendicular to jointing. Bulging of the tunnel wall along an axis perpendicular to jointing may be due to a buckling failure mechanism as described by Guenot (1979).

The deformation mechanism changes significantly in the broken zones as compared with intact rock mass zones. Physical deterioration of the tunnel wall is coincident with physical alteration of rock structure, for example, bulging

of the tunnel wall. Also, coincident with the local bulging mechanism, the effective size of the opening increases. Accordingly, local rupture apparently causes local stress redistribution around broken zones. However, study of local rupture requires small scale instrumentation to record local details.

3.9 CONCLUSIONS

The time-independent and time-dependent deformation behavior of the test specimen change during the test program. The most significant change in deformation behavior occurs with test MC1.11. Figure 3.4 shows the change in the apparent deformation modulus with test MC1.11. Also, radial extensometers respond to local deformation processes and exhibit more compression near the tunnel and more extension further from the tunnel. Therefore, an "Equivalent Opening" (EO) develops to a size of about 25-35% larger than the initial tunnel size. A "weakened" or "softened" region must develop around the tunnel which causes stress to redistribute away from the tunnel to regions of higher confinement. In tests with N=1 and in the latter part of the test program, this stress redistribution process insignificantly alters the deformation behavior, at least with respect to tunnel closure.

The magnitude of delayed deformations depend on the loading rate. In particular, after reducing the loading rate at 10 MPa field stress, delayed deformations lead to

more tunnel closure. Relative to the longterm deformation behavior, the magnitude of the time-dependent change in the delayed tunnel closure will depend on loading rate and is referred to as a delayed EO.

The magnitude of the delayed EO also depends on loading history. In particular, the size of the delayed EO in test MC1.14 is about one-half of that in test MC1.9. Figure 3.5 illustrates the difference in the change of the fast and slow moduli due to test MC1.11. Less delayed radial strains occur in test MC1.14, as shown by comparing curves shown in Figures 3.11 to 3.14. In addition, more extension strain rates occur in Zone B with only slight changes occurring in Zone A, after test MC1.11. The tunnel closure rate parameters change insignificantly during the test program (Figure 3.6). In the first "Non-hydrostatic Episode", the closure rate parameters change slightly as shown in Figure 3.8, especially for the 90-270 diameter. Superposition of deformations due to isotropic and deviatoric stress and the load history dependent deformation behavior complicates evaluation of the delayed EO.

The second test with a non-hydrostatic field stress, test MC1.16, influences the EO only slightly. Also, the tunnel closure behavior changes insignificantly after the specimen ruptures along jointing in test MC1.18. However, the radial strain results show appreciable irrecoverable radial strain after test MC1.16. Also, in test MC1.19, the radial strain pattern varies, in particular due to broken

zones. Thus, the deformation mechanisms that lead to alteration of the equivalent opening size in test MC1.11 are not significantly reactivated in the later tests.

The test specimen exhibits linear elastic and linear visco-elastic behavior in general and especially in tests with hydrostatic field stress. Insignificant irrecoverable radial strains develop, especially in comparison with changes in the deformation behavior. In particular, loading path dependent compaction of the specimen occurs in tests with a "Bimodal Loading Rate". Also, a binary visco-elastic formulation may simulate alteration of the radial strain rate behavior depending on loading rate.

Deformation behavior depends on loading history. Moreover, loading or stress history must be considered when comparing the deformation results. Variations in the closure rate behavior depending on stress increment magnitude, loading rate and stress level illustrate the necessity for specifying the loading history in comparison of deformations. Finally, stress redistribution processes evidently control deformation behavior in detail. Local creep and yielding or strength loss control local stress redistribution and represent the most significant deformation mechanism.

Kaiser and Morgenstern (1981) describe the time-dependent yielding process. The creep behavior evidently depends on load increment. At higher field stress, yielding actively occurs and is characterized by a

decrease of the closure rate parameters. Closure rates stabilize and stress redistribution processes evidently control the stabilization. In particular, according to Kaiser and Morgenstern (1981), the actual closure rate depends on the local rock mass properties whereas the unfractured rock mass controls the rate of decrease of the closure rate.

Prior to rupture at the tunnel wall on the 315 radius during test MC1.9, small tunnel closures and low closure rates occur. With rupturing, tunnel closures increase while closure rate parameter b decreases and n increases. The local rupture differs from general yielding in that the decrease in closure rate with time occurs more rapidly. Perhaps progressive yielding may have continued at higher stresses, however, the rupture apparently stabilizes with the unloading and reloading test history. Although radial strain does not change immediately, in subsequent tests radial strain changes markedly. Thus, the deformation behavior depends on the rock mass condition.

The behavior due to test MC1.11 differs slightly from the response around the local rupture. After test MC1.11, tunnel closures increase and closure rate parameter b increases and n decreases slightly. The rock mass condition must change with test MC1.11. This causes the lower potential for closure and more gradual decrease in closure rate. Correspondingly, the magnitude of the delayed EO decreases. This is consistent with observations concerning

the active time-dependent yielding process. Thus, the yielding process evidently occurs primarily during the short-term test MC1.11.

Considering tunnel closure only may lead to a misinterpretation of the mechanisms of behavior. The radial strain measurements are necessary to evaluate the mechanisms causing the alteration of the deformation behavior in detail. For example, deterioration of the tunnel wall during test MC1.9 correlates with alteration of radial strain behavior during subsequent tests. Thus, knowledge of the condition of the rock mass at the extensometer augments interpretation of test results. In addition, tunnel closure measurements indicate an elliptical EO develops in response to test MC1.11. However, radial strain results exhibit a radially symmetric pattern. Even after the specimen failed along jointing in a low confinement field stress test, the tunnel closure behavior changes insignificantly. Some radial strain measurements change, particularly for extensometers located in broken portions of the test specimen. However, superposition of crack closure and continuum deformation complicates evaluation of the average radial strain results. Indeed, the extensometers respond to superposed deformation modes. Suitable deformation gauges would be required to monitor the local, small scale deformations. Correspondingly, small scale mapping of the rock structure would augment analysis. However, this maybe practically useless. The PST is designed to study the

deformation behavior as a response to local effects.

In the preliminary tests, enlarging the tunnel size causes alteration of the time-dependent tunnel closure. In particular, short-term closure rates occur with an increase in total delayed closure. Thus, the magnitude of the delayed EO increases.

Testing prior to test MC1.8 complicates evaluation of the preliminary tests. Expansion of the equivalent opening during tests prior to test MC1.8 may also explain the observed behavior. In particular, assuming tests with the smaller tunnel lead to "softening" or "weakening" of the rock elements located near the tunnel, the stresses redistribute further inside the specimen. Subsequently enlarging the tunnel size effectively removes these rock elements. Then, loading during test MC1.8 causes increased stress concentration around the tunnel and an associated increase of time-dependent tunnel closure, perhaps comparable with test observations. Further testing is required to investigate this process.

Also, since this material exhibits nonlinear, stress-dependent creep (da Fontoura, 1980), the response to enlarging the tunnel is not readily apparent. Consideration of scale effects, discussed in Chapter 4, also complicates evaluation of changing the tunnel diameter.

a.

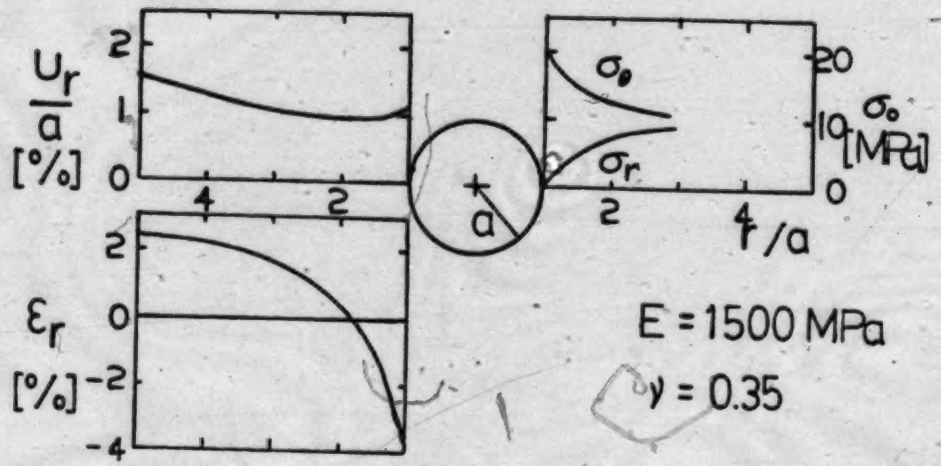

b.

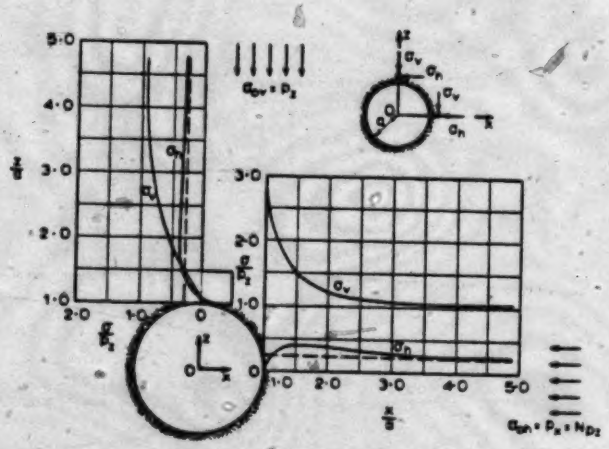

Figure 3.1 a. Linear Elastic Stress, Strain and Displacement for the PST; N=1.0
b. Linear Elastic Stress; N=0.25 (Terzaghi & Richter, 1952)

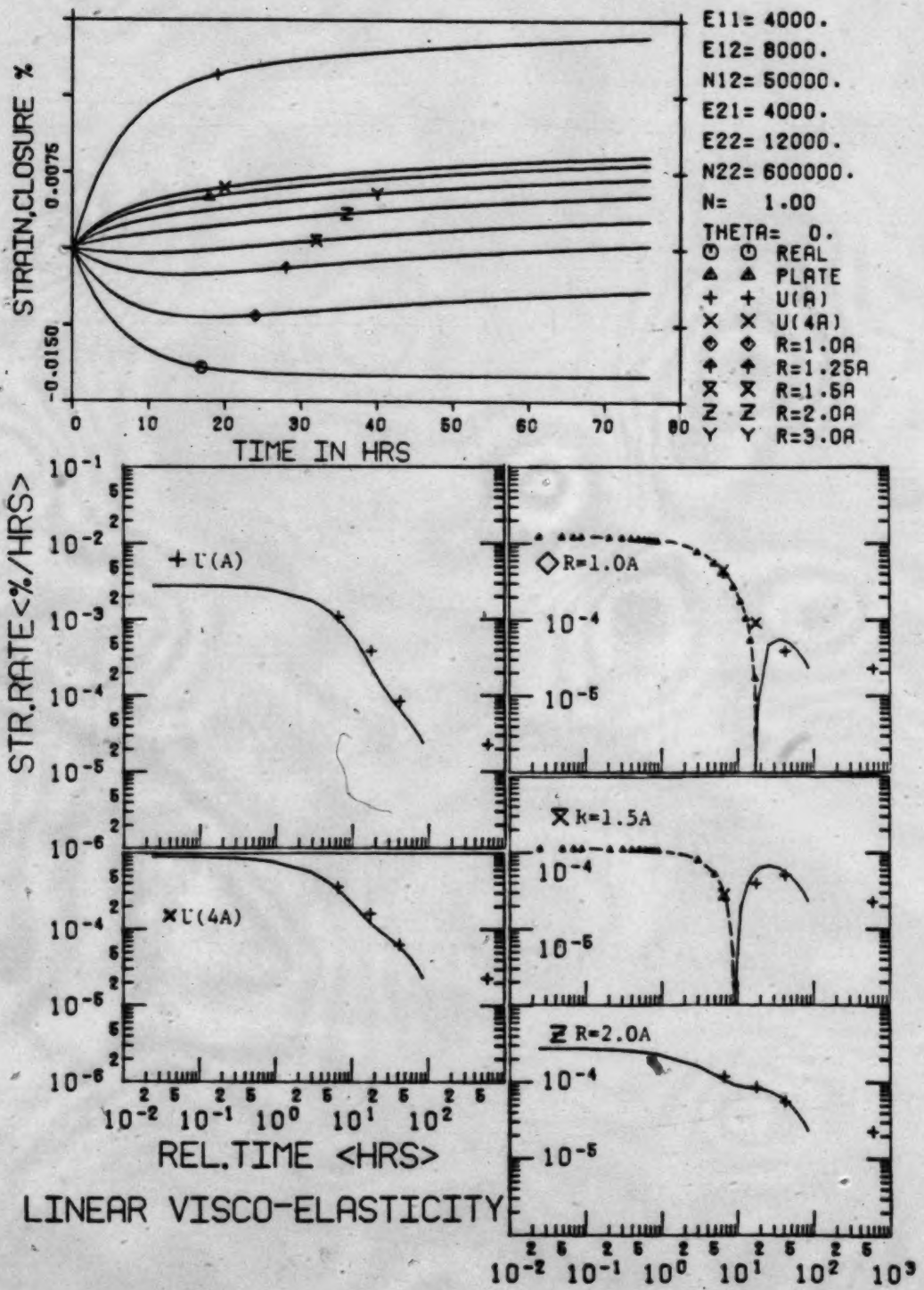

Figure 3.2 Linear Visco-elastic Creep For Binary (Isotropic and Deviatoric) Formulation (Kaiser, 1979)

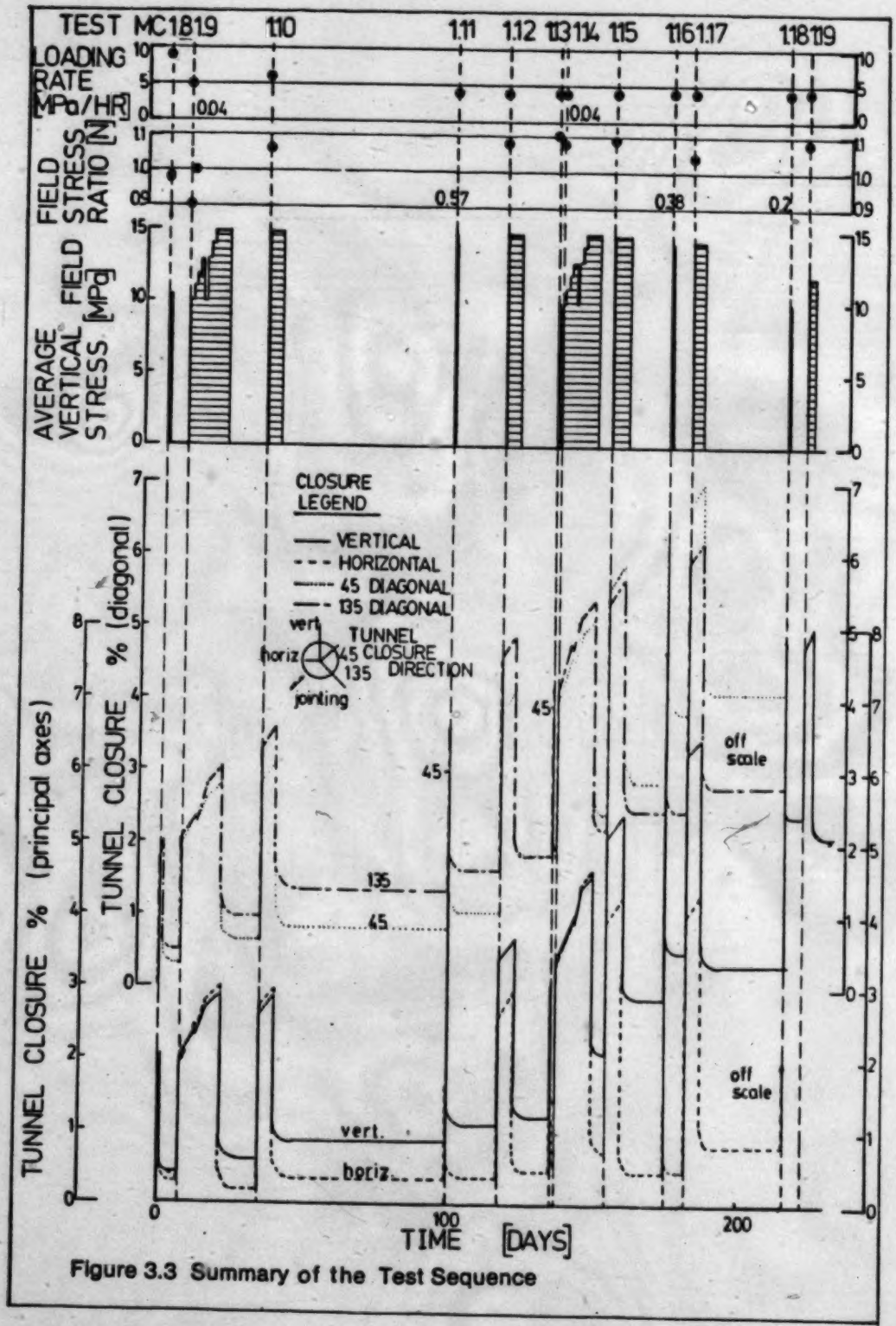

Figure 3.3 Summary of the Test Sequence

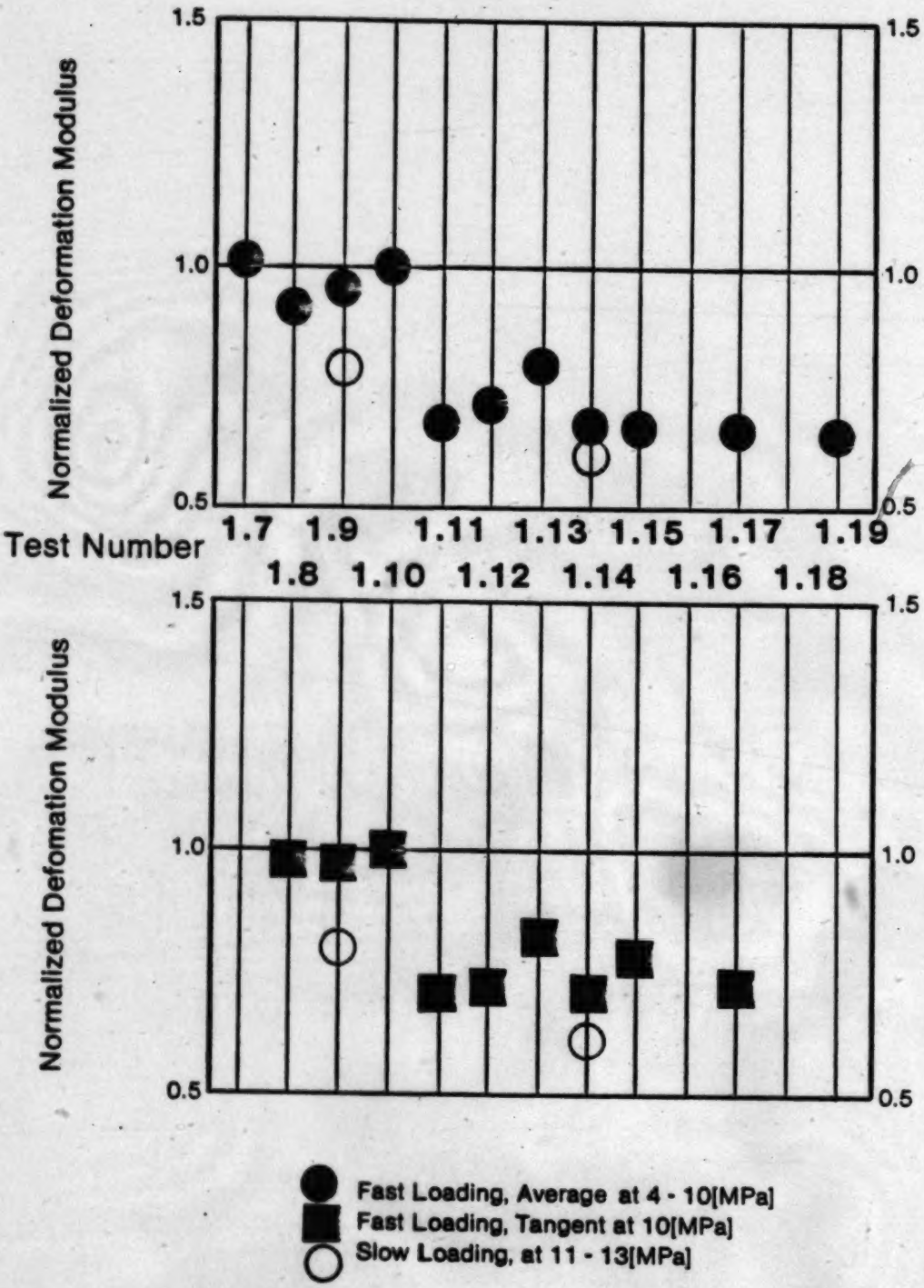

Figure 3.4 Average Deformation Modulus for each Test Normalized to Test MC 1.10

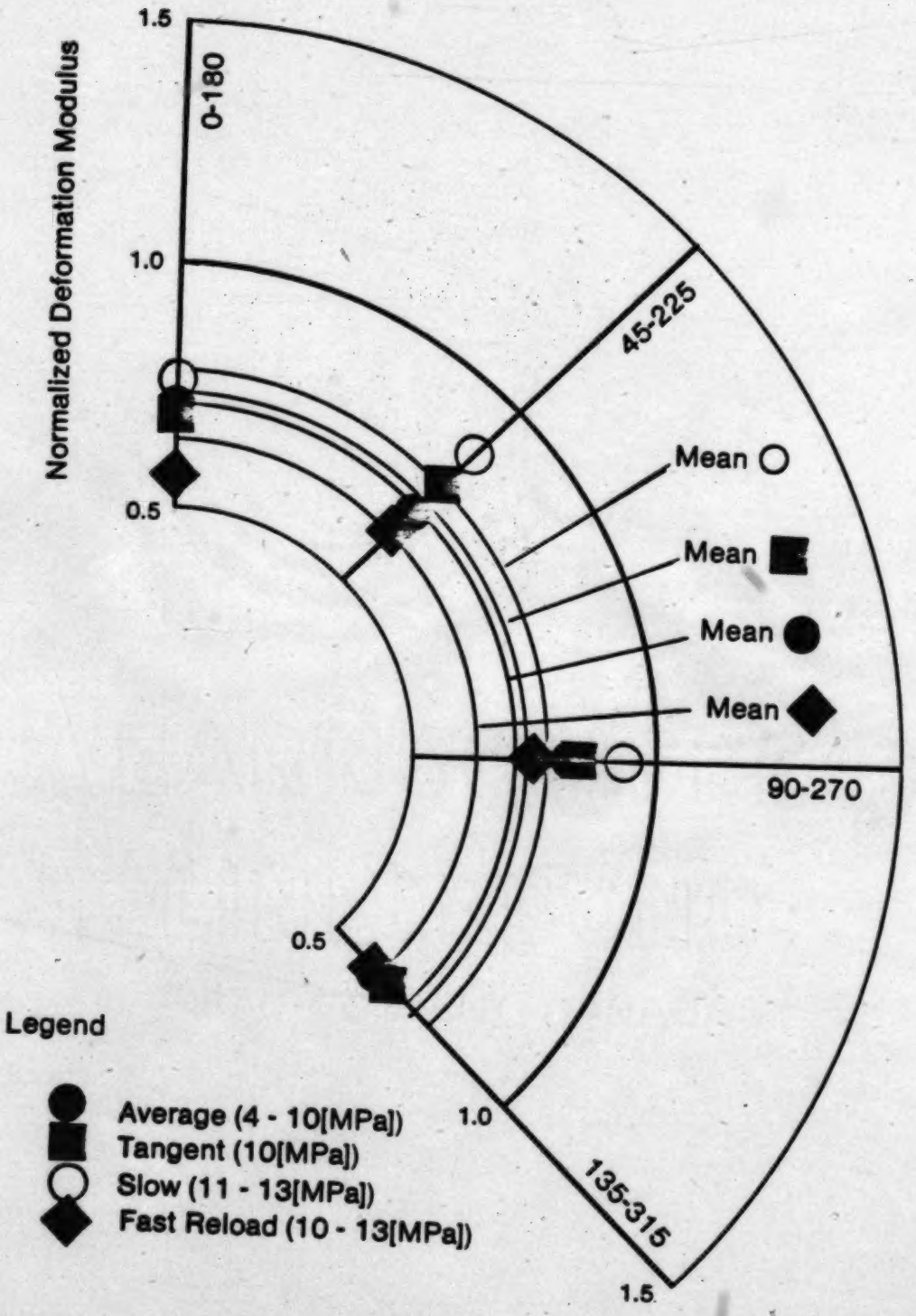

Figure 3.5 Average Deformation Moduli for Test MC 1.14 Normalized to Test MC 1.9

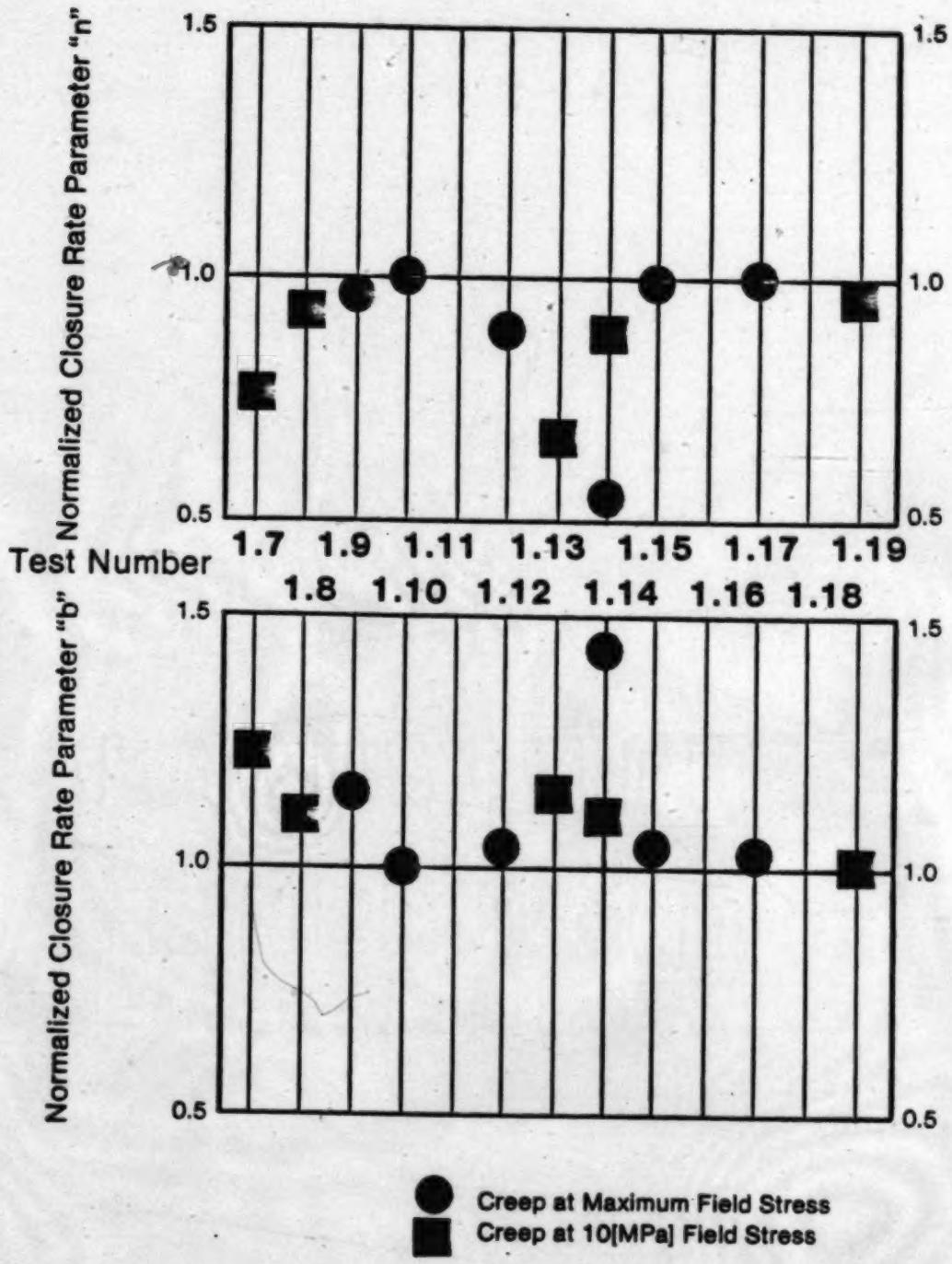

Figure 3.6 Average Closure Rate Parameters for Each Test Normalized to Test MC 1.10 at 15 [MPa] Field Stress

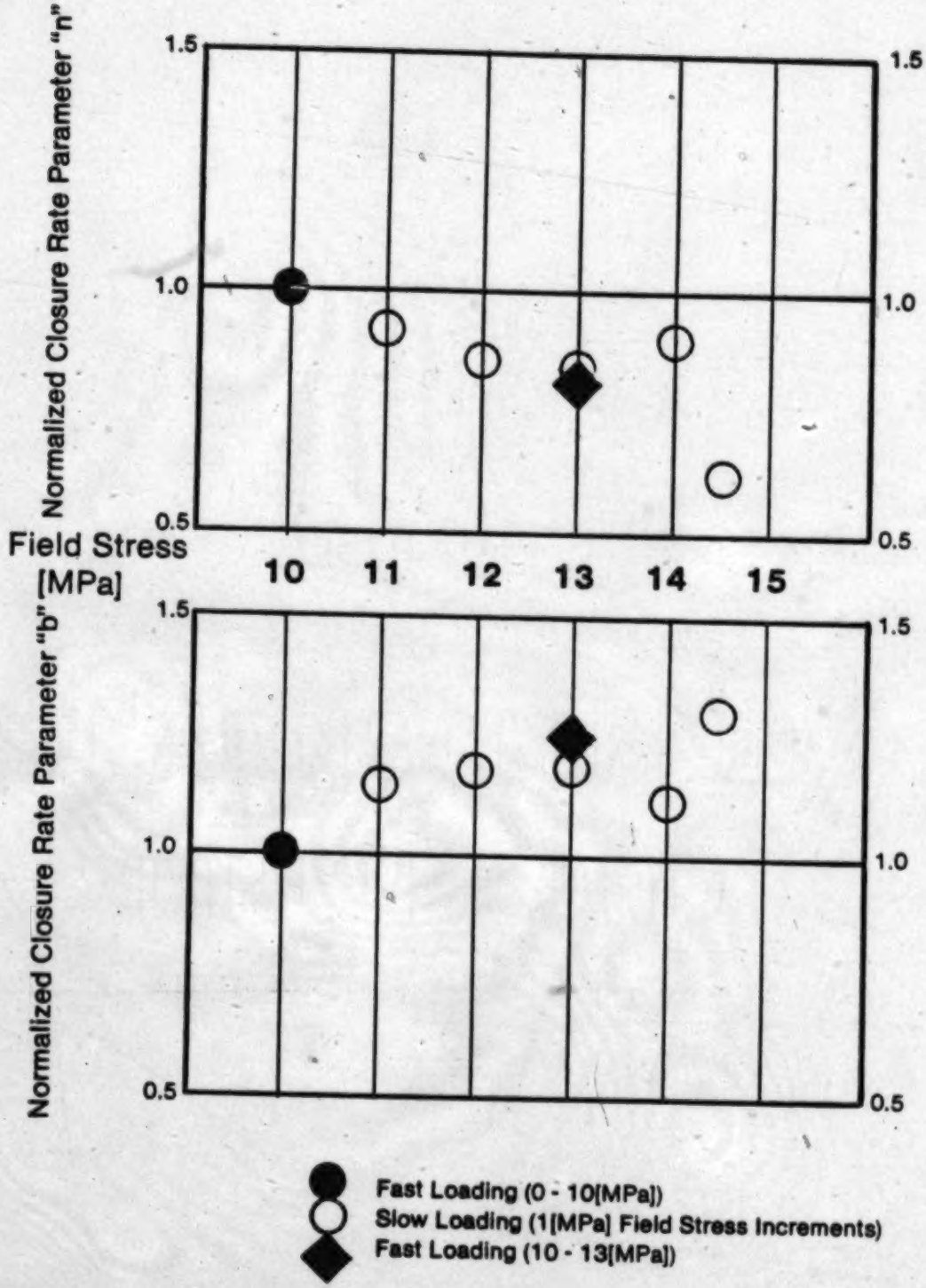

Figure 3.7 Average Closure Rate Parameters for Test MC 1.14 Normalized to the 10 [MPa] Field Stress

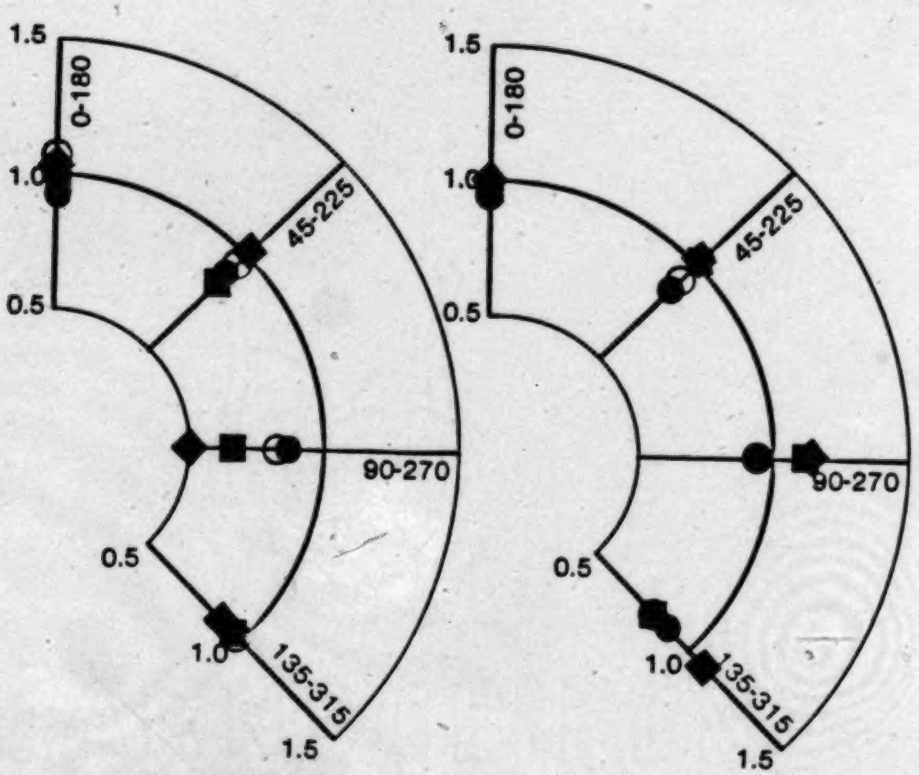

Note:N =1.05 for MC 1.14
N = 1.0 for MC 1.9

Field Stress
○ 11[MPa]
■ 12[MPa]
◆ 13[MPa]
● 14[MPa]

Figure 3.8 Closure Rate Parameters for Test MC 1.14 Normalized to Test MC 1.9

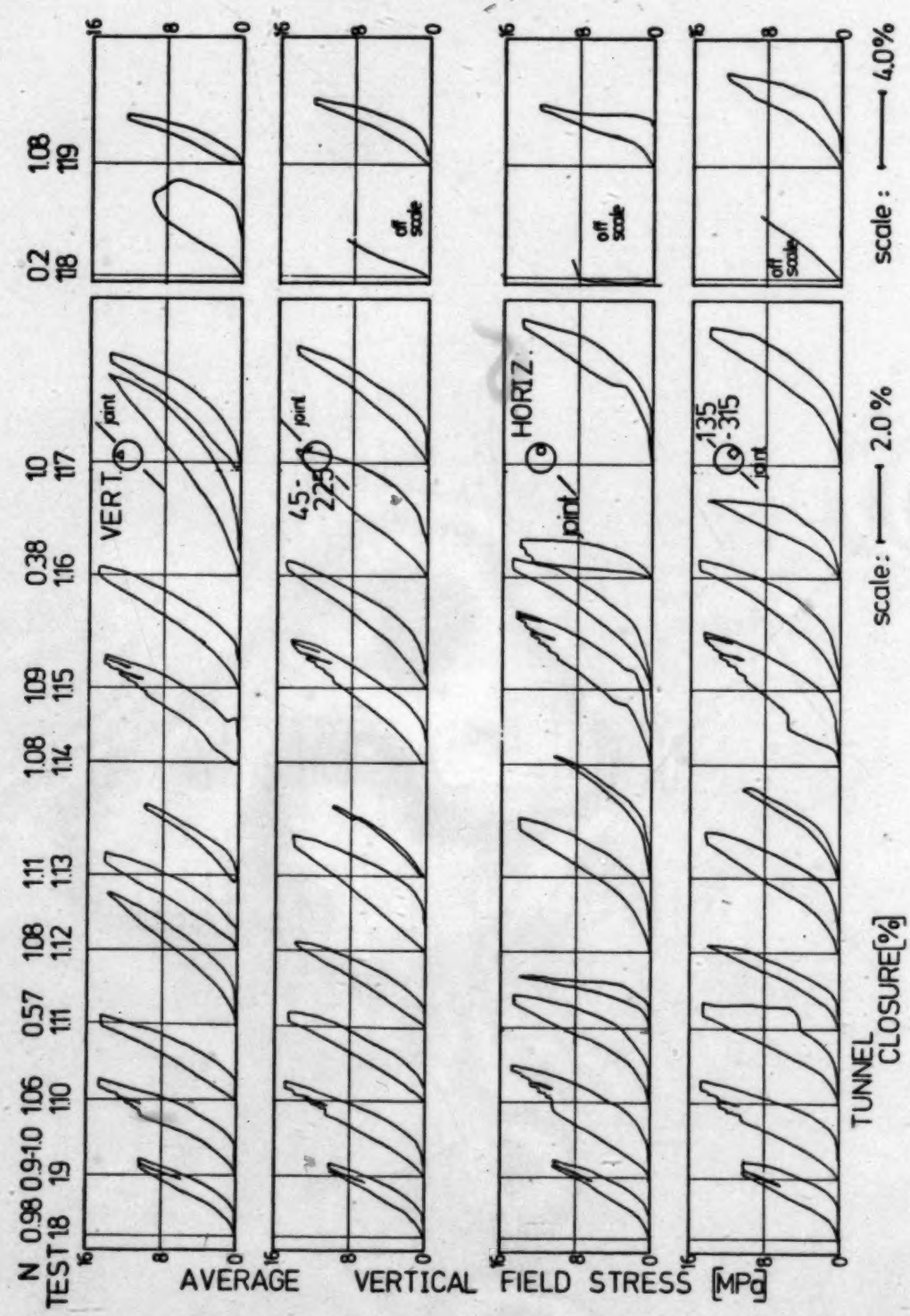

Figure 3.9 Field Stress Versus Tunnel Closure

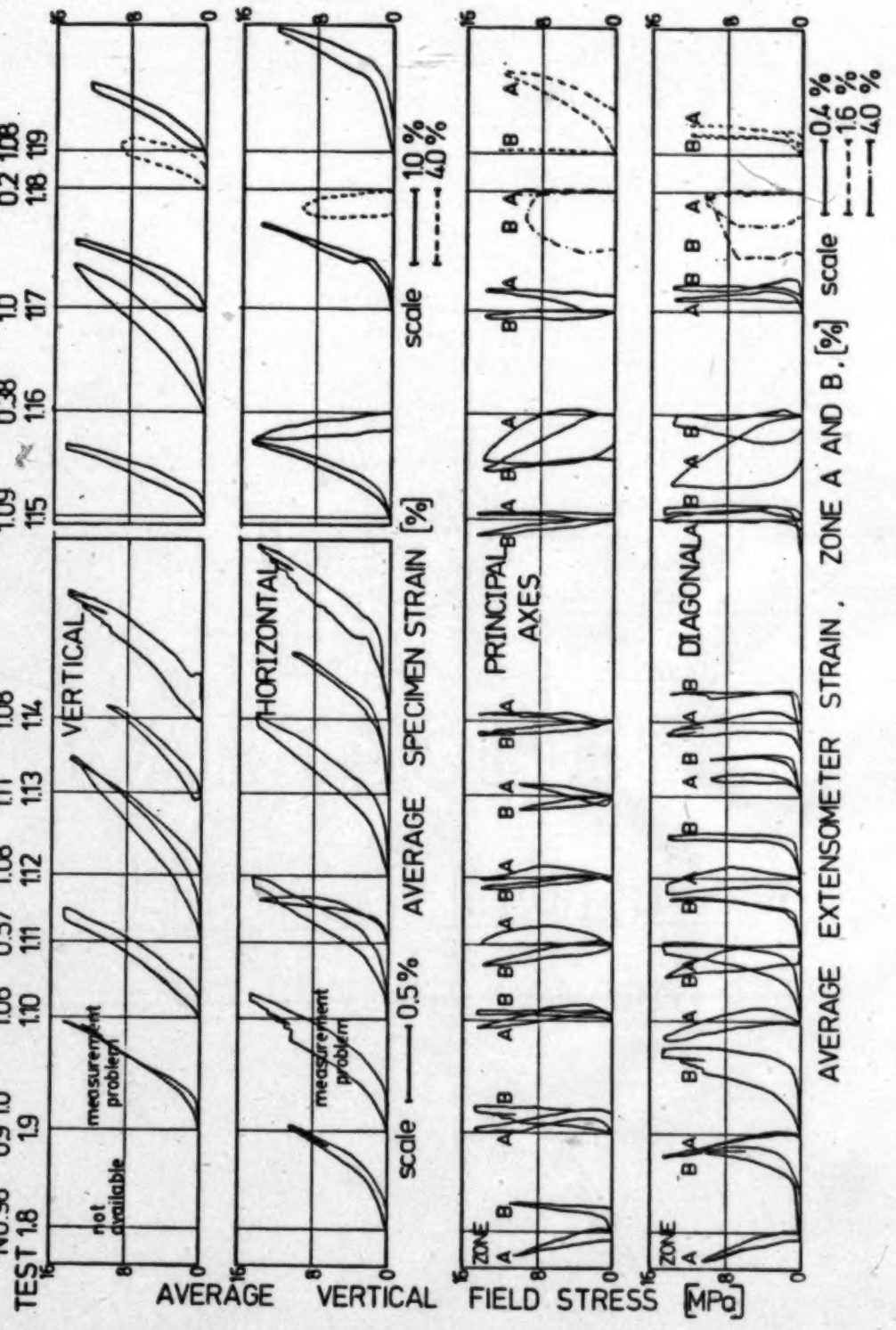

Figure 3.10 Summary of Field Stress Versus Strain

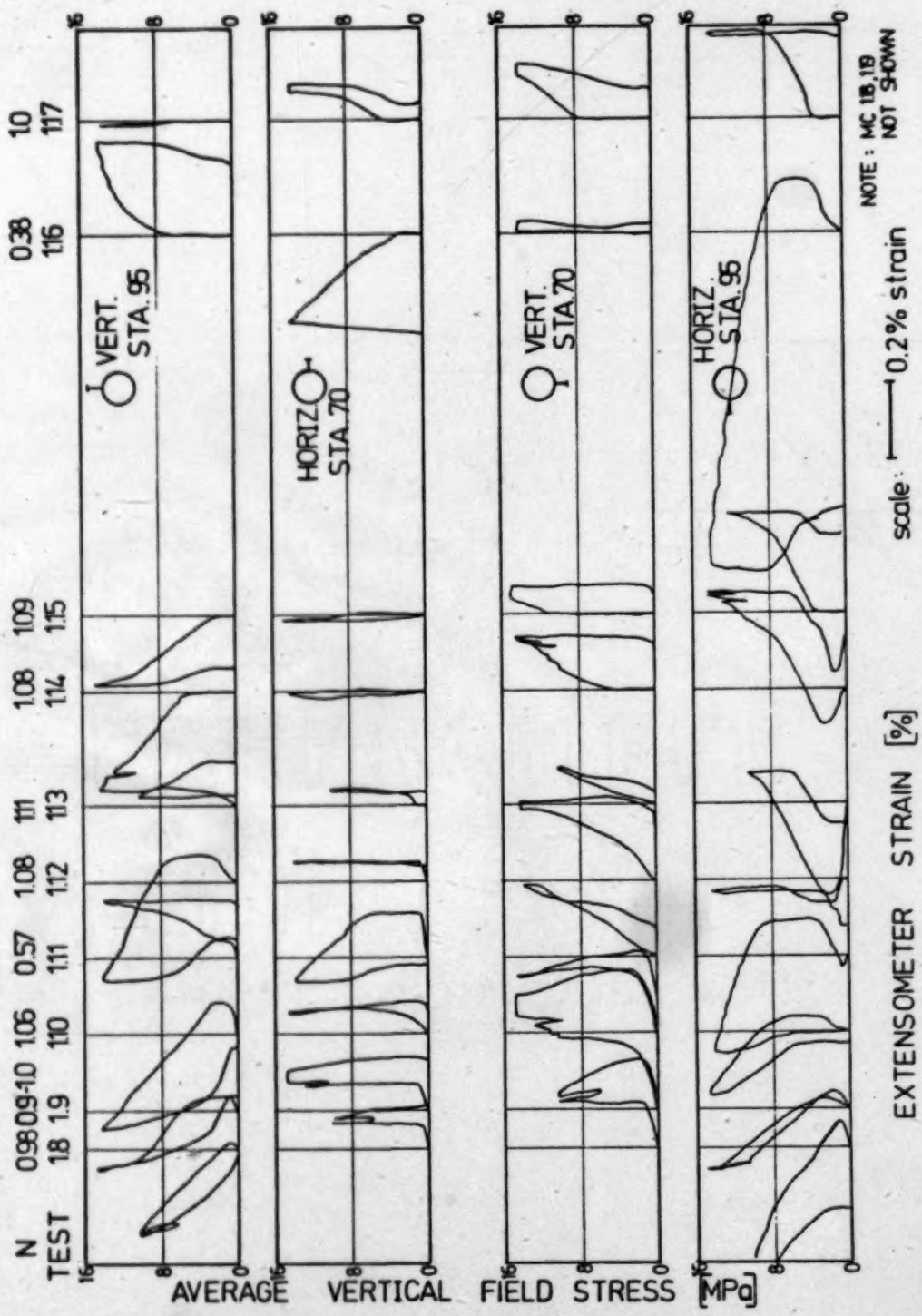

Figure 3.11 Field Stress Versus Average Radial Strain; Zone A, Principal Axes Extensometers

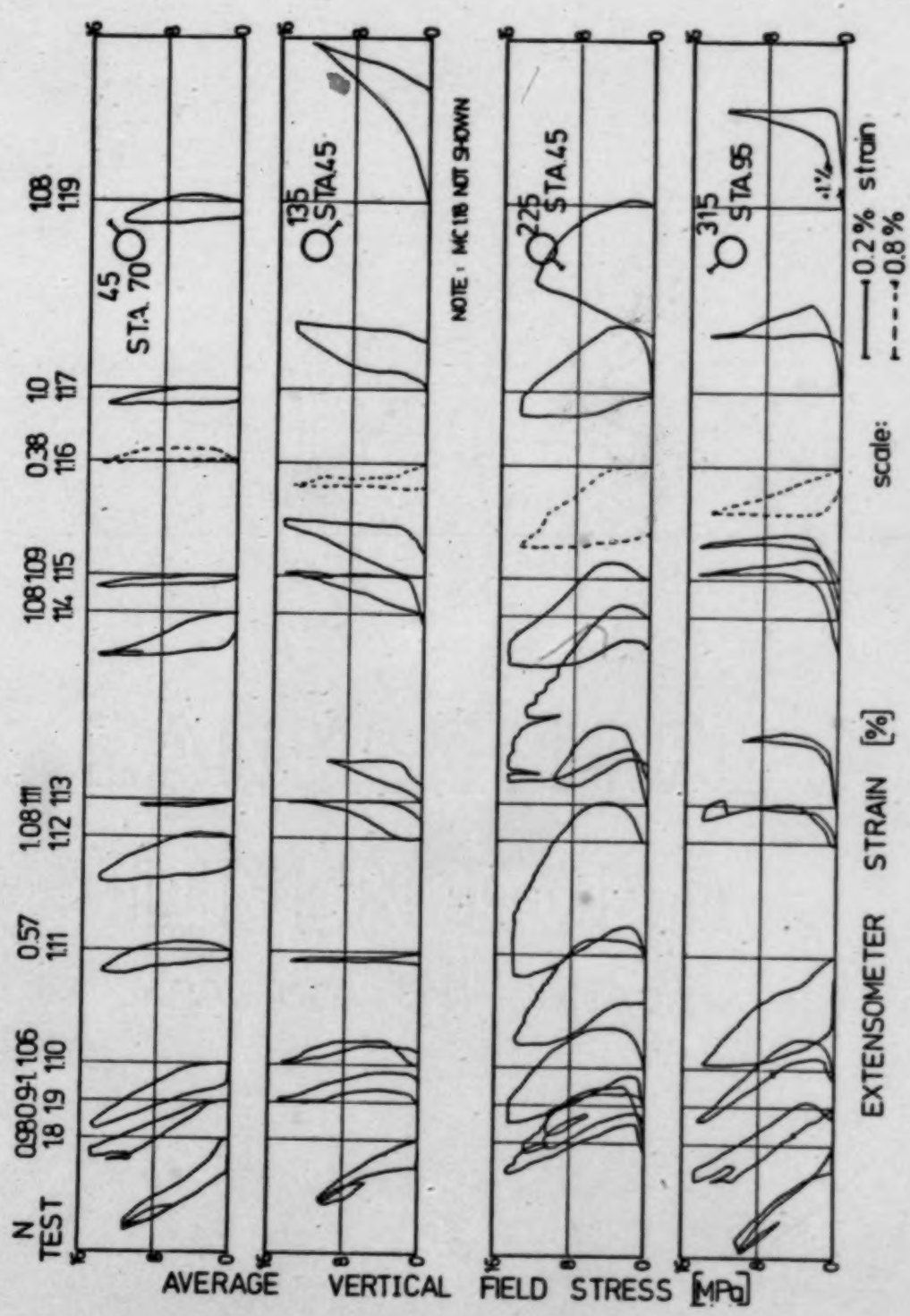

Figure 3.12 Field Stress Versus Average Radial Strain; Zone A, Diagonal Extensometers

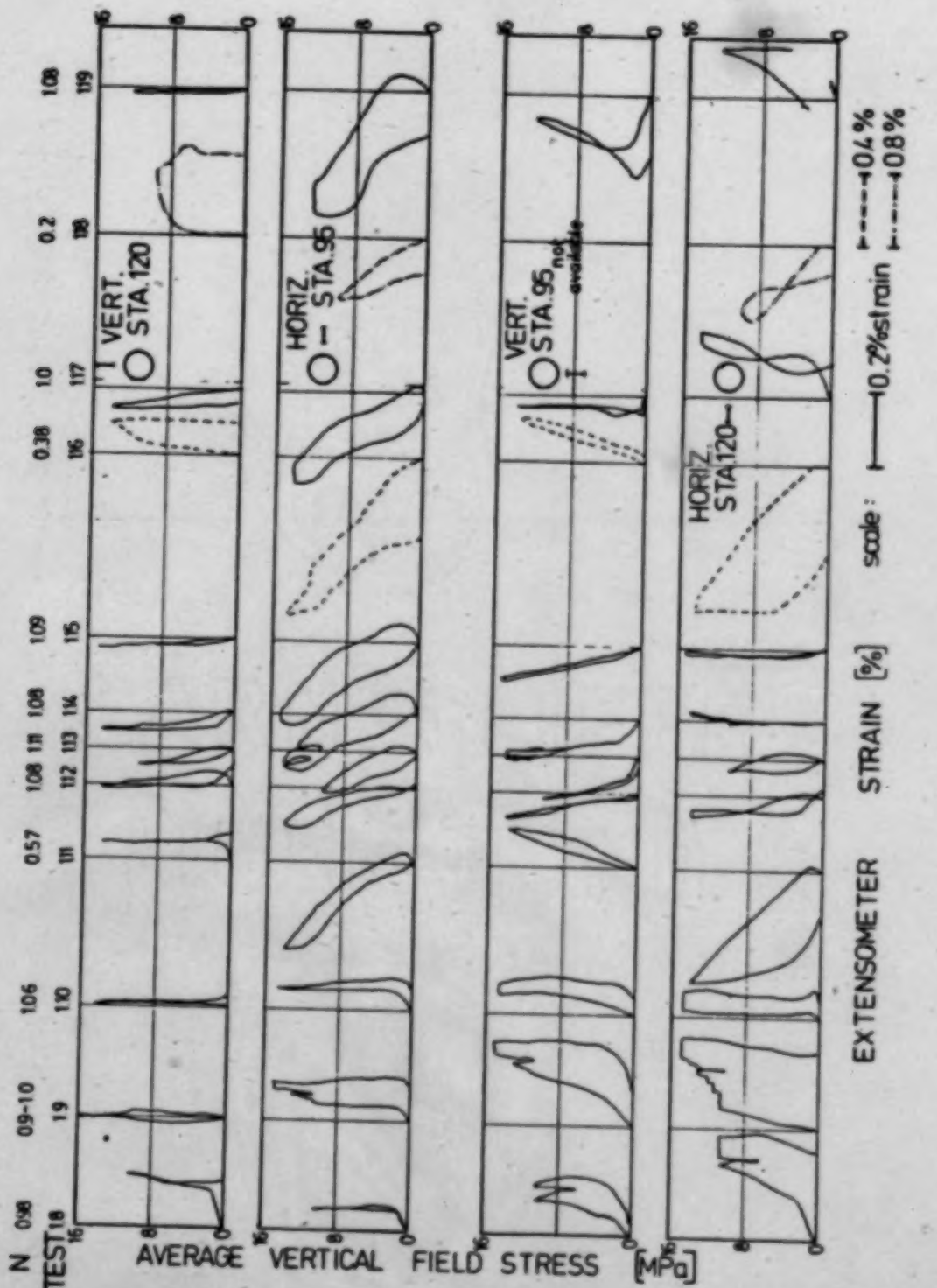

Figure 3.13 Field Stress Versus Average Radial Strain; Zone B, Principal Axes Extensometers

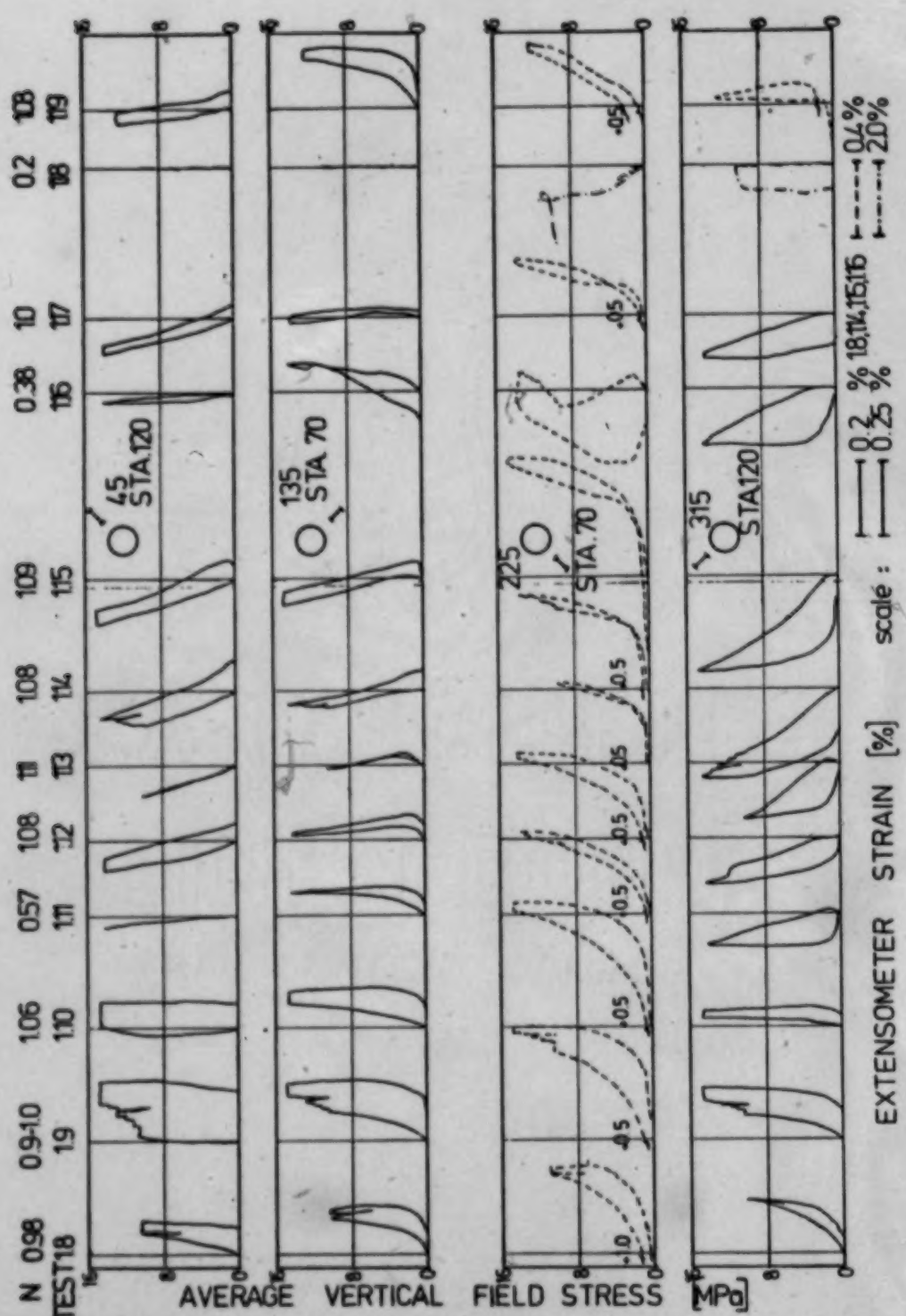

Figure 3.14 Field Stress Versus Average Radial Srain; Zone B, Diagonal Extensometers

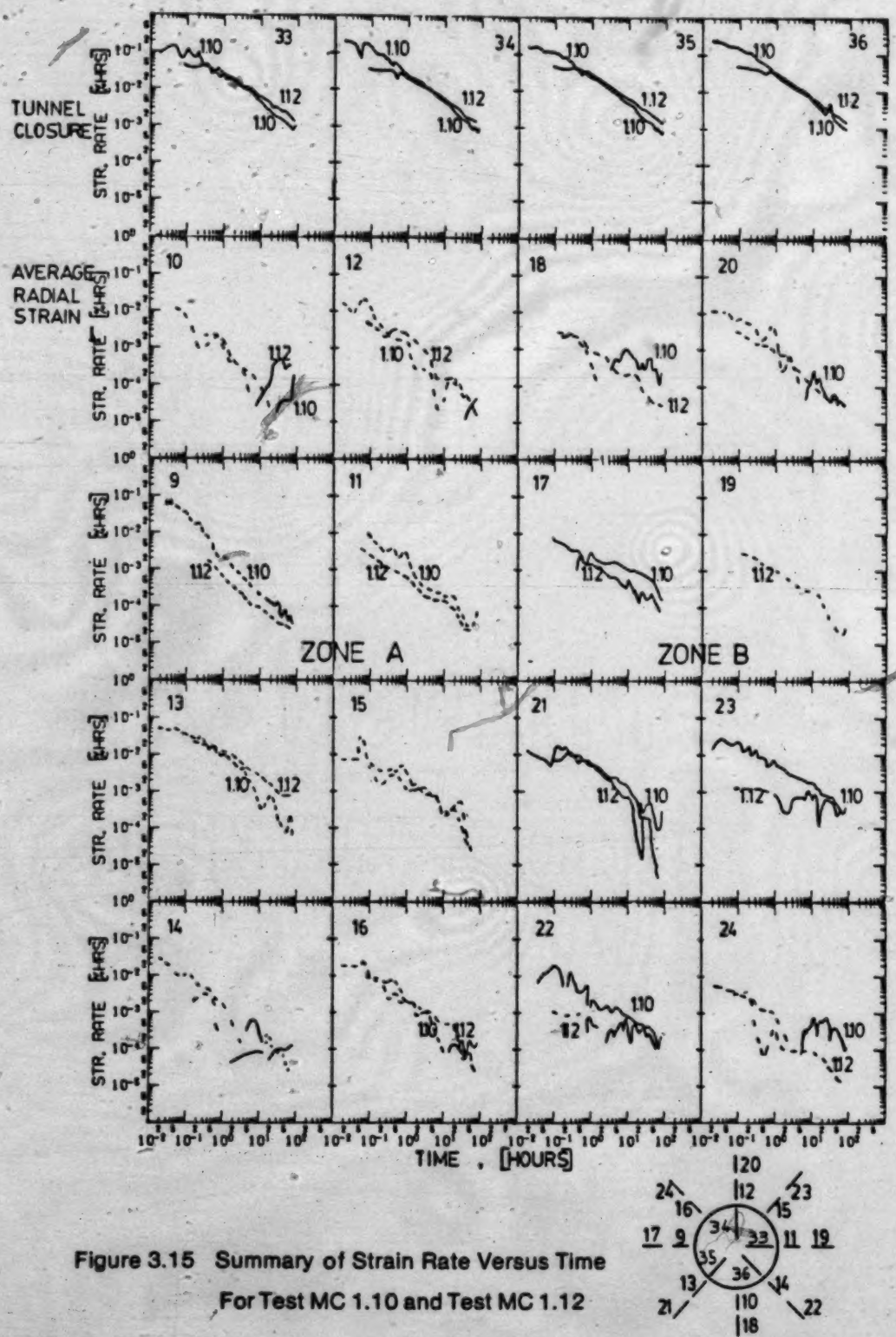

Figure 3.15 Summary of Strain Rate Versus Time For Test MC 1.10 and Test MC 1.12

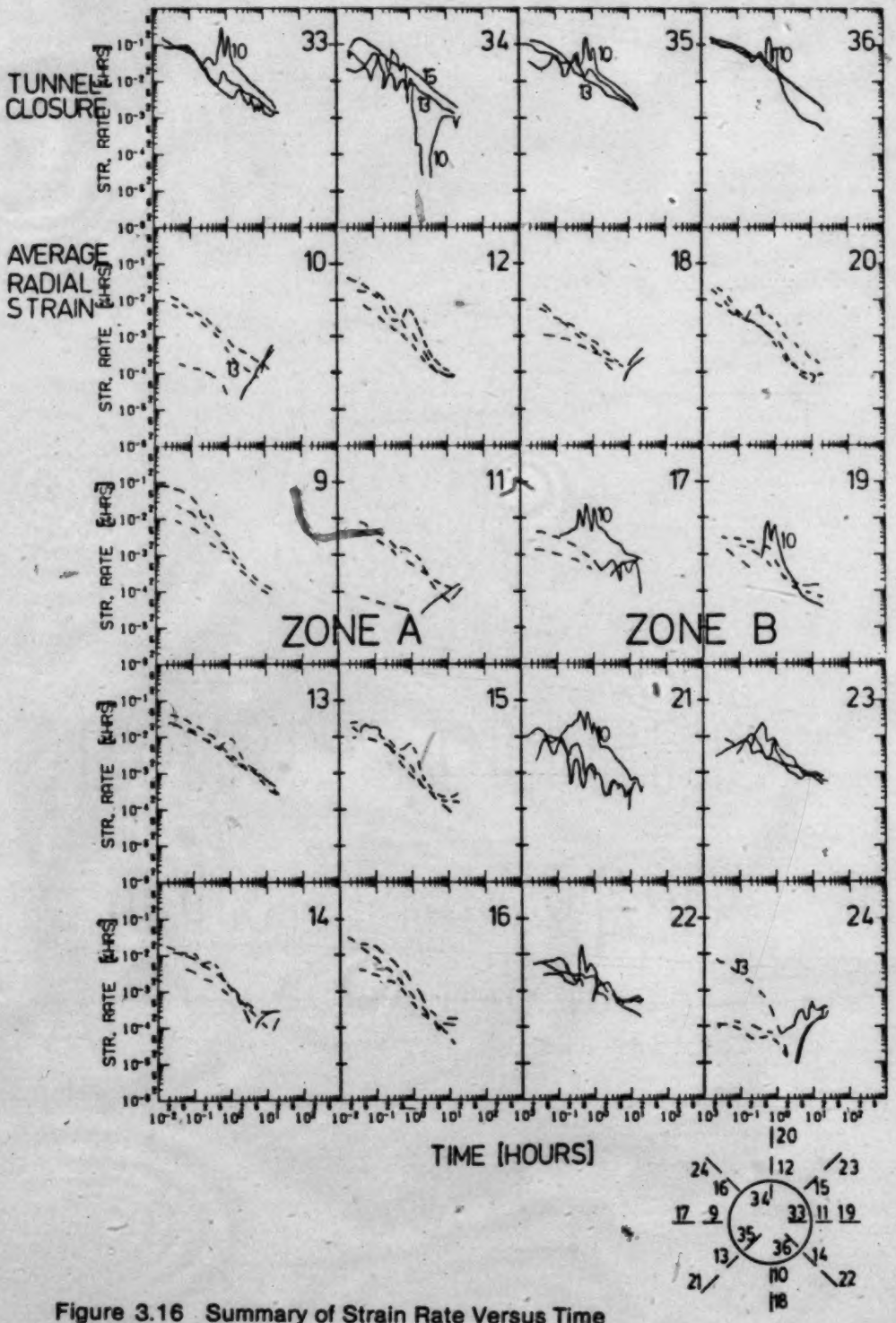

Figure 3.16 Summary of Strain Rate Versus Time For Test MC 1.9

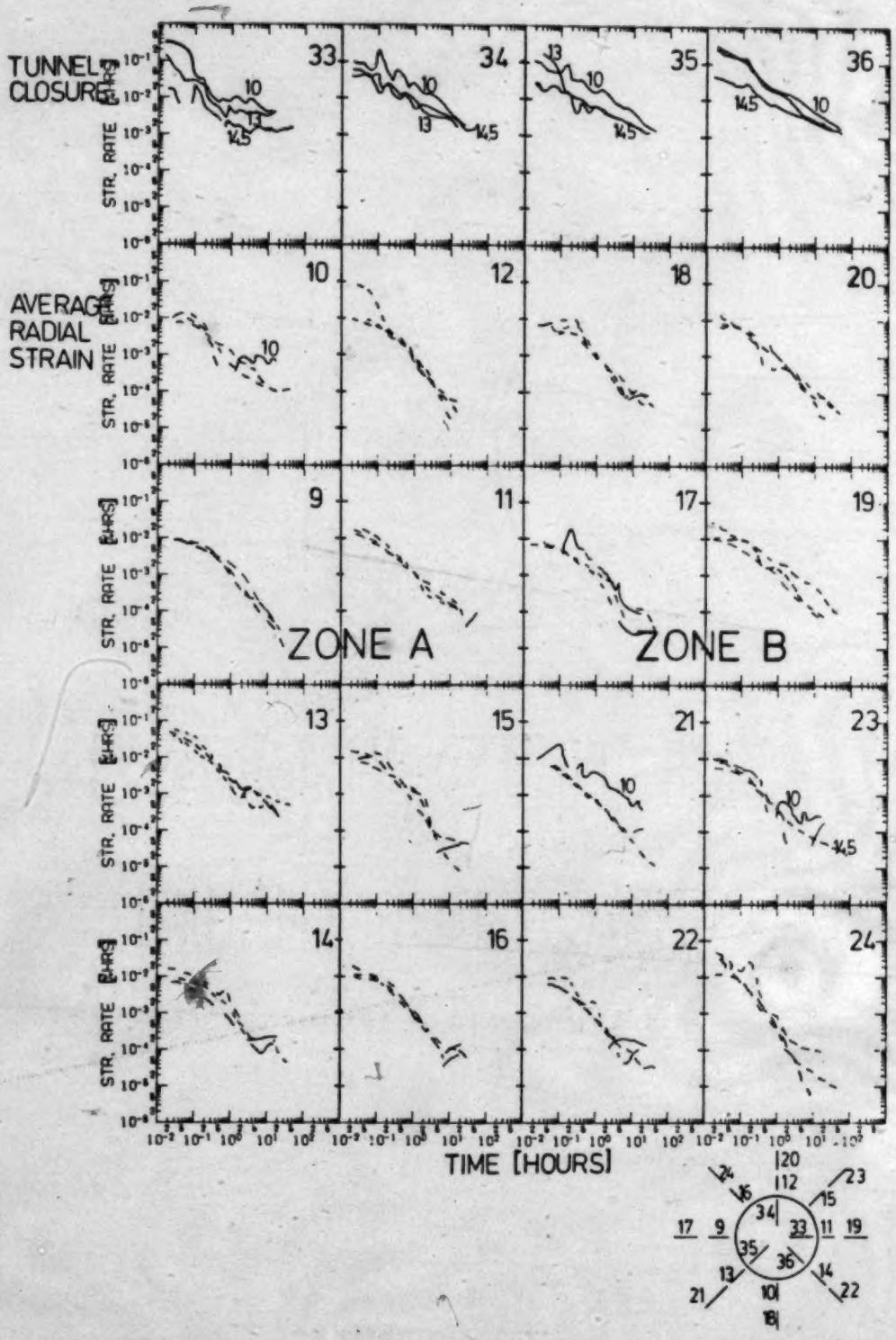

Figure 3.17 Summary of Strain Rate Versus Time For Test MC 1.14

4. CHAPTER IV

ANALYSIS OF TEST RESULTS

4.1 INTRODUCTION

The objective of this chapter is to simulate test results by analysis, when possible, and otherwise to qualitatively explain test behavior. A closed form solution with homogeneous elastic deformation properties and a finite element analysis with non-homogeneous elastic deformation properties simulates some test observations. The phenomenological model for a strain-weakening rock with time-dependent strength and deformation properties, developed by Kaiser and Morgenstern (1981a), provides the basis for qualitative discussion of the PST behavior. In the preliminary tests, consideration of scale effects lends understanding, too.

Tunnel closure, average radial strain and also average specimen strain have been simulated for tests MC 1.10, MC1.11 and MC 1.12. The associated stress distribution has also been calculated. These results provide an additional basis for qualitative discussion of test behavior.

The measured apparent deformation properties of the PST specimen, assuming homogeneous behavior, vary with stress magnitude and between different tests. Assuming values for Poisson's Ratio of between 0.3 and 0.35, the average Young's Modulus, ranges between 1800 MPa and 1000 MPa for fast loading and between 1560 MPa and 925 MPa for slow loading.

However, a significant reduction of the apparent deformation properties occurs with test MC1.11, as shown in Figure 3.4.

The linear elastic simulation provides a simple technique for evaluation of the trends observed in the deformation behavior of the specimen. Detailed analysis of the yielding mechanism may benefit by analytical formulation and attention to local deformation mechanisms including stress redistribution.

4.2 HOMOGENEOUS LINEAR ELASTIC SIMULATION

The predicted deformation behavior, assuming a homogeneous linear elastic formulation for the PST, is consistent with the observed deformation behavior of test MC1.10. The predicted deformation behavior changes significantly when varying the elastic parameters over the range of values back-calculated from test measurements. Assumption of elastic parameters back-calculated from tunnel closure measurements for test MC1.10 predicts the observed average radial strain behavior, particularly in Zone B.

For the boundary condition in the PST, the elastic tunnel closure depends more on the choice of the shear modulus, G, than on the choice of the bulk modulus, K. The elastic average radial strain changes with a variation in the shear or bulk modulus.

The theoretical tunnel closure and average radial strain assuming a homogeneous linear elastic material are shown in Figure 4.1. The upper graph in Figure 4.1 shows

two plots of normalized tunnel closure as a function of Young's Modulus and Poisson's Ratio. Tunnel closure is normalized to closure for a Young's Modulus of 1500 MPa and a Poisson's Ratio of 0.3. The solid line represents constant Poisson's Ratio and the dashed line represents a constant Young's Modulus. The center diagram shows average radial strain for three values of Young's Modulus, with a constant Poisson's Ratio. The bottom diagram shows average radial strain for three values of Poisson's Ratio. The average radial strain is calculated as a displacement difference between two points divided by the distance between the points, to correspond to the PST calculation procedure. In Figure 4.1, the average radial strain is shown for the two zones, A and B, and is plotted at a scale similar to Figures 3.11 to 3.14.

With a decrease in Young's Modulus, the tunnel closures increase and the average radial strains become more negative in Zone A and less positive in Zone B (Figure 4.1). The tunnel closures change insignificantly with a decrease in Poisson's Ratio however the average radial strains change markedly (Figure 4.1). Tunnel closure varies mostly with Young's Modulus and radial strain with Young's Modulus and Poisson's Ratio. Finally, reducing Young's Modulus and Poisson's Ratio over the range of interest in this test program produces increased tunnel closure with a correspondingly increased positive average radial strain.

The tunnel closure and average radial strain for a

Young's Modulus of 1500 MPa and Poisson's Ratio of between 0.3 and 0.35 is consistent with PST results prior to test MC1.11. For test MC1.10 at 10 MPa field stress, the measured tunnel closure is about 1.15% to 1.2% and the measured average specimen strain is about 0.35% to 0.4%. For tests MC1.8 to MC1.10, the back-calculated value of Young's Modulus ranges from 1500 to 1600 MPa and Poisson's Ratio ranges from 0.31 to 0.35. Finally, the elastic average radial strain for a Young's Modulus of 1500 MPa and a Poisson's Ratio of 0.35, shown in Figure 4.1, is consistent with linear segments of the observed average radial strain prior to test MC1.11. The similarity between calculated and observed radial strain is illustrated by comparing Figure 4.1 with Figures 3.11 to 3.14.

The assumption of linear elastic properties approximates the test results, however stress dependency is evident in the test results. For example, at low field stress, tunnel closure is typically nonlinear (Figure 3.9). Kulhawy (1975a) illustrates the importance of considering stress dependency in a study of stresses and displacements around an opening in rock. In particular, as the stress dependent modulus increases the tunnel displacement decreases. For simplicity, neglecting stress dependency allows evaluation of the change in the deformation behavior with test MC1.11.

Homogeneous elasticity fails to approximate test results after test MC1.10. The observed tunnel closure

increases and the average radial strain in Zone B tends toward more negative values after test MC1.10, as discussed in Chapter 3.

4.3 NON-HOMOGENEOUS LINEAR ELASTIC SIMULATION

In this simulation, a selected spatial arrangement of material deformation properties simulates the radial alteration of the rock mass in the PST specimen. By trial and error, various deformation properties are specified in annular regions near the tunnel until the calculated results are consistent with the observed tunnel closure, average radial strain and average specimen strain. In this way, the test observations provide the basis for selection of an appropriate non-homogeneous property distribution.

4.3.1 FINITE ELEMENT CALCULATION

A non-linear construction finite element program designed by Simmons (1980) was used for the non-homogeneous simulation. Economical calculations costing approximately two dollars per solution were obtained with this program. The program is designed for stepwise construction analysis. In addition, considerable flexibility is allowed for material specification (Simmons, 1980).

The finite element mesh used in the analysis is shown in Figure 4.2. It represents one plan quadrant of the PST specimen and consists of two types of isoparametric elements. Small size, eight node quadratic elements are

located near the tunnel, in the region with non-homogeneous deformation properties, and larger size, six node linear elements are located away from the tunnel (Figure 4.2). The quadratic elements satisfy interelement compatibility at corner and side nodes. Element stresses are evaluated at four Gauss points within each element and then extrapolated to the element nodes.

For homogeneous material, the finite element stresses and displacements are generally consistent with the values obtained from a closed form solution. At the tunnel wall, the average nodal tangential stress exceeds the closed form calculated tangential stress by 5% to 7%. Also, the nodal displacements exceed the closed form displacements by 3% to 4%. The closed form solution assumes an infinite distance to the specimen boundary. The two solution methods differ and hence some discrepancy may be anticipated. This discrepency is not significant for the purposes of this analysis.

4.3.2 SIMULATION OF PST MEASUREMENTS ASSUMING NON-HOMOGENEOUS ELASTIC BEHAVIOR

The predicted deformation behavior, assuming non-homogeneous elastic deformation properties in the annular region near the tunnel, is consistent with the measured time-independent deformation behavior observed in tests MC1.11 and MC1.12.

4.3.2.1 SIMULATION OF TEST MC1.12

The tunnel closure and average specimen strain calculated assuming a low value of Young's Modulus in the regions near the tunnel are shown in Figure 4.3. The table in Figure 4.3 shows the elastic properties specified for three regions around the tunnel. The elastic properties for region 1 are the same as values found to simulate test MC1.10. The graphs show the normalized tunnel closure and average specimen strain under hydrostatic field stress as a function of the size of the non-homogeneous region. The tunnel closure and average specimen strain are normalized to values calculated assuming homogeneous properties with a Young's Modulus of 1500 MPa and a Poisson's Ratio of 0.35.

The average radial strain assuming a non-homogeneous property distribution is shown in Figure 4.4. The material properties for Case I in Figure 4.4 correspond to those shown in Figure 4.3. The material properties for Case II differ from Case I in that the value of Poisson's Ratio is lower in the region near the tunnel. Thus, for Case II, the region near the tunnel is more compressible. The average radial strain calculation procedure shown for Zones A and B corresponds to the PST strain calculation. The radial strain for the homogeneous case corresponding to test MC1.10 (.ie. for $R^1=R^2=a$) is shown for reference as a dashed line.

The predicted tunnel closure after reducing the magnitude of Young's Modulus near the tunnel is consistent with the observed tunnel closure of test MC1.12. In Figure

4.3, the tunnel closure for R^2=1.5a and R^1=1.75a corresponds to a 30 to 35% increase in tunnel closure observed between tests MC1.10 and MC1.12 (Figure C5-3). However, the change in average specimen strain for R^2=1.5a and R^1=1.75 is about one half of the observed change. Moreover, the average radial strain for Zone A also tends toward more negative values, as shown for Case I in Figure 4.4. This is contrary to the test results as shown by comparing Figure 4.4 with Figures 3.11 to 3.14.

The predicted deformation behavior after reducing Poisson's Ratio in the region near the tunnel together with a reduction of Young's Modulus is consistent with the alteration of the observed behavior between tests MC1.10 and MC1.12. Case II shown in Figure 4.4, illustrates the effect of reducing both Young's Modulus and Poisson's Ratio. Reducing Poisson's Ratio by 15% insignificantly affects the shear modulus, but the bulk modulus decreases substantially, as illustrated by comparison of the deformation properties for Cases I and II, shown in Figure 4.4. Thus, for Case II, the predicted tunnel closure decreases by about 5%, a relatively insignificant change as shown in Figure 4.3 (R^2=1.5a,R^1=1.75a). In addition, the change in average specimen strain increases to about 15% as shown in Figure 4.3, which is closer to the observed 20% alteration. Finally, the calculated average radial strain for Case II tends toward compression in Zone A and extension in Zone B relative to the homogeneous behavior. This is comparable to

the observed trend between tests MC1.10 and MC1.12. The similarity of the radial strain for Case II and test results is illustrated by comparing the radial strain shown in Figure 4.4 to the results shown in Figures 3.11 to 3.14.

4.3.2.2 SIMULATION OF TESTS MC1.11 AND MC1.16

The non-homogeneous property distribution for Case II also simulates the tunnel closure, the average radial strain and, to a lesser degree, the average specimen strain for test MC1.11. Also, the homogeneous formulation, assuming elastic property values back-calculated from test MC1.12, simulates the tunnel closure and average specimen strain for test MC1.11. For both assumptions, the calculated tunnel closure is consistent with measured values for test MC1.11, except for the variable results observed for the diagonal closures. However, the homogeneous formulation is not consistent with the observed radial strain behavior. The deformation property distribution and average radial strain for a homogeneous case, Case III, and the non-homogeneous case, Case II, are shown in Figure 4.5. Comparison of the calculated radial strain shown in Figure 4.5 and the measured radial strain shown in Figures 3.11 to 3.14 illustrates the similiarity between the non-homogeneous formulation and test results. In particular, the non-homogeneous formulation simulates the positive radial strain along the maximum load axis in Zone A.

The property distributions given in Figure 4.5 fail to

predict the deformation behavior of test MC1.16. For a field stress of 10 MPa and a field stress ratio of 0.4, the calculated tunnel closure is about 2.1 - 2.2% for the maximum loading axis and about 0.02% for the minimum loading axis. For the comparable condition in test MC1.16 the measured closure is about 3% and 0.25% respectively. Moreover, reducing the elastic parameters in the region near the tunnel to 60% of the values in region 1 produces a maximum tunnel closure of 2.5%.

Assumption of an elliptical shaped non-homogeneous region apparently reduces the amount of tunnel closure. Thorough analysis of the shape effect requires modification of the finite element mesh shown in Figure 4.2. However, calculations using this mesh indicate that the ellipse orientation influences the tunnel closure in a non-hydrostatic field stress. In particular, for N=0.4, when the major axis of an elliptical shaped non-homogeneous region coincides with the minimum loading axis, less tunnel closure occurs as compared to a circular region. In addition, when the major axis of the ellipse coincides with the maximum loading direction, even less tunnel closure occurs.

Any discontinuity around the tunnel influences the tunnel closure. Studying the stresses and displacements around an opening in rock containing a planar elastic discontinuity, Kulhawy (1975b) shows the effect of the orientation of a soft planar discontinuity under

non-hydrostatic field stress. When the planes of the discontinuity and the initial minimum principal stress coincide, the maximum principal stress decreases and the least inward displacements occur relative to when the discontinuity is offset 90°. Also, these changes are very significant with initial softening in the discontinuity. Thus, any discontinuity will markedly alter the behavior (Kulhawy,1975b). In a companion paper, Kulhawy (1975c) shows that stress-dependency of the discontinuity significantly affects the opening behavior. Thus, the discontinuity must be modelled correctly.

These results illustrate the importance of correctly identifying the deformation mechanism in order to predict the deformation behavior of an opening. A non-hydrostatic field stress causes non-uniform tunnel closure for a circular non-homogeneous region. In addition, an elliptical non-homogeneous region and elastic or inelastic discontinuities create non-uniform stress distributions and tunnel closures. Moreover, the tunnel closure may not be simply implied since non-uniform tunnel closure may occur due to radially symmetric property distribution as well as due to non-hydrostatic field stress.

4.3.2.3 CALCULATED STRESS DISTRIBUTION

The average nodal values for the minimum and maximum principal stress and deviatoric stress for a homogeneous and a non-homogeneous property distribution at 10 MPa field

stress are shown in Figure 4.6. The homogeneous case, with a Young's Modulus of 1500 MPa and a Poisson's Ratio of 0.3, shown in Figure 4.1, corresponds to the deformation behavior of test MC1.10. The non-homogeneous case, Case II in Figure 4.4, corresponds to the deformation behavior of test MC1.12. The stress distribution for the non-homogeneous Case II exhibits a lower deviatoric and confinement stress level adjacent to the tunnel with a correspondingly greater deviatoric and confinement stress level away from the tunnel.

Compatibility of deformations at the contacts between each region creates a discontinuity in the average nodal stress distributions, particularly for the maximum principal stress distribution. The curves for Gauss point stresses illustrate the variation of the stresses within each region. In particular, the 'ground cylinder' condition described by Terzaghi (1946) occurs within each elastic region and the stresses increase closer to the tunnel. In the specimen, greater softening would likely occur nearer the tunnel, perhaps in a continuous manner and stresses would then vary accordingly.

4.4 PHYSICAL BEHAVIOR OF COAL

The time-dependent failure process of coal specimens has been investigated by Kaiser and Morgenstern (1978). Figure 4.7 shows the schematic stress-strain curve developed by Kaiser and Morgenstern (1978) to illustrate, in a

phenomenological manner, the various processes of time-dependent strength and deformation behavior. Figure 4.8 (Kaiser and Morgenstern, 1981a) shows a simple version of a phenomenological model with mechanical elements which simulates the deformational behavior of Zones A, B and C, shown in Figure 4.7. The model is shown to simulate published test results from creep tests, relaxation tests and variable strain rate tests (Kaiser and Morgenstern, 1981a).

The phenomenological model consists of time-independent units with elastic and yield elements (Figure 4.8). A number of A - and B - units with different properties arranged in parallel would simulate nonlinear, stress dependent behavior; typical of this coal. At stress levels prior to failure, Zone A in Figure 4.7, and below the long term strength, deformation behavior of a rock specimen is rate-dependent and load transfers from the B - units to the A - units in time. For stress levels at yielding of some A- and/or B - units, friction sliding or strength loss occurs in some yield elements and load transfers to other units. The load transfer causes more overall deformation in the model.

4.5 PHENOMENOLOGICAL BEHAVIOR AND THE PST BEHAVIOR

The phenomenological model given by Kaiser and Morgenstern (1981a) and the elastic simulation methods shown in this chapter provide a basis for qualitative discussion

of the observed PST deformation behavior. Likely, finite element formulation could be used to apply the phenomenological model, and finally such a method will be necessary for analytical verification of any qualitative evaluation.

In the finite element formulation, each element may exhibit a particular behavior depending on the element deformation character and the inter-element compatibility. A rock element experiencing yielding transfers load to neighbouring rock elements. In general, for a physical system in which yielding and strength loss may occur, stress redistribution should minimize stress differences and reduce stress concentrations. Therefore, deformation compatibility would primarily influence simulation of this deformation process.

4.5.1 TIME-INDEPENDENT YIELDING AND PROPERTY ALTERATION

In the tests on the PST specimen with $N<1$, radially symmetric loading rates, stress concentrations along the minimum load axis and lower confinement stress in general leads to stress redistribution, as illustrated by test measurements shown in Chapter 3. On the basis of a comparison of the non-homogeneous simulation and test observation, discussed in section 4.3, a non-homogeneous stress distribution exists during test MC1.11.

In the simulation method, softer rock elements correspond with a "yielded" or "softened" zone near the

tunnel. The phenomenological model indicates that yielding of some A - and/or B - units cause an alteration of the model stiffness. The alteration of stiffness occurs in response to displacement induced overstressing, thereby activating the stress dependent yield elements.

In addition, test results indicate radially symmetric alteration of deformation behavior, as described in section 3.6. More time-independent closure occurs along the 90-270 axis after test MC1.11. Perhaps the observed radial symmetry could be simulated by techniques incorporating the phenomenological model.

4.5.2 TIME-DEPENDENT YIELDING AND PROPERTY ALTERATION

In test MC1.9, more tunnel closure and positive radial strain occur with slow loading rates.

The rate dependent behavior of the phenomenological model depends on the load transfer from B - units to A - units, controlled by the viscous element in the B - unit. For slow loading, more load is taken by A -units as compared to fast loading.

After test MC1.11, the slow loading deformation modulus and the size of the delayed EO decrease. The closure rate behavior changes slightly. Assuming the slow loading modulus represents a time-independent response (.ie., the B - units have transferred load to the A -unit without extensive yielding), reduction of the slow loading modulus would correspond with an alteration of the A -unit property

distribution. Reduction of the delayed EO could represent alteration of the B -unit property distribution. Slight alteration of the closure rate may represent an insignificant change in load level on the viscous element.

Test results discussed in Chapter 3 indicate a non-homogeneous alteration of the PST specimen after test MC1.11. Radial strain and strain rate behavior change with more negative strains occurring away from the tunnel. Also, delayed radail strains decrease, especially in Zone A. The non-homogeneous formulation approximates the yielding near the tunnel. Coupling of a non-homogeneous elastic and a visco-elastic formulation may well approximate the observed alteration of the delayed deformation behavior.

4.5.3 SCALE EFFECTS

Scale effects may often concern tunnel designers, particularly when they are extrapolating results of small size test tunnels to the prediction of larger size tunnel behavior. Enlarging the tunnel size in the PST causes increased time-dependent closure and more total closure, as discussed in Chapter 3.

The fracture in the test specimen, shown in Figure 2.4 is a fair example of a large scale defect which may influence the specimen behavior. Enlarging the tunnel size effectively relocates the fracture nearer to the tunnel. Thus the macro-scale conditions change test MC1.7.

The compressive strength and deformation behavior of

coal specimens depends on specimen size. In an extensive literature study, Heuze (1980) found that the compressive strength of coal specimens decreases substantially with an increase in the specimen size. In addition, deformability of test specimens may decrease in a similiar manner, however inconsistencies in the reported results precludes positive conclusions about deformability (Heuze, 1980).

Increasing the tunnel size effectively increases the length of rock elements located at the tunnel wall. For a given tangential angle, enlarging the tunnel size by 25% also increases the arc length of the tunnel surface.

Hence, yielding or strength loss for unconfined rock elements at the larger size tunnel wall would occur at lower field stress as compared to the smaller size tunnel. Yielding would cause stress redistribution with an associated reduction of the deformation modulus. Apparently, this process occurs rapidly since closure rate parameters change insignificantly in the latter part of the test program.

Scale effects may influence tunnel behavior as the EO size changes. Direct correlation of analytical methods with tunnel performance may incorporate scale effect.

4.6 CONCLUSIONS

1. A homogeneous elastic formulation predicts deformation behavior that is consistent with results for test MC1.10.

2. A non-homogeneous elastic formulation with an annular region of reduced stiffness around the tunnel predicts deformation behavior that is consistent with results for test MC1.12. Also, the non-homogeneous formulation predicts deformation behavior that is consistent with results for test MC1.11, the test with a non-hydrostatic field stress. Consideration of loading path effects for the specification of material properties may improve predictions. Alteration of deformation behavior evidently proceeds rapidly since the elastic property distributions are the same for the simulation of tests MC1.11 and MC1.12.
3. To simulate test results in the non-homogeneous simulation, Young's Modulus and Poisson's Ratio must be reduced in the annular region around the tunnel. Thus, the stiffness of this region is reduced.
4. Caution is neccessary when interpreting tunnel closure measurements since non-uniform tunnel closure may occur due to a radially symmetric property pattern as well as due to non-hydrostatic field stress. Consideration of extensometer results improves evaluation of deformation mechanisms.
5. The phenomenological model developed by Kaiser and Morgenstern (1981) provides a basis for explaining the correlation between a linear elastic formulation and test observation. In particular, in terms of the model, a rock element may yield under stress with an associated

alteration of the stiffness character. The non-homogeneous linear elastic technique presented here predicts deformations that are consistent with the alteration of the deformation behavior observed with test MC1.11. The PST specimen manifests an elastic behavior and local yielding leads to a regional alteration of stiffness character. Thus, the phenomenological model seems a convenient characterization of the observed behavior.

6. Large and small scale effects may influence the preliminary test results.

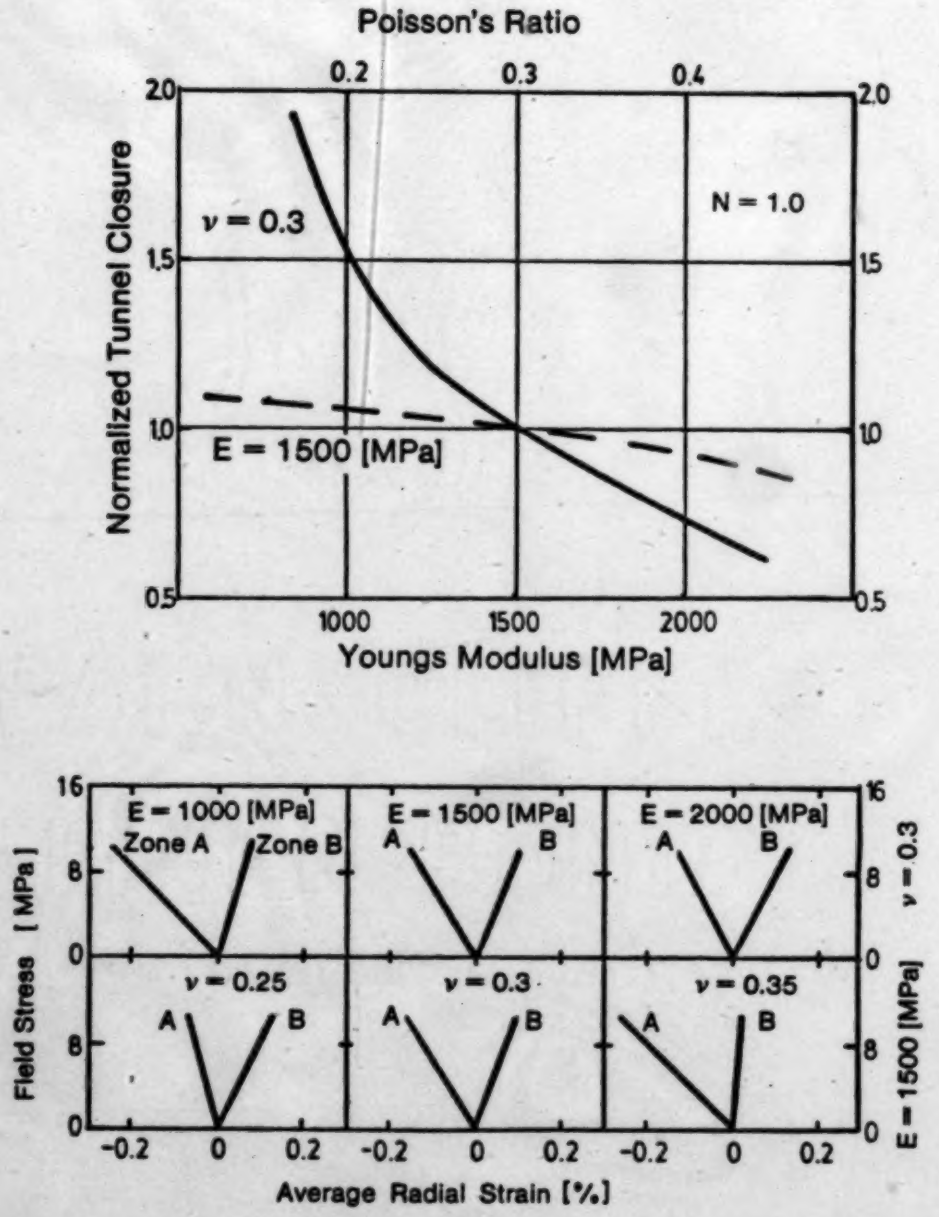

Figure 4.1 Tunnel Closure and Average Radial Strain Assuming a Homogeneous Linear Elastic PST Specimen.

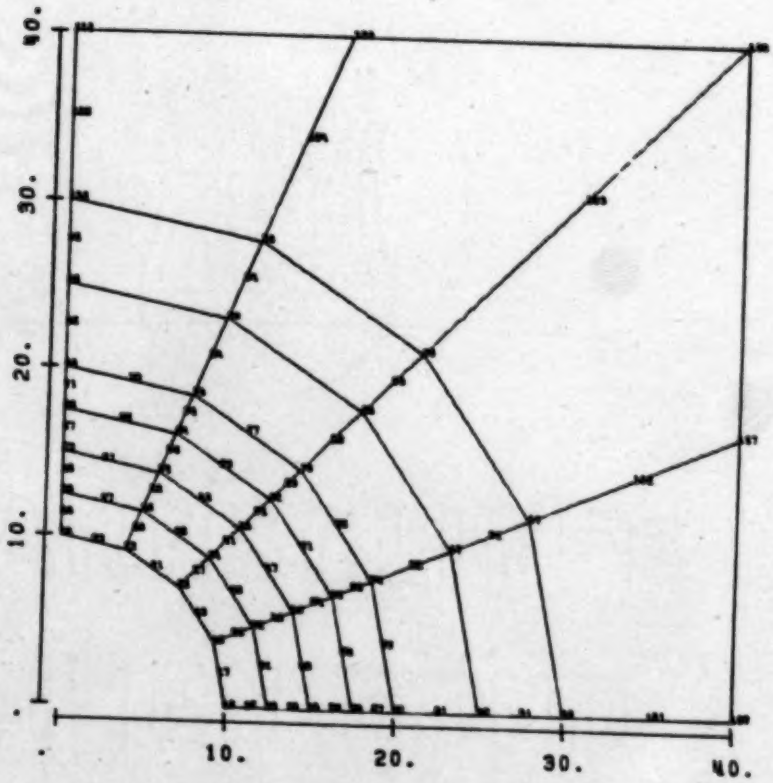

Figure 4.2 Finite Element Mesh

CASE I	MATERIAL PROPERTIES			
REGION	E [MPa]	ν	K [MPa]	G [MPa]
1	1500	0.35	1666	555
2	1200	0.35	1333	444
3	800	0.35	889	292

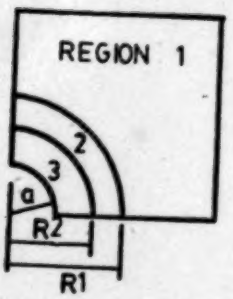

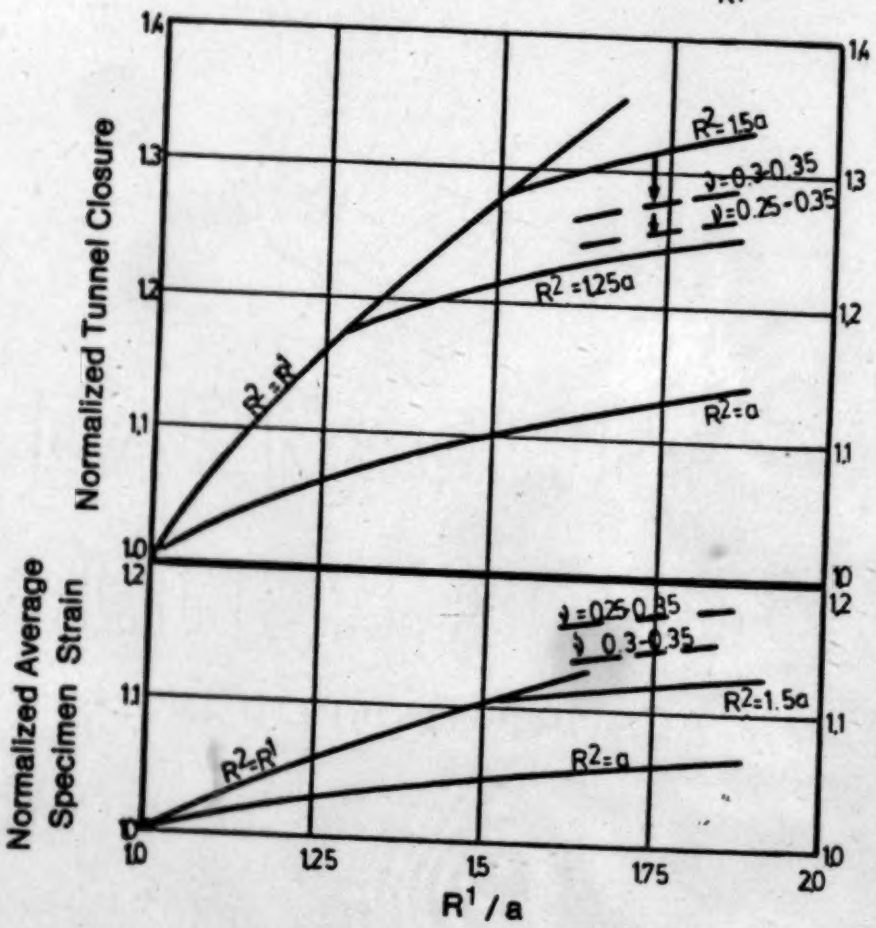

(Note: Measurements are normalized to the Homogeneous Elastic Values with the Material Properties shown for Region 1)

Figure 4.3 Tunnel Closure and Average Specimen Strain Assuming a Non-Homogeneous Linear Elastic PST Specimen.

CASE I	MATERIAL PROPERTIES			
REGION	E [MPa]	ν	K [MPa]	G [MPa]
1	1500	0.35	1666	555
2	1200	0.35	1333	444
3	800	0.35	889	292

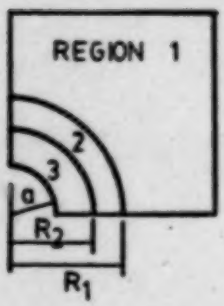

CASE II	MATERIAL PROPERTIES			
REGION	E [MPa]	ν	K [MPa]	G [MPa]
1	1500	0.35	1666	555
2	1200	0.325	1142	452
3	800	0.3	666	308

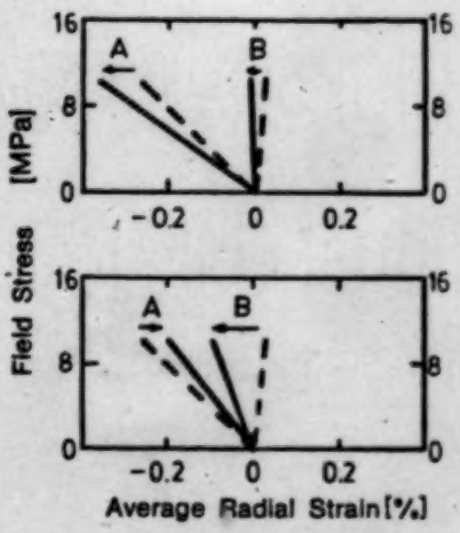

CASE I
$R_1 = 1.75a$
$R_2 = 1.5a$

CASE II
$R_1 = 1.75a$
$R_2 = 1.5a$

Figure 4.4 Average Radial Strain Assuming a Non-Homogeneous Linear Elastic PST Specimen

CASE II	MATERIAL PROPERTIES			
REGION	E [MPa]	ν	K [MPa]	G [MPa]
1	1500	0.35	1666	555
2	1200	0.325	1142	452
3	800	0.3	666	308

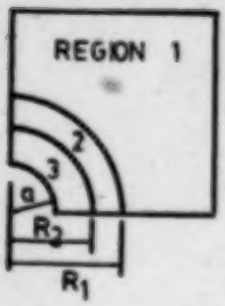

CASE III	MATERIAL PROPERTIES			
REGION	E [MPa]	ν	K [MPa]	G [MPa]
1	1150	0.35	1250	426

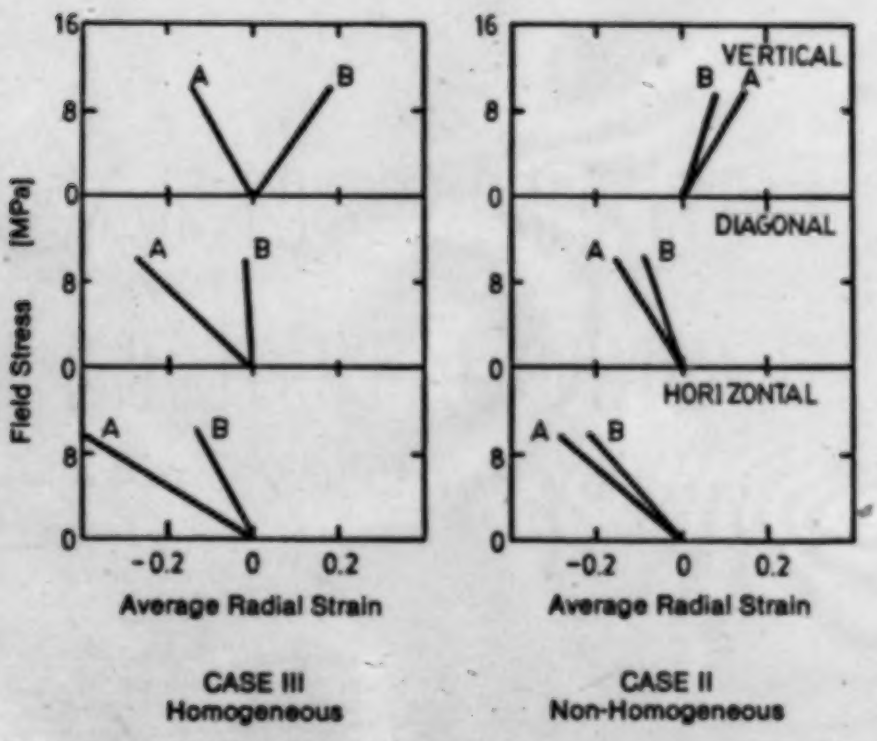

Figure 4.5 Average Radial Strain for a Homogeneous Case and a Non-Homogeneous Case; with a Field Stress Ratio of 0.6.

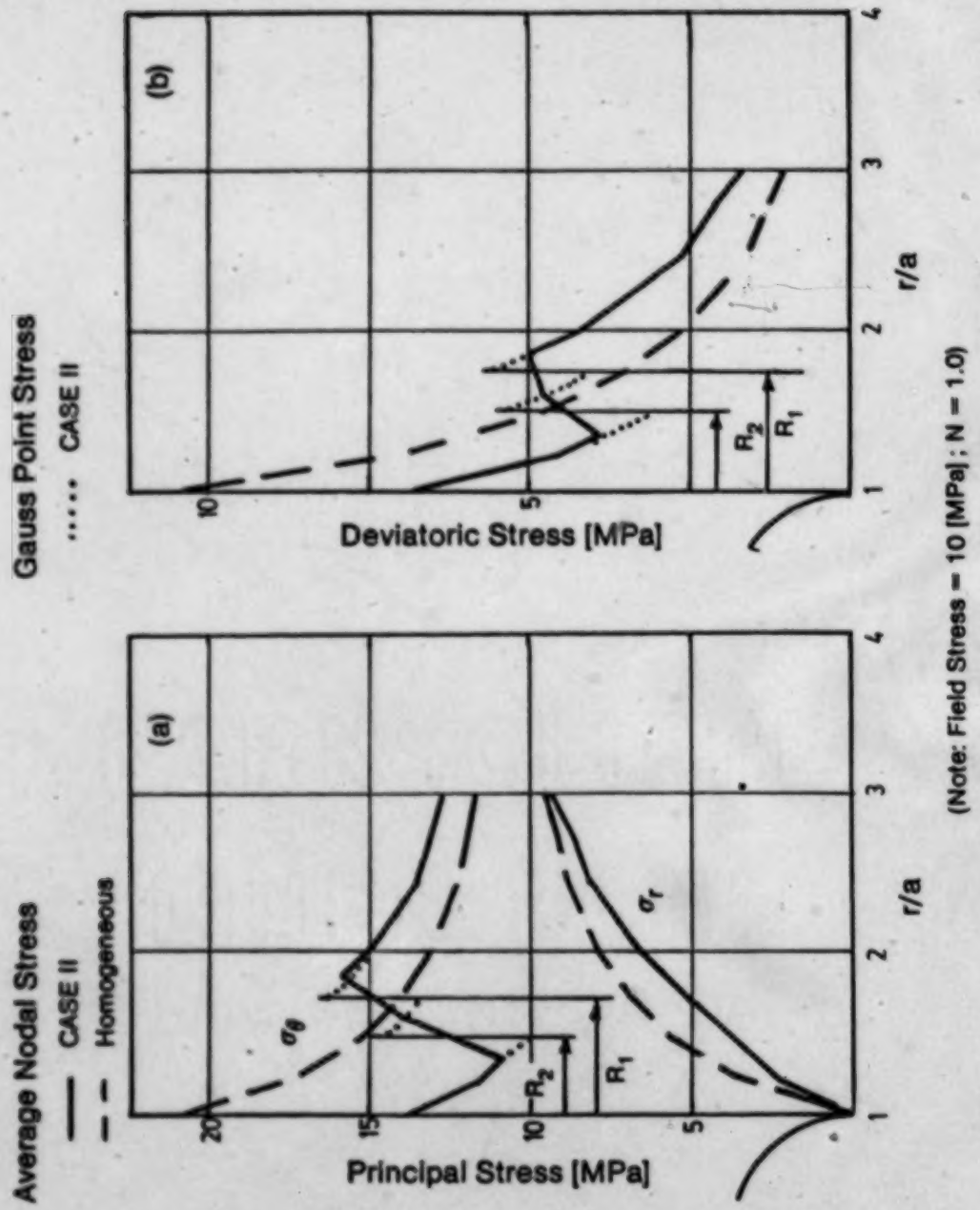

Figure 4.6 a. Homogeneous and Non-Homogeneous Linear Elastic Maximum And Minimum Principal Stress Distribution.
b. Homogeneous and Non-Homogeneous Linear Elastic Deviatoric Stress Distribution.

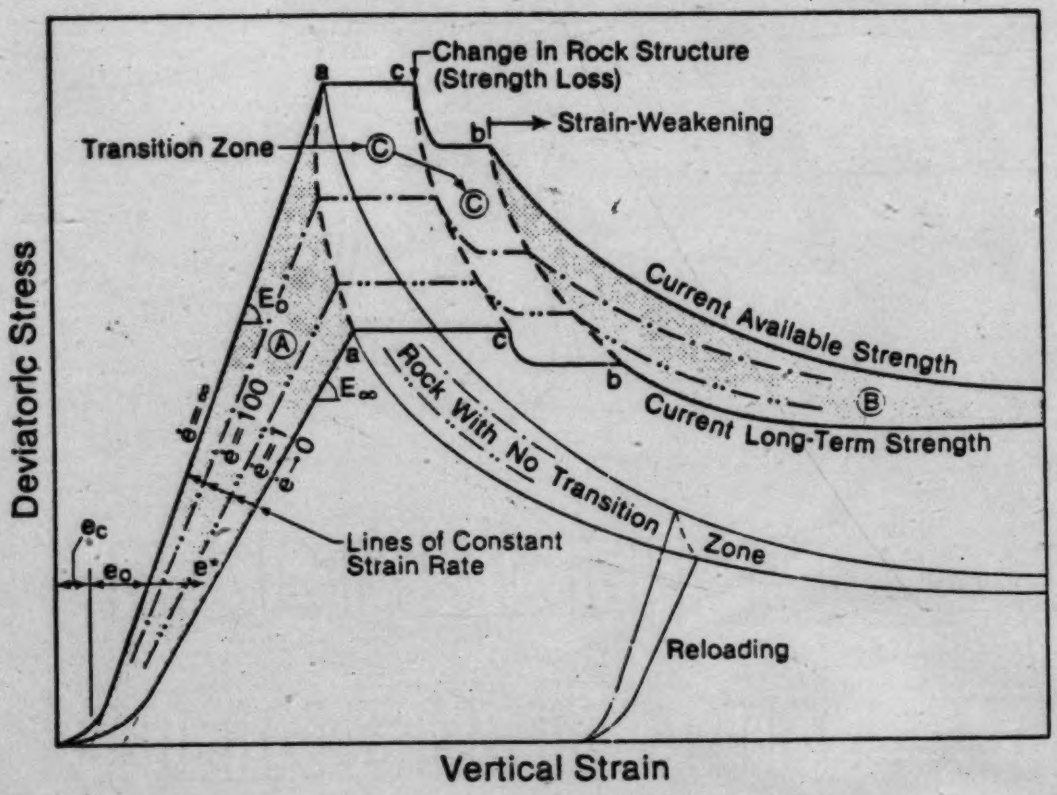

Figure 4.7 Schematic Stress-Strain Diagram of Rock (Kaiser and Morgenstern, 1978)

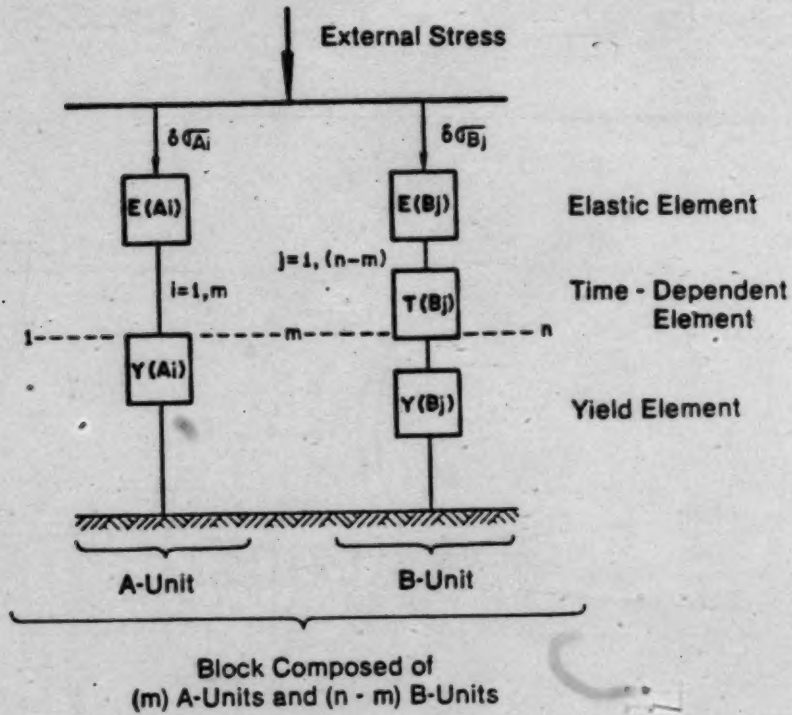

Schematic diagram of model

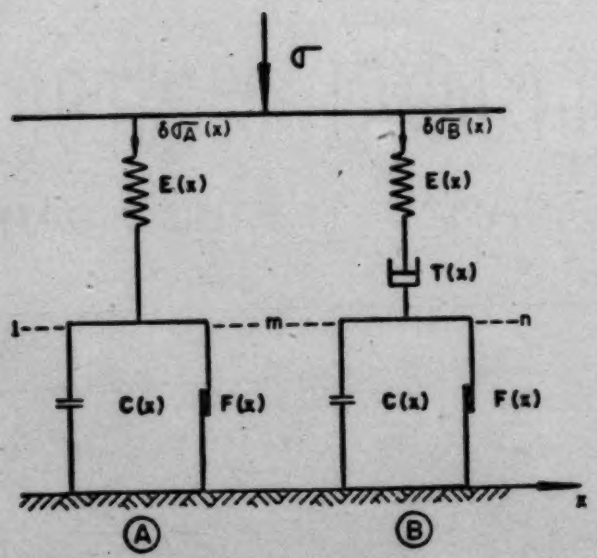

Figure 4.8 Schematic Diagram of Phenomenological Model and a Simple Version of the Model With Mechanical Elements (Kaiser and Morgenstern, 1981)

5. CHAPTER V

CONCLUSIONS

5.1 STATEMENT OF THE TEST STUDY

A Process Simulation Test (PST) facility has been used to study the response of one small diameter unlined tunnel in a naturally jointed coal specimen. Pre-failure deformation processes, some associated rate effects and stress redistribution have been investigated.

In response to a series of repeated loadings, the condition of the block of coal changed, particularly near the tunnel. However, the tunnel remained self-supporting with total tunnel closures of about 3.5% to 4%.

Tunnel closure, average specimen strain and average radial strain measurements as well as visual inspection of the tunnel during testing showed the alteration of the rock mass near the tunnel. The test specimen displayed time-independent and time-dependent deformation behavior which was nonlinear and stress-dependent. However, linear elastic and linear viscoelastic formulations adequately approximated some deformation results.

The deformation behavior of the test specimen changed during the test program. The greatest alteration in deformation behavior occurred with test MC1.11, a test with a non-hydrostatic field stress. This lead to an expansion of the equivalent opening (EO) size and shape with an associated decrease in the magnitude of the delayed

equivalent opening. Moreover, closure rate parameters changed only slightly for tests with a hydrostatic field stress. The stress redistribution was caused by "yielding" or "weakening" of rock elements near the tunnel wall.

Inappreciable deformational change occurred after the second test with non-hydrostatic field stress and after the specimen ruptured along jointing. In particular, tunnel closures and closure rates changed insignificantly, but radial strains changed slightly, especially in broken zones near the tunnel. Thus, the extensometers responded to local deformation processes. The stress redistribution process stabilized and was only reactivated by stress concentrations not previously experienced by the specimen. Moreover, the rupture inappreciably affected the immediate and delayed tunnel closure response.

The deformation behavior of this test specimen depends on loading history (.ie. loading rate, stress increment, stress path and field stress magnitude). Therefore, loading history must be considered in comparisons of deformation results. Superposition of deformation due to isotropic and deviatoric stresses complicated the evalution of history dependent behavior.

Long lasting and changing elevated field stresses compressed the test specimen slightly. However, relatively insignificant irrecoverable strains remained in comparison to the deformation changes that occurred with a change in the loading rate or field stress ratio.

After increasing the tunnel diameter by 25%, the magnitude of the delayed EO increased with an associated increase in the immediate tunnel closure. However, test history, material nonlinearity and scale effects complicated the interpretation of the preliminary tests.

5.2 SIMULATION OF THE SPECIMEN BEHAVIOR

A linear elastic formulation was used to simulate the deformation behavior for the tests prior to test MC1.11. A non-homogeneous elastic analysis was used to simulate the alteration of the deformation behavior due to the first low confinement test.

In the non-homogeneous elastic analysis, the magnitude of both Young's Modulus and Poisson's Ratio was reduced in an annular region near the tunnel. This adequately simulated the effect of the initial low confinement episode. The stress distribution was calculated.

This analysis illustrates the necessity of considering strain results for simulation of deformation behavior. Consideration of the shape of the non-homogeneous region and the loading paths of rock elements may improve simulation of the tests with a non-hydrostatic field stress.

5.3 MODES OF DEFORMATION

The following modes of deformation affect the deformation behavior of this test specimen in response to

increasing and constant elevated field stress:

1. local macro-scale brittle rupture at the tunnel wall or local strength loss and strain-weakening behavior;
2. disintegration and fracturing or local yielding;
3. compaction of the test specimen;
4. loosening, in particular, slip and adjustment along joints and fractures;and
5. squeezing due to rheological behavior.

Evidently, swelling does not contribute to the observed deformation, at least at the scale of the above modes of deformation.

The character of the local macro-scale rupture illustrates the effect of local conditions on the deformation behavior. Prior to the local rupture along the 315 radius at the tunnel wall, the closure stiffness is greater and the propensity for delayed closure is lower than for other diameters. Then, with rupturing, immediate and delayed closures increase, a crack appears on the tunnel wall and coal dust appears in the tunnel. However, the rate of decrease of the closure rate increases quickly. Incidently, this is generally consistent with the behavior observed upon increasing the tunnel size. In particular, the immediate and delayed equivalent openings increase and short-term closure rates occur. Extensometers along the 315 radius only respond to the rupture later in test MC1.10, in much the same fashion as in test MC1.12. In particular, more extension strain occurs away from the tunnel and more

compression strain occurs near the tunnel. Thus, the local rock mass condition affects the specimen behavior.

The gradual, active yielding process has been discussed by Kaiser and Morgenstern (1981). In particular, in a test with a non-hydrostatic field stress and at a stress that causes active yielding, the delayed tunnel closure rates increase and continue for a longer duration than otherwise. The closure rates may stabilize to values observed prior to the onset of yield.

The deformation behavior in test MC1.12 differs from previous tests. In particular, the size of the time-independent EO increases by 25% while the magnitude of the delayed EO decreases by 10%. The delayed closure rates also decrease slightly, thus the propensity for delayed closures decrease. This yielding process is consistent with the active yielding process described by Kaiser and Morgenstern (1981).

The predicted deformation using the same non-homogeneous elastic properties is consistent with results for tests MC1.11 and MC1.12. Rock elements near the tunnel must have a lower load resistance. The radial strain and strain rate exhibit extension away from the tunnel. Therefore, short duration loading in test MC1.11 may be associated with a rapid fracturing and disintegration in the rock mass adjacent to the tunnel.

The EO size changes insignificantly in the later tests with non-hydrostatic field stress. The extensometers

indicate some local alteration of response. However, the local yielding processes evidently do not affect the tunnel closure behavior.

The physical character of the disintegration and fracturing is evident during testing. In particular, the visual texture of the tunnel wall changes over the test program. Also, for example, in test MC1.18, a block of coal fell from the tunnel wall at only 2 MPa field stress. However, no macro-scale ruptures occur at the tunnel wall. Therefore, smaller scale processes must lead to "yielding" or "weakening" of the rock at the tunnel wall and this must proceed rapidly. The exact processes may vary around the tunnel however the overall behavior is generally consistent. Finally, the insignificant alteration in later tests may occur due to the combination of higher confinement away from the tunnel which inhibits this process and due to lower departure from previously experienced stress levels.

The deformation measurements indicate compaction of the test specimen. In particular, on average for tests with hydrostatic field stress, about 0.4% irrecoverable tunnel closure and about 0.1% irrecoverable specimen strain remain after each test. Also, on average, about 0.1% irrecoverable radial strain occurs except after tests with a non-hydrostatic field stress. Compaction of the specimen insignificantly affects the modes of deformation outlined above. In particular, test measurements are repeatable except when yielding near the tunnel caused stress

redistribution.

The difference between irrecoverable tunnel closure and average specimen strain in tests with N=1 indicates some loosening occurs in the rock at the tunnel wall. Slip and adjustment on joint surfaces and perhaps even failure at some locations may be anticipated as the field stress is applied to the specimen. The effect of loosening insignificantly affects the specimen behavior, at least in comparison with the local yielding processes.

The squeezing mode evidently causes the delayed deformation behavior. However, due to the loading conditions in the PST, superposition of deformation due to isotropic and deviatoric stresses complicates evaluation of the rheological behavior.

5.4 PRACTICAL IMPLICATIONS

The practical implications of these test results generally apply to tunnels and particularily to tunnels in strain-weakening rock masses with time-dependent strength and deformation properties.

The PST illustrates the importance of correct monitoring for evaluation of deformation behavior. The extensometers respond to local deformation processes and to enhance evaluation of the measurements, the local condition of the rock mass should be known. Tunnel closure measurements may respond poorly to the onset of yielding processes.

The loading history generally influences the tunnel behavior and in particular local processes affect the integrity of the tunnel. Local rupture in test MC1.9 and local yielding in test MC1.11 generally cause stress to redistribute to zones away from the tunnel. Thus, stabilizing processes in real tunnels may depend on this deformation behavior.

For this test series, the time-dependent tunnel behavior depends primarily on loading history. Therefore, when evaluating deformations of a tunnel in similiar rock masses, loading history may be important.

The deformation behavior of the "softened" or "weakened" rock mass in the PST specimen has been simulated using a non-homogeneous linear elastic formulation. Perhaps, delayed deformation behavior may be approximated by assuming such non-homogeneous character coupled with time-dependent deformation parameters. Local processes create this non-homogeneous character. Active yielding processes would cause more tunnel closure. Perhaps, longterm evaluation of real tunnels may be accomplished by considering the non-homogeneous character evident in the PST results.

The characteristic behavior of this specimen has been simulated by considering the nature of the deformation behavior in the 'ground cylinder'. In particular, local deformation processes control stress redistribution. For example, in the PST specimen, local yielding and weakening

processes control stress redistribution. In general, consideration of the deformation in the 'ground cylinder' is necessary to proper understanding of the tunnel behavior. Then, with proper consideration of initial and boundary conditions, derivation and solution of the governing physical equations may proceed rationally.

Analysis of tunnel deformation behavior depends on appropriate evaluation of tunnels Analysis of real tunnel behavior may benefit by practical application of the results presented here.

REFERENCES

AFTES 1978. Analysis of tunnel stability by the convergence confinement method. Underground Space, Vol. 4, No. 6, 1980, pp. 297-311.

Brusau, C.T., Alred, G.J. and Olui, W.E. 1976. Handbook of technical writing. St. Martins Press, N.Y. 571p.

Chou, P.C., and Pagano, N.J. 1967. Elasticity. Van Nostrand. 300p.

Coates, D.F. 1970. Rock mechanics principles. Mines Branch Monograph 874. Mining Research Centre, Mines Branch, Dept. of Energy Mines and Resources.

Fairhurst, C., and Daemen,J.J.K. 1980. Practical inferences from research on the design of tunnel supports. Undergound Space, Vol. 4, No. 5, pp. 297-311.

Findlay, W.N., Lai, J.S., and Onaran, K. 1976. Creep and relaxation of nonlinear viscoelastic materials. North-Holland Pub. Co., Amsterdam-N.T.-Oxford. 367p.

Guenot, A. 1979. Investigation of tunnel stability by model tests. M.Sc. Thesis, Department of Civil Engineering, University of Alberta, Edmonton, Alberta. 217p.

Guttman, I., and Wilks, S.S. 1965. Introductory engineering statistics. John Wiley and Sons. 257p.

da Fontoura, S. 1980. Time-dependent response of rock masses during tunnelling. Ph.D. Thesis, Department of Civil Engineering, University of Alberta, Edmonton, Alberta. 314p.

Heuer, R.E., and Hendron, A.J. 1969,71,73,74. Geomechanical

model study of the behavior of underground openings in rock subjected to static loads. U.S. Corps of Engineers Report, Report 1-4, Contract No. DACA 39-67-C-0009.

Heuze,F.H. 1980. Scale effects in the determination of rock mass strength and deformability. Rock Mechanics, Vol. 12/3-4, pp.167-192.

Jordan, Stello. 1971. Handbook of technical writing practice. Wiley-Interscience. 733p.

Kaiser, P.K. 1979. Time-Dependent behavior of tunnels in jointed rock masses. Ph.D. Thesis, Department of Civil Engineering, University of Alberta, Edmonton, Alberta. 395p.

Kaiser, P.K. 1980. Effect of stress-history on the deformation behavior of underground openings. 13th Canadian Rock Mechanics Symposium, Toronto.

Kaiser, P.K., and Morgenstern, N.R. 1978. Time-Dependent deformation of rock near failure. Proceedings, Fourth International Congress on Rock Mechanics, Montreux, Switzerland, Vol.1, pp.195-202.

Kaiser, P.K., and Morgenstern, N.R. 1981. Time-Dependent deformation of small tunnels. Part 1. Experimental Facilities. Part 2. Typical Test Results. Int. J. Rock Mech. Min. Sci. and Geomech. Abstr., Vol. 18, in press.

Kaiser, P.K., and Morgenstern, N.R. 1981a. Phenomenological model for rock with time-dependent strength. Int. J.

Rock Mech. Min. Sci. and Geomech. Abstr., Vol. 18, in press.

Kersten, R.D. 1969. Engineering differential systems. McGraw-Hill. 236p.

Korbin, G.E. 1976. Simple procedure for the analysis of deep tunnels in problematic ground. 17th U.S. Symposium on Rock Mechanics, Site Characterization, pp.1A3-1-1A3-7.

Kulhawy, F.H. 1975a. Stresses and displacements around openings in homogeneous rock. Int. J. Rock Mech. Min. Sci. and Geomech. Abstr.,Vol. 12, pp.43-57.

Kulhawy 1975b. Stresses and displacements around openings in rock containing an elastic discontinuity. Int. J. Rock Mech. Min. Sci. and Geomech. Abstr.,Vol. 12, pp.59-72.

Kulhawy 1975c. Stresses and displacements around openings in rock containing an inelastic discontinuity. Int. J. Rock Mech. Min. Sci. and Geomech. Abstr.,Vol. 12, pp.73-78.

Ladanyi, B. 1974. Use of the long-term strength concept in the determination of ground pressure on tunnel linings. Proceedings, 3rd Int. Congr. on Rock Mech., Denver, Colorado, Vol. 2B, pp. 1150-1156.

Mitchell, J.K. 1976. Fundamentals of soil behavior. John Wiley and Sons. 422p.

Morgenstern, N.R. 1975. Stress-strain relations for soils in practice. Proceedings, 5th Pan American Conf. on

Soil Mechanics and Foundation Engineering, Buenos Aires, Vol. 1, pp.1-41.

Morgenstern, N.R., and Noonan, D.K.J. 1974. Fractured coal subjected to direct shear. Proceedings, Third Congress of the International Society of Rock Mechanics, Denver, Colorado, Vol.2A, pp.282-287.

Obert, L., and Duvall, W.I. 1967. Rock mechanics and the design of structures in rock. John Wiley and Sons, New York. 650p.

Pender, M.J. 1980. Elastic solutions for a deep circular tunnel. Technical Note, Geotechnique, 30, No.2,pp.216-222.

Poulos, H.G., and Davis, E.H. 1974. Elastic solutions for soil and rock mechanics. New York: John Wiley and Sons.

Sargent, D.W.J. 1980. Users manual. PST Computer Program Package, Department of Civil Engineering, University of Alberta, Edmonton, Alberta.

Scott, R.F. 1963. Principles of soil mechanics. Addison-Wesley Publishing Co. 550p.

Simmons, J.V. 1981. Users manual. Nonlinear Construction Program (NLCP), Department of Civil Engineering, University of Alberta, Edmonton, Alberta.

Stagg, K.G., and Zienkiewicz, O.C. editors, 1968. Rock mechanics in engineering practice. John Wiley and Sons. 442p.

Terzaghi, K. 1943. Theoretical soil mechanics. John Wiley and Sons, New York.

Terzaghi, K. 1946. Rock defects and loads on tunnel supports. Section I, Rock Tunnelling With Steel Supports, R.V. Proctor and T.L. White. The Commerical Shearing and Stamping Co., Youngstown, Ohio, pp17-99.

Terzaghi, K., and Richart, F.E. 1952. Stresses in rock about cavities. Geotechnique,3,pp.57-93.

Zienkiewicz, O.C., and Cheung, Y.K. 1967. Finite element method in structural and continuum mechanics. McGraw-Hill.

Zienkiewicz, O.C., Brotton, D.M., Morgan, L. 1976. A finite element primer for structural engineering. The Structural Engineer, Vol. 54, No. 10, pp.387-397.

APPENDIX A1

LINEAR ELASTIC FORMULATION FOR A TUNNEL IN AN INFINITE PLATE WITH A PLANE STRAIN BOUNDARY CONDITION

DEFINITIONS:

The polar coordinate system is used and the components of stress and strain are signified by a subscript. For example, in the radial direction, stress and strain are δ_r, ϵ_r. In the tangential direction, they are δ_θ, ϵ_θ. The components of displacement are u and v in the radial and tangential directions respectively. The coordinate radius is signified by r and the tunnel radius by a.

The field stress is applied at infinity. A longitudinal stress, δ_l, is also present for a plane strain boundary condition. The field stresses are signified by δ_v in the vertical direction (0-180 axis) and δ_h in the horizontal direction (90-270 axis). The ratio of field stress is signified by $N = \delta_h/\delta_v$.

For this reference system, compressive stresses and strains are positive. Extension strains are negative. Radial displacement is positive when it is directed toward the tunnel. Angles are measured counterclockwise from the horizontal axis in the first quadrant.

The independent elastic parameters are signified by E for Young's Modulus and υ for Poisson's Ratio. Young's Modulus is defined as the ratio of uniaxial

stress to axial strain. Poisson's Ratio is defined as the ratio of lateral to axial strain in uniaxial loading.

The shear and bulk moduli are signified by G and K respectively. The shear or rigidity modulus is defined as the ratio of shear stress to shear strain. The bulk modulus is defined as the ratio of mean stress to volumetric strain. For a plane strain boundary condition, the shear and bulk moduli may be written as:

$$G = E/2(1+\upsilon) \; ; \; K = E/3(1-2\upsilon).$$

CONTINUUM MECHANICS REQUIREMENTS

A. Assumptions:

-isotropic continuum;
-homogeneous continuum;
-infinitesimal deformations;

B. Physical conditions in the differential system, governing equations:

-Static Equilibrium, .ie.differential equations of equilibrium;

-Condition of Compatibility for Strain-displacement Relations;

-Material Behavior : Hooke's Law.

C. Boundary Conditions:

-Plane strain;
-Field stress appied at infinity;
-No pressure inside the tunnel.

SOLUTION OF THE TWO-DIMENSIONAL ELASTIC PROBLEM

In the stress formulation, with constant body forces, terms in the governing equations may be eliminated to obtain

the Biharmonic equation:

$$\nabla^4 \Phi = 0$$

Solution of this equation is obtained using the following Airy stress function:

$$\Phi = A \log r + B r^2 + [C r^2 + D r^4 + E\ 1/r^2 + F] \cos 2\theta$$

In polar coordinates, the stress components are given by (Pender, 1980):

$$\delta = 1/r\ \Phi'_r + 1/r^2\ \Phi''_{\theta\theta}$$

$$\delta = \Phi''_{rr}$$

Constants are evaluated knowing the stresses at r=a and r=infinity.

By back-calculation, the elastic stress-strain relationship gives strain:

$$\epsilon_r E = (1+\upsilon)\ [(1-\upsilon)\ \delta_r - \upsilon \delta_\theta]$$

$$\epsilon_\theta E = (1+\upsilon)\ [(1-\upsilon)\ \delta_\theta - \upsilon \delta_r]$$

Integration of these strain-displacement equations:

$$\epsilon_r = u'_r$$

$$\epsilon_\theta = u/r + v'_\theta\ 1/r$$

gives the displacement.

The constants of integration are obtained by considering displacements at r = infinity.

The radial displacement equation is given by Pender (1980):

$$uE = 0.5\delta_v [(1-\upsilon^2)[(1+N)(r+a^2/r) - (1-N)(r-a^4/r^3+4a^2/r)\cos 2\theta]$$
$$-\upsilon(1+\upsilon)[(1+N)(r-a^2/r) + (1-N)(r-a^4/r^3)\cos 2\theta]]$$

At the tunnel wall, radial displacement is:

$$uE = \delta_v a(1-\upsilon^2)[(1+N)-2(1-N)\cos 2\theta]$$

APPENDIX A2

LINEAR VISCOELASTIC RELATIONS

The elastic-viscoelastic correspondence principle may be used to determine the linear viscoelastic relations (Findlay, 1976). Linear elastic behavior is a limiting condition of the linear viscoelastic formulation. The following procedure may be used for a viscoelastic formulation:

1. obtain the Laplace transform of the elastic equations;
2. substitute the corresponding material parameters in terms of the transformed variable (s);
3. solve the transformed equation; and
4. apply the inverse Laplace transform to obtain the desired quantities with a time variable.

The equivalent to E and υ for a viscoelastic material in terms of linear differential operators is given by (Findlay, 1976):

$$E(t) = 3\,Q_1 Q_2/(P_2 Q_1 + 2P_1 Q_2)$$

$$\upsilon(t) = (P_1 Q_2 - P_2 Q_1)/(P_2 Q_1 + 2\,P_1 Q_2)$$

This follows from the analogy between elastic and viscoelastic constitutive equations, in particular:

$$S_{ij} = 2G\,d_{ij} \text{ and } P_1 S_{ij}(t) = Q_1 d_{ij}(t)$$

$$\delta_{ii} = 3K\,\epsilon_{ii} \text{ and } P_2 \delta_{ii}(t) = Q_2 \epsilon_{ii}(t)$$

where:

S_{ij}, δ_{ii} - deviatoric and isotropic stress tensors

d_{ij}, ϵ_{ii} - deviatoric and isotropic strain tensors

G,E - shear and bulk moduli

P,Q - linear differential operators with respect to time, containing material constants.

For the PST formulation shown in Appendix A1 (N=1,r=a), in brief terms, the viscoelastic formulation is as follows (Kaiser, 1979):

- $u = 2a\ \delta_v(1-\upsilon^2)/\ E = 2a\ \delta_v f$
- Laplace transform gives: $u = 2a\ \delta_v f(s)/s$ since $\delta(s) = \delta_v/s$
- substitute material properties
- inverse transform: $u(t) = 2a\ \delta_v f(t)$

(Note: The stresses for this formulation are independent of the material constants.)

APPENDIX B1

REVIEW OF ELECTRICAL MONITORING DEVICES

This appendix describes the transducers, their calibration procedures and their degree of uncertainty. Load cell calibration relates voltage to load measured with a Baldwin-Southwark compression machine. LVDT calibration relates voltage to displacement measured with a screw micrometer. A least squares method determines the calibration equation and the 95% confidence interval defines the degree of uncertainty.

Load cell calibrations were done after tests MC1.15 and MC1.19. Previously determined calibration equations were used for some calculations however the average vertical stress calculated by each set of equations differs insignificantly. LVDT calibrations were done in the spring of 1979, prior to test MC1.7.

DESCRIPTION OF TRANSDUCERS

A load cell (Dynamometer) is a device for measuring force. It consists of a bonded resistance strain guage as the tranducing element which converts deflection of on annular aluminum ring into changes in electric current. Four resistance strain gauges are mounted inside the annular ring, two orientated axially and two orientated circumferentially. The load cells are fitted with two types

of interchangeable end platens to provide a flat bearing surface. The moveable end platen consists of two metal discs machined to contact at a concave-convex lubricated surface thereby to allow small seating movements during testing. The flat end platen consists of a metal discs also machined to fit onto the annular ring. Two sizes of load cells are used, the lateral load cells (10 cm O.D., 10 cm length) operate to approximately 1 MN and the longitudinal load cells operate to 0.25 MN. The sensor range is 0 to 20-23 millivolts with a smallest reading of 0.002 millivolts. (The longitudinal load cells were not calibrated during this test program).

A LVDT-Linear Voltage Differential Transformer is a device for measuring displacement using an "iron core travelling inside an electric coil as the transducing element. A change of the relative position of the core and coil causes a voltage change. Five sizes of LVDT's are used. The LVDT voltage ranges are ±5, ±7 or ±10 volts at 6 or 22 volt excitation with displacement ranges of ±12.5 mm (two boundary displacement LVDT's), ±6. mm (extensometers) and ±2.5 mm (tunnel). The sensor sensitivity (dQ in /dQ out) is between 0.0001 and 0.0003 and strain sensitivity (smallest reading/measurement length) is at least 0.001% for the tunnel and extensometers and 0.03% for two boundary displacements.

DESCRIPTION OF THE TEST PROCEDURE

Load cell calibrations were done in three sessions, once in February 1980 and twice in April 1980, using a continuous reading compression machine (1% accuracy) located in the Civil Engineering Building. The first two calibrations were done with a proving ring (1% accuracy) located in series with a stack of 3 load cells thus to optimize time. Flat end platens were located between load cells. Moveable bearing surfaces were located at the ends of the stack, like a pinned column. During the third session, some load cells were tested individually and all were tested in a stack of 2 load cells with one flat and one moveable end platen plus, in a stack of 4 load cells. To randomize tests, the load cells were moved between each test but always connected to the same electrical lines and conditioner channels at least 15 minutes before a test.

A typical calibration test was done by increasing load in 0.045 MN increments to 0.85 MN and decreasing load in 0.225 decrements while recording voltage at each load setting.

Arithmetic and double log coordinate systems were investigated to seek suitable calibration equations. A student-t statistical evaluation for linear calibration equations was done for increasing load data on an average of 3 or 4 category A test per load cell (catagory A tests were done with one flat and one moveable end platen, catagory B tests were done with two flat end platens). Thus, the confidence interval of y given x equals plus or minus, the

student t statistic times the square root of: all of the estimated standard deviation of predicted y, squared; plus an estimate of variance (standard deviation of y about the regression line squared). This method gives a relatively uniform confidence interval in the range of interest and differs only slightly from ASTM E 74.

The LVDT calibration procedure was carried out by setting twenty displacement values at equal increments over the transducer range and recording voltage at each setting. First order polynomial equations were determined for each LVDT. Regression statistics were investigated for one LVDT.

SUMMARY OF RESULTS

First order polynomial calibration equations adequately represent calibration results for load cells in the loading range of 25% to 100% of maximum. The degree of uncertainty is less than ±0.025 MN in this range, except for LC 19 (±0.047 MN) and LC 25 (±0.036 MN). Operating in a range above 0.25 MN provides better than 10% error for most of the load cells. Inherent non-linearity of the test data restricts the validity of statistical inferences about uncertainty. Results for tests on load cells with two flat end platens generally estimate a 10% lower mid range load than when both types of end platens are used. Acceptable drift stability occurs during short-term loading (not studied for long term), however, hysterisis affects unloading calibration. Hence, load cell calibration should

be done for the range of interest and by duplication of the loading conditions in the PST.

The LVDT's seem to comply with manufacturers specifications of at least 0.5% linearity error. For the analysis of regression on one LVDT, the residuals exhibit a normal distribution with a 0.027 volt standard deviation and the plot of residuals over the sensor range exhibits a sinuisoidal distribution with peaks at ±50% of the transducer scale.

APPENDIX C1

SOME TEST RESULTS

TABLE C1-1

DETAILS OF THE TEST PROGRAM

TEST	PURPOSE	TEST DIFFICULTIES	ACCOMPLISHMENTS
Preliminary MC1.7,1.8	-explore effect of changing the tunnel size. -operator familiar.	-incorrect plane strain control,.ie. longitud. stress about 25% too high. -R/I in test MC1.7. -Power failure during recovery in test MC1.8.	-observed a "size effect" -establish correct equipment operation procedures.
Non-hydrostat. Episodes MC1.10,1.11, 1.12	-damage the rock near the tunnel.(non-hydrostatic field stress). -do tests with hydrostatic field stress to evalute non-hydr. test.	-Partial unloading at constant field stress in test MC1.7, stop test to replace faulty air regulator.	-measure alteration of deformation behavior. -establish procedure to interactively monitor the field stress ratio during loading(MC1.11,1.12). -hear rock noise in test MC1.16.
Bimodal Loading Rate Tests MC1.9, MC1.14	-explore effect of reducing the loading rate at 10 MPa field stress.	-abort initial loading for test MC1.14 (test numbered MC1.13). -field stress changed by 5% at 10MPa in test MC1.9. -power failure during 14 MPa constant load. -anisotropic loading to 3.5 MPa in test MC1.14 specimen quickly unloaded; and restart test.	-crack observed on tunnel wall in test MC1.9. -measure loading rate effect.
Breaking the Specimen MC1.17,1.18, 1.19	-continue low confinement tests. -test a ruptured specimen.	-specimen ruptured along jointing at 10 MPa vertical field stress in test MC1.18.	-test a completely altered test specimen.

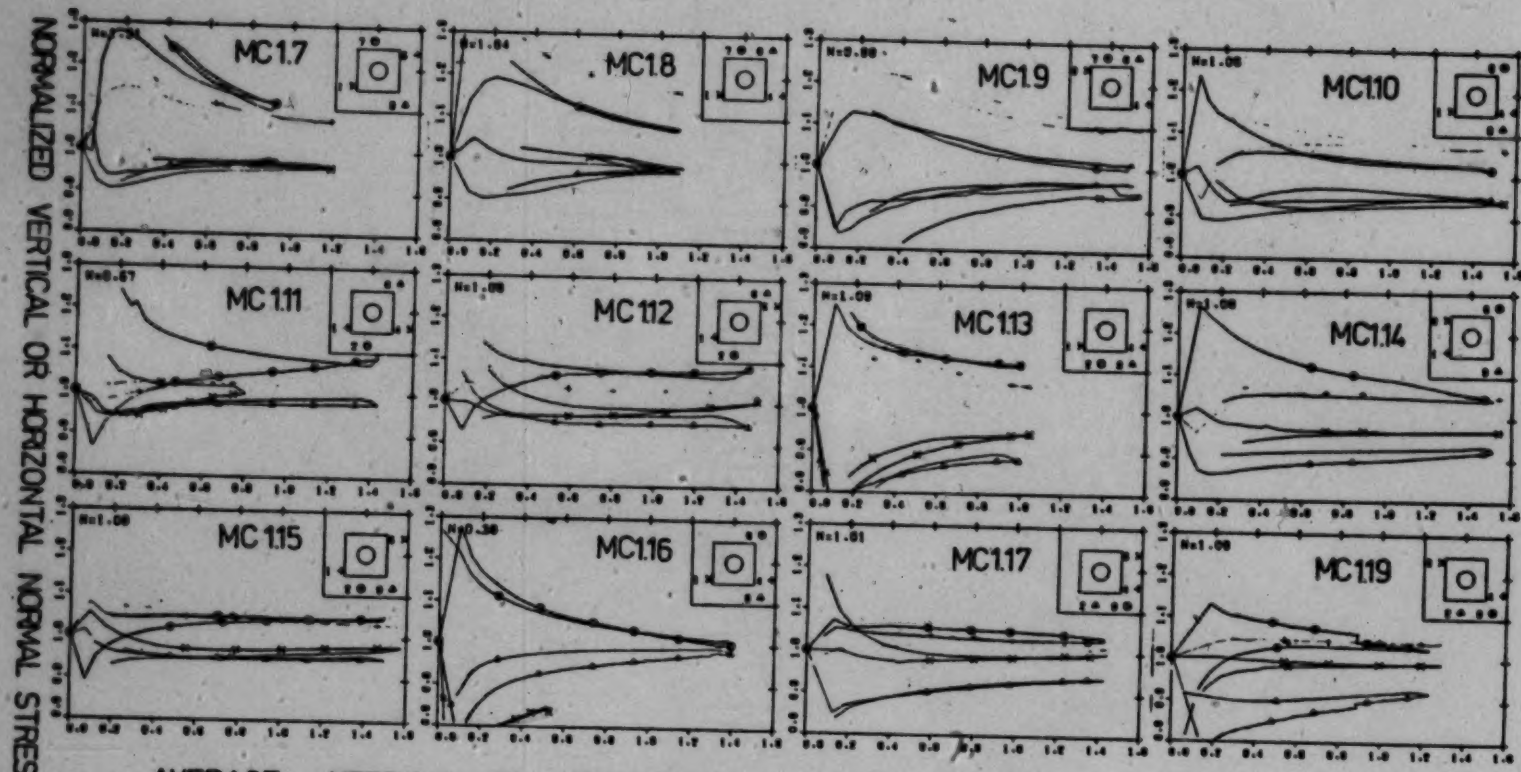

MC1.18 not shown

maximum and minimum normal stress shown normalized to the average stress for vertical & horizontal direction during loading.

FIGURE C2-1 RANGE OF BOUNDARY NORMAL STRESS

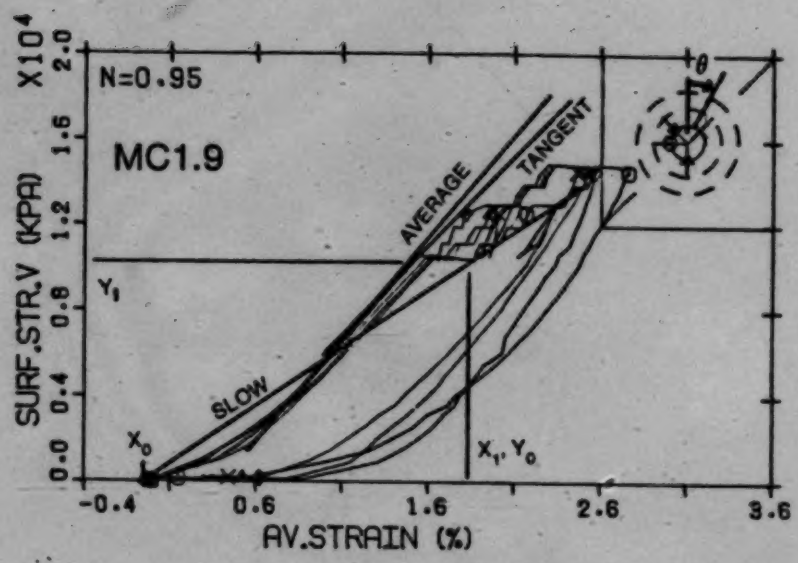

Deformation Moduli are Derived Assuming a Linear Elastic Formulation, Thus:

$$\frac{E}{(1-\nu^2)} = \frac{(Y_1 - Y_0)}{(X_1 - X_0)} \cdot [(1+N)+2(1-N)\cos 2\theta]$$

Figure C3-1 (a) Determination of Apparent Deformation Modulus

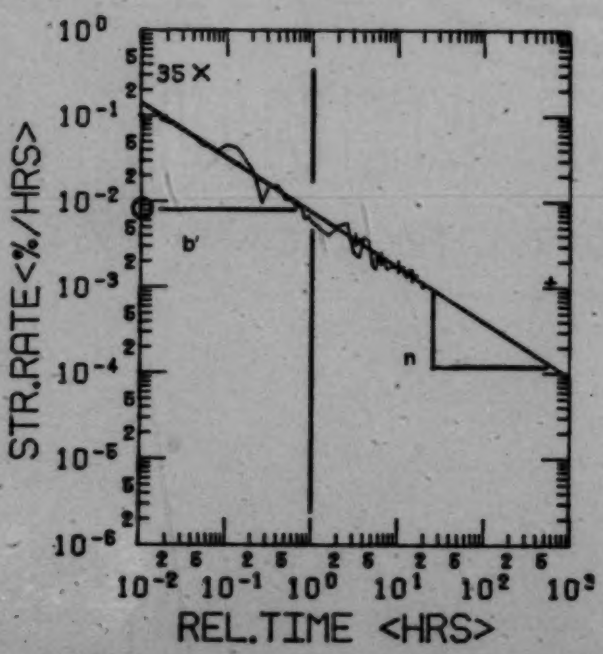

Closure Rate Parameters:

b = log b'

n = geometric straight line slope

Figure C3-1 (b) Determination of Closure Rate Parameters

TABLE C4-1

DEFINITION OF GRAPHICAL SYMBOLS

Graphical Plot	Symbol	Definition
Stress-Strain	O △ X ◇	-Data curve and LVDT position Note: For the combination of two LVDT measurements, the location symbol is shown along the measurement axis
	N	-Field stress ratio, the ratio of horizontal to vertical field stress.
Strain-Time	O △ X ◇	-Data curve and location symbols
	SIGMAV	-Average vertical field stress
	TZERO	-Time at start of constant field stress
Strain Rate - Time	33 O	-Strain Rate - Time curve corresponds to curve 33 shown in the strain-time plot
	———	-Positive Strain Rate
	+	-Positive trend
	▲	-Negative strain rate
	X	-Negative trend

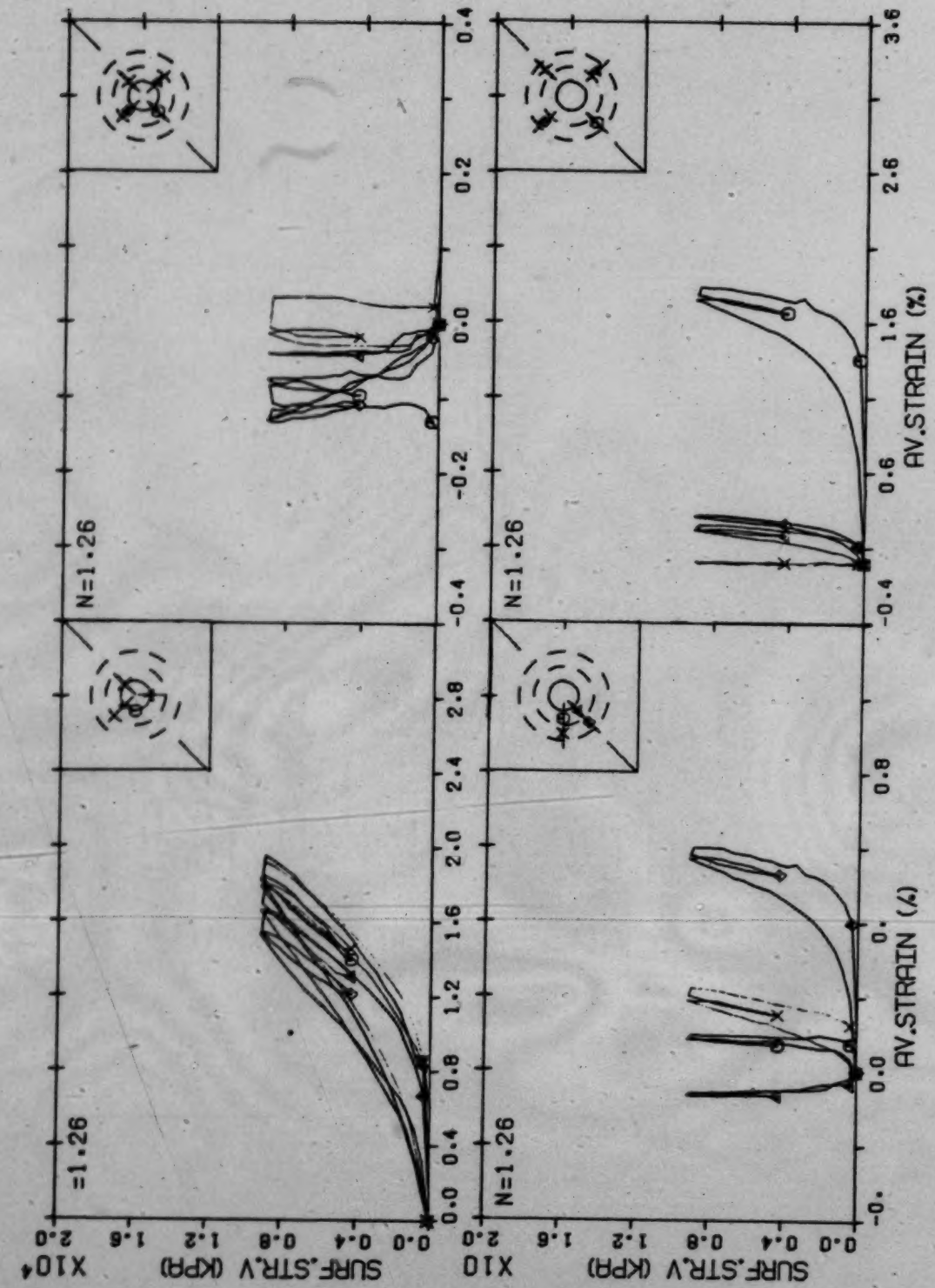

Figure C4-1 Field Stress Versus Strain Curves For Some Locations For Test MC 1.7

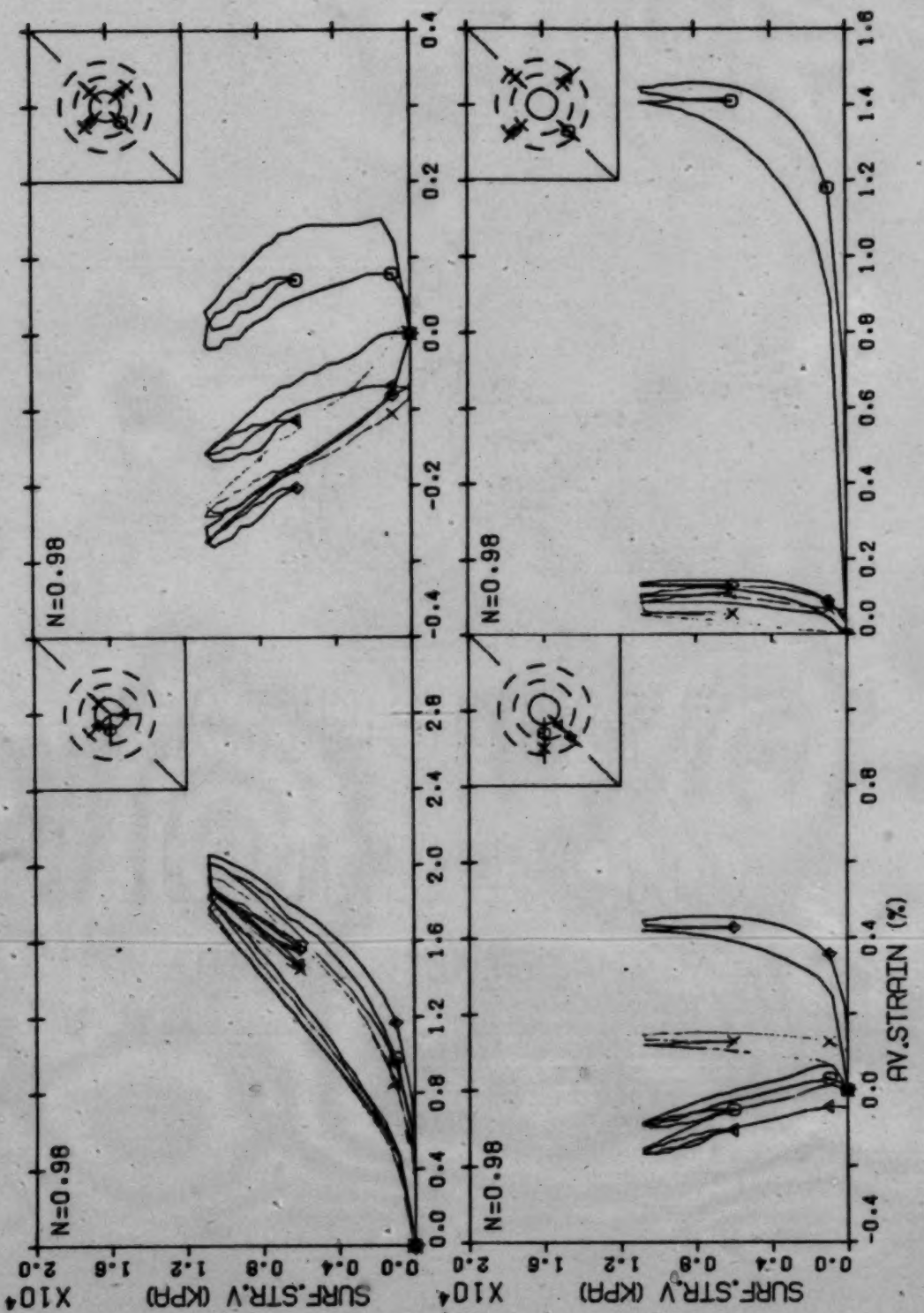

Figure C4-2 Field Stress Versus Strain Curves For Some Locations For Test MC 1.8

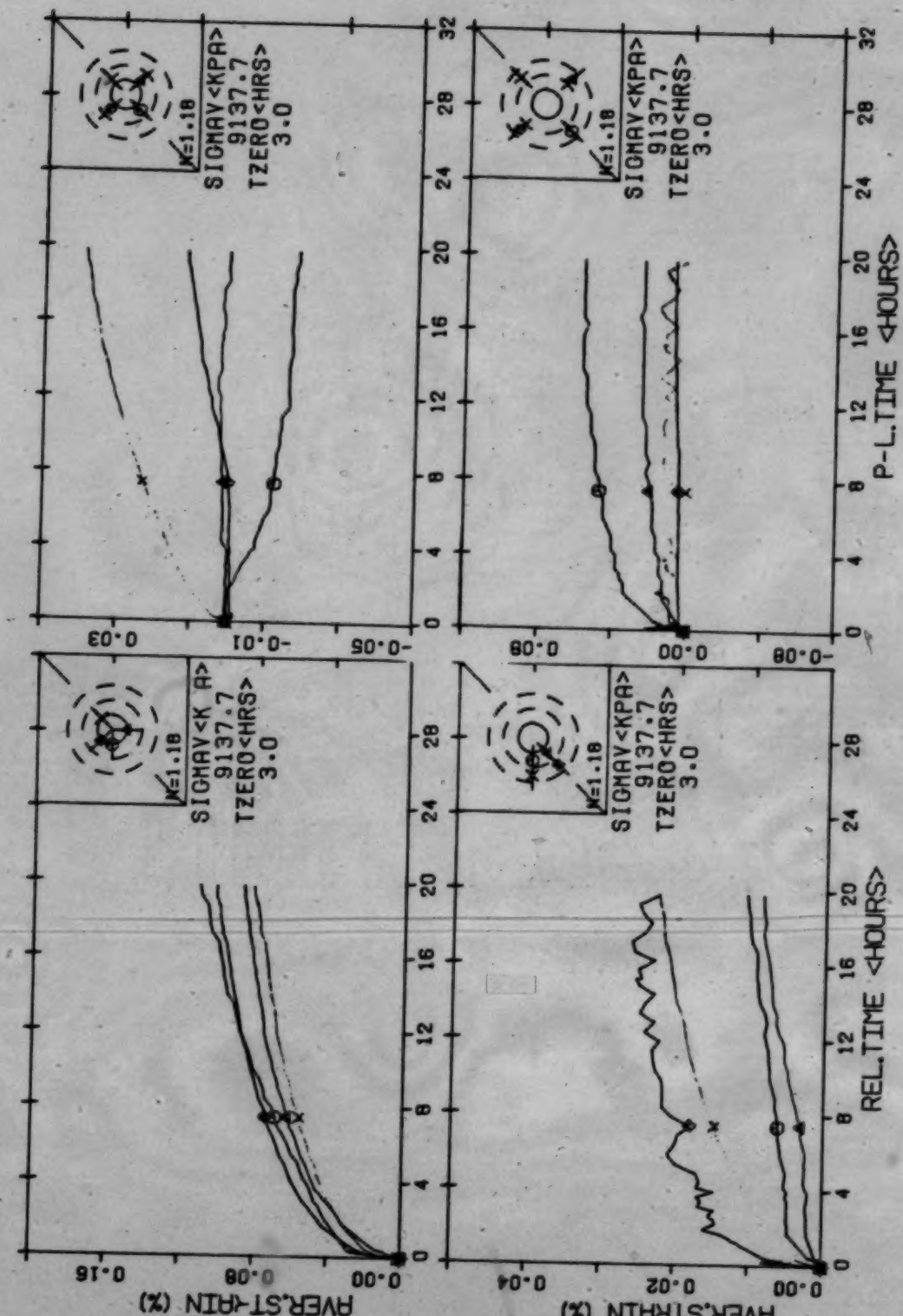

Figure C4-3 Strain Versus Time Curves For Some Locations For Test MC 1.7

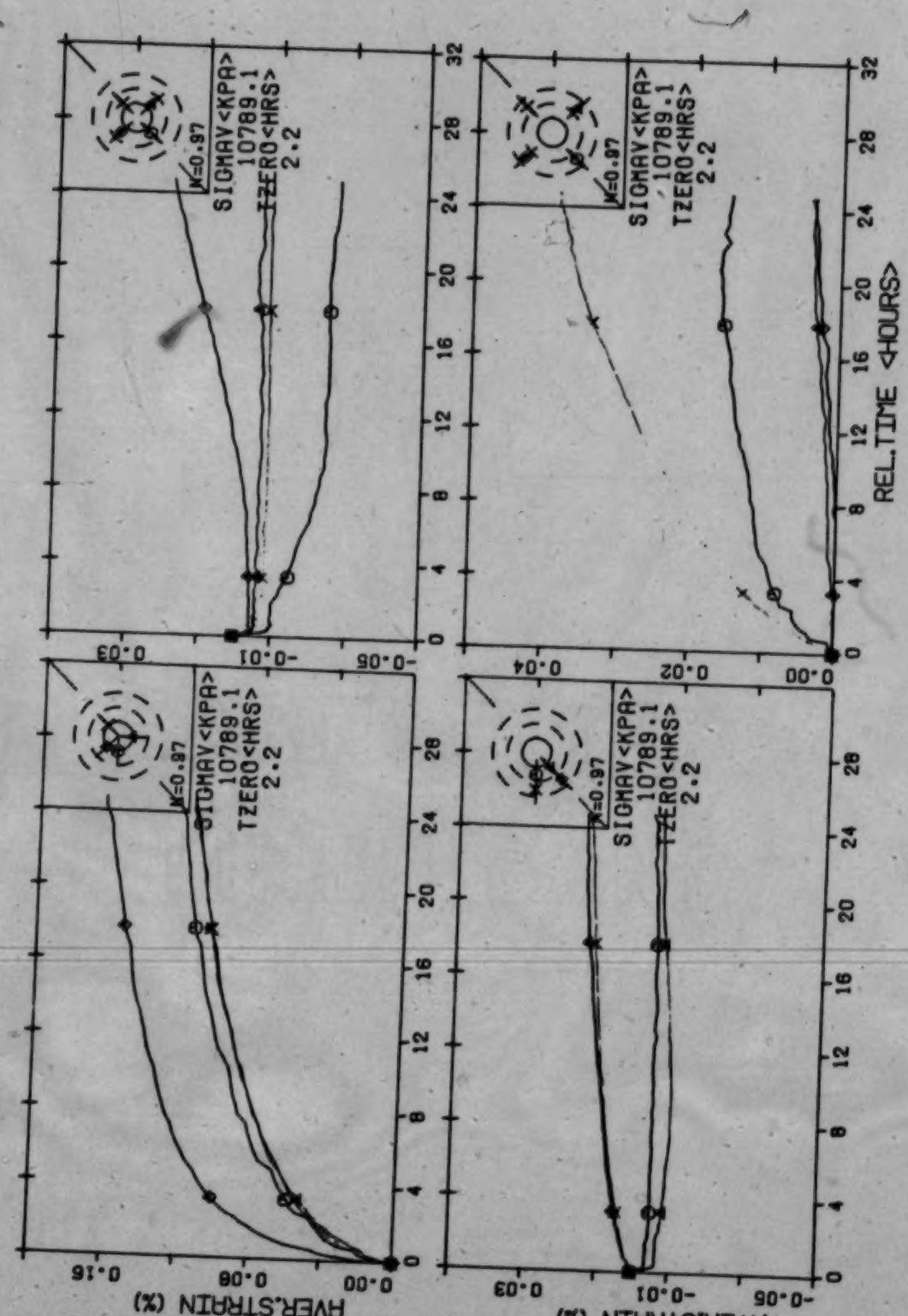

Figure C4-4 Strain Versus Time Curves For Some Locations For Test MC 1.8

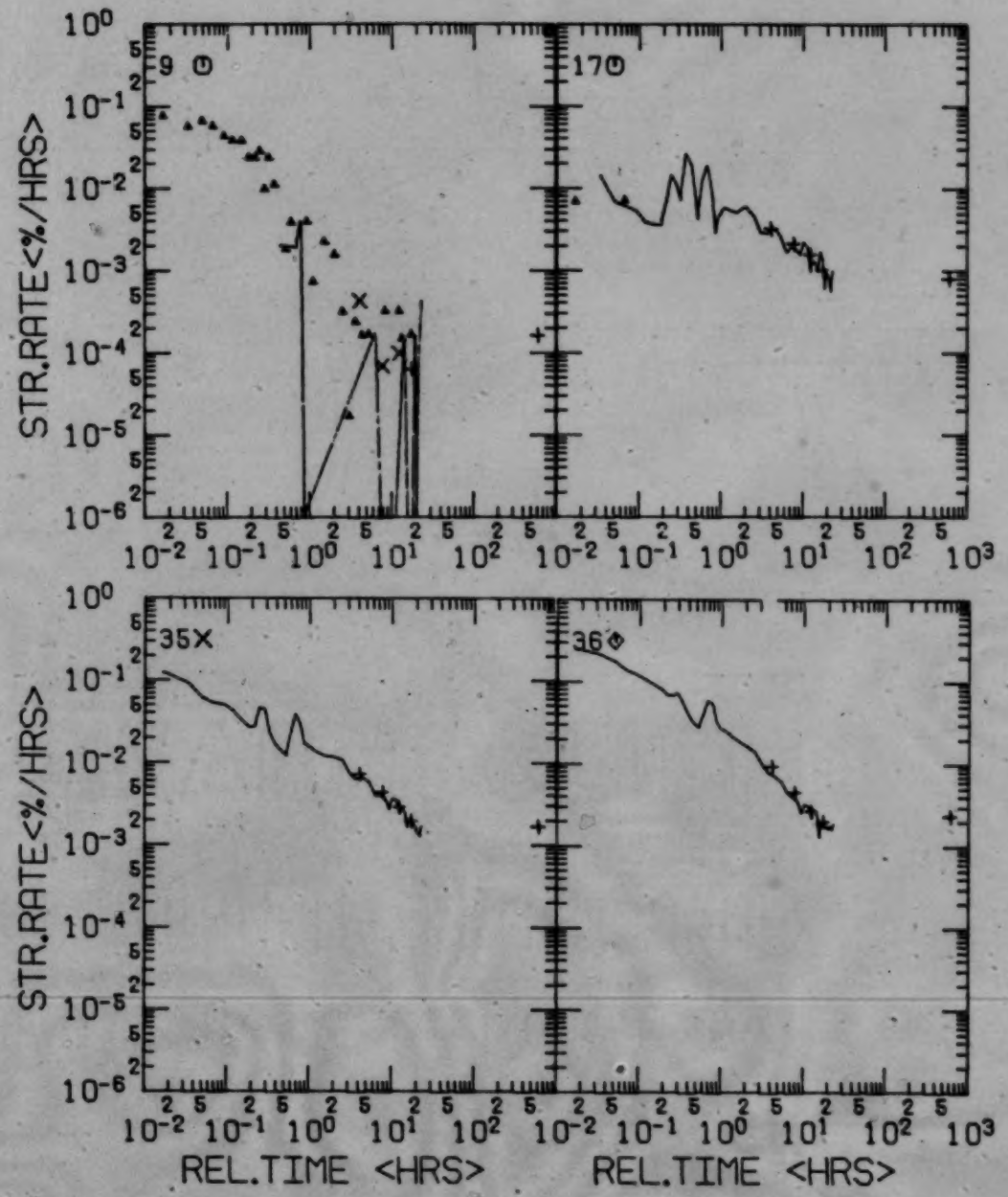

Figure C4-5 Strain Rate Versus Time Curves For Some Locations For Test MC 1.8

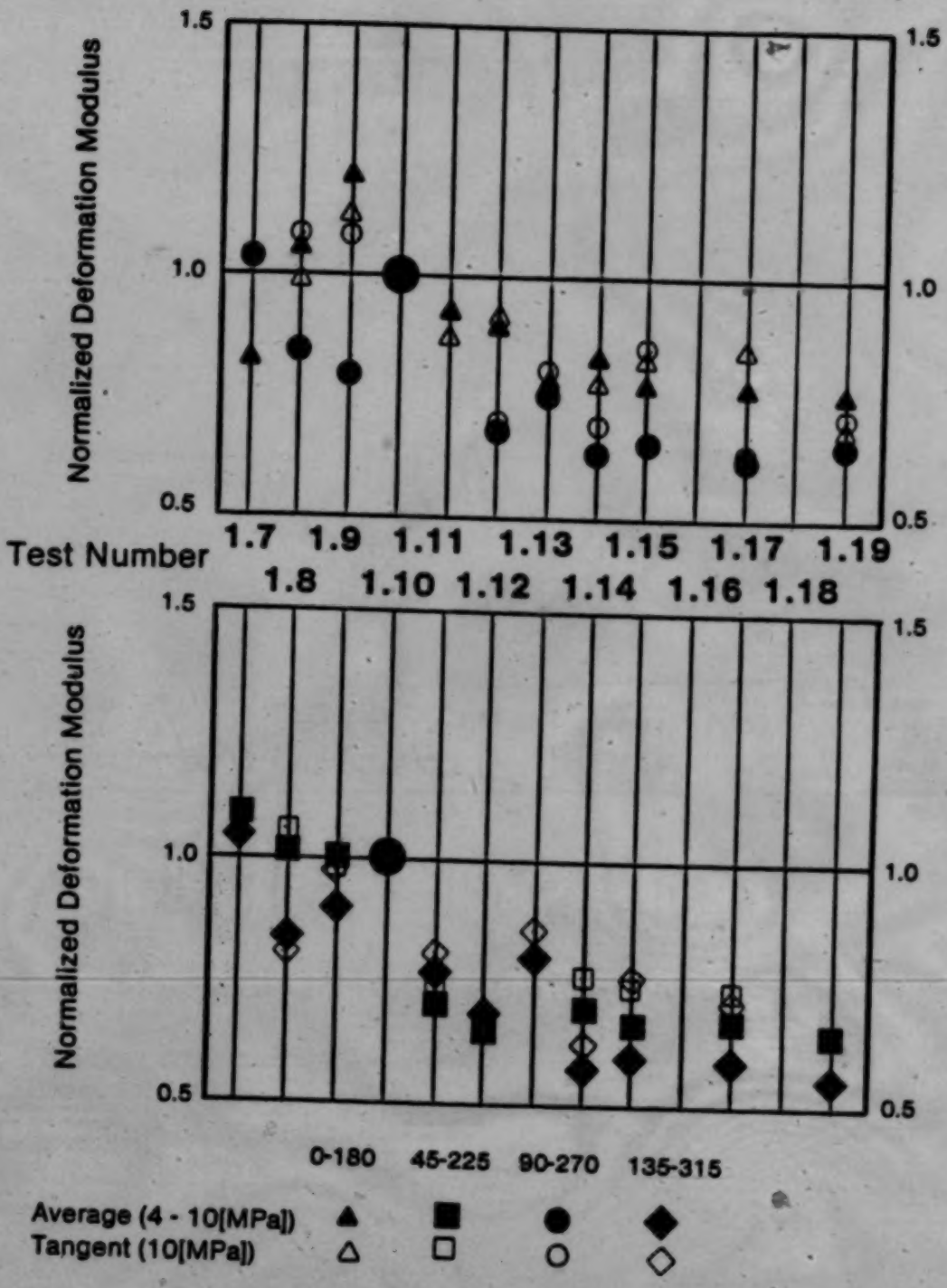

Figure C5-1 Deformation Modulus Along the Four Tunnel Diameters in Each Test Normalized to Test MC 1.10

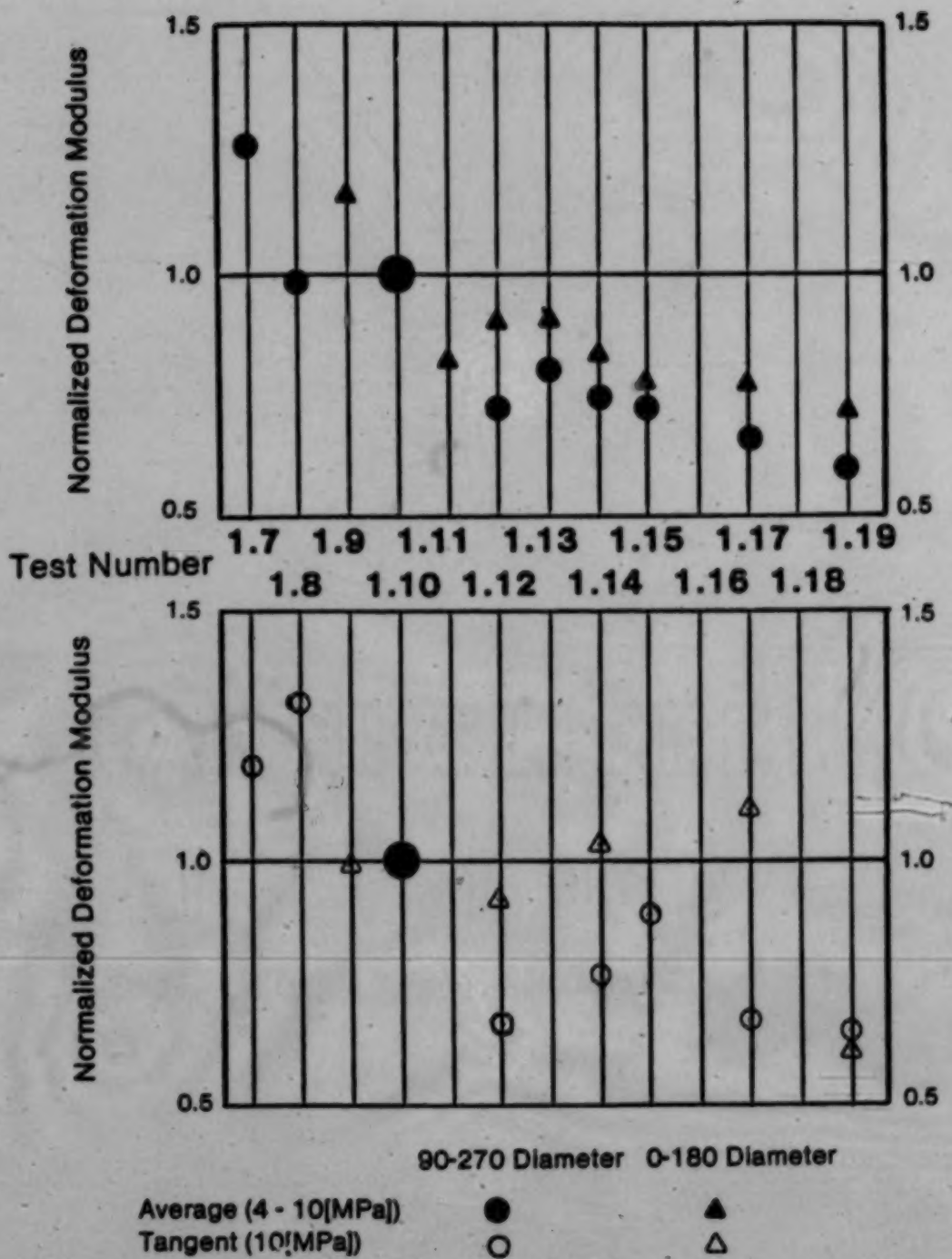

Average Specimen Strain;

Figure C5-2 Deformation Modulus for EachTest Normalized to Test MC 1.10

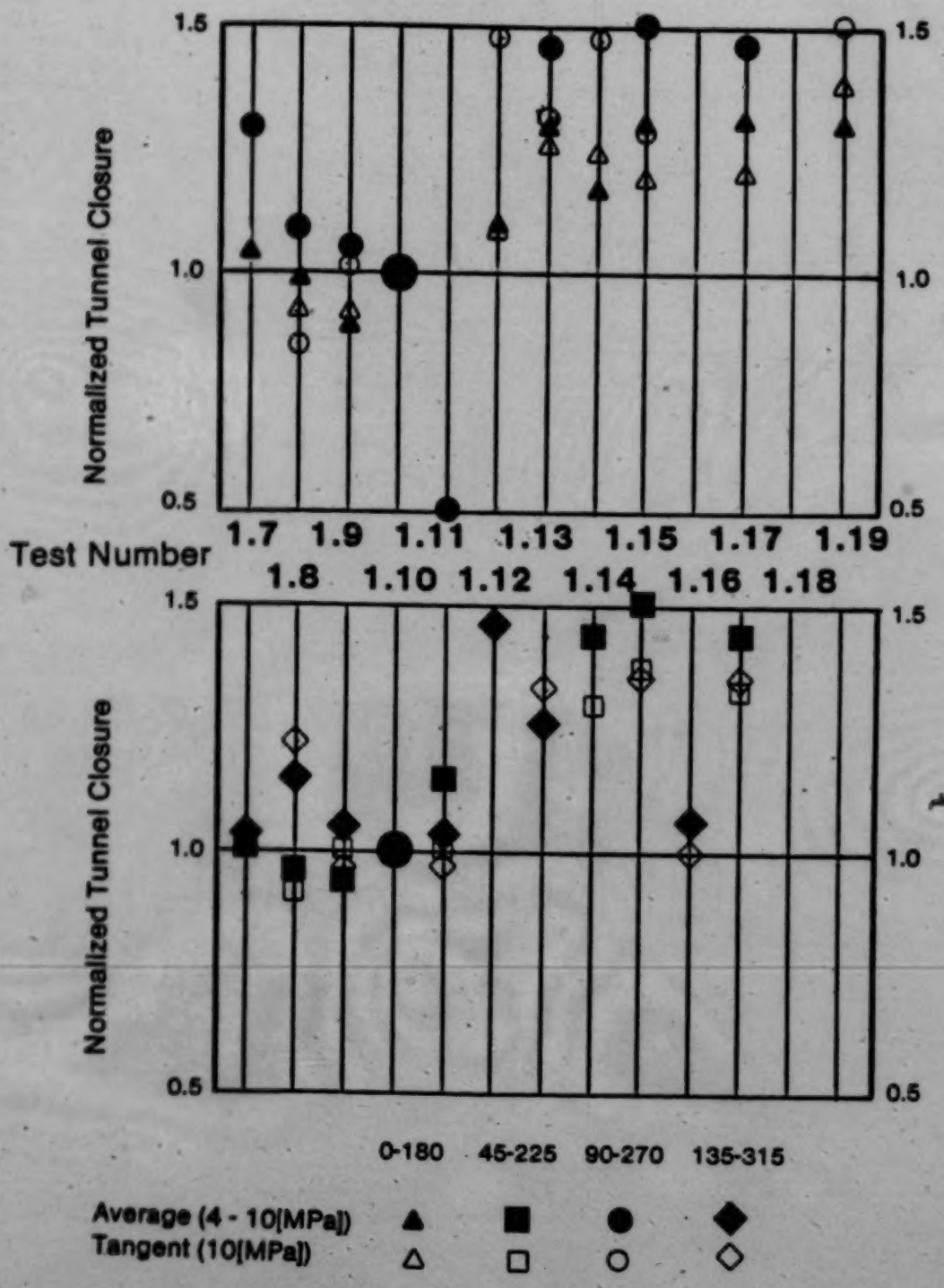

Figure C5-3 Tunnel Closure Along the Four Tunnel Diameters in Each Test Normalized to Test MC 1.10

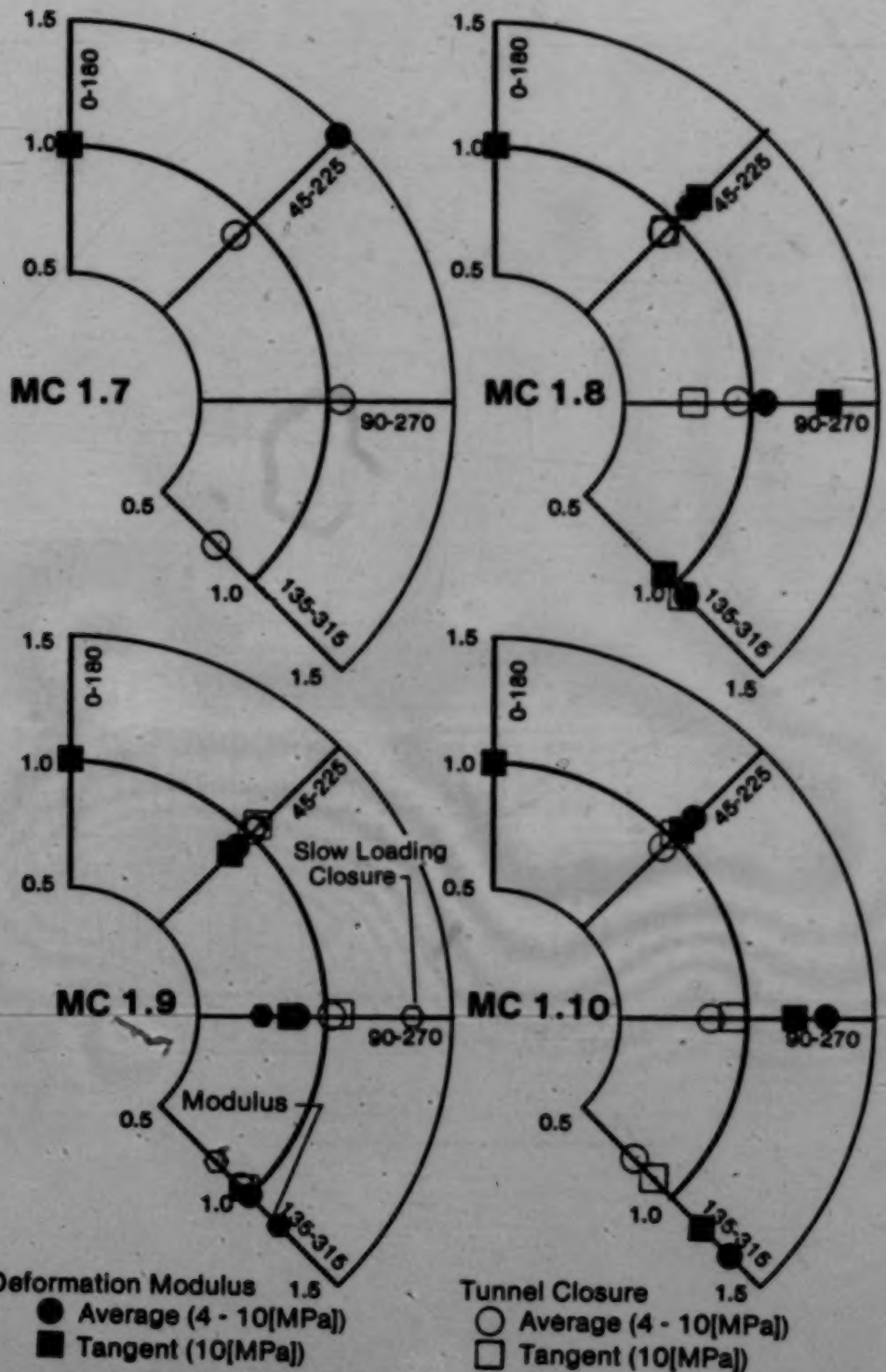

Figure C5-4 Deformation Modulus and Tunnel Closure For Tests MC 1.7 To MC 1.10 Normalized To The 0-180 Diameter

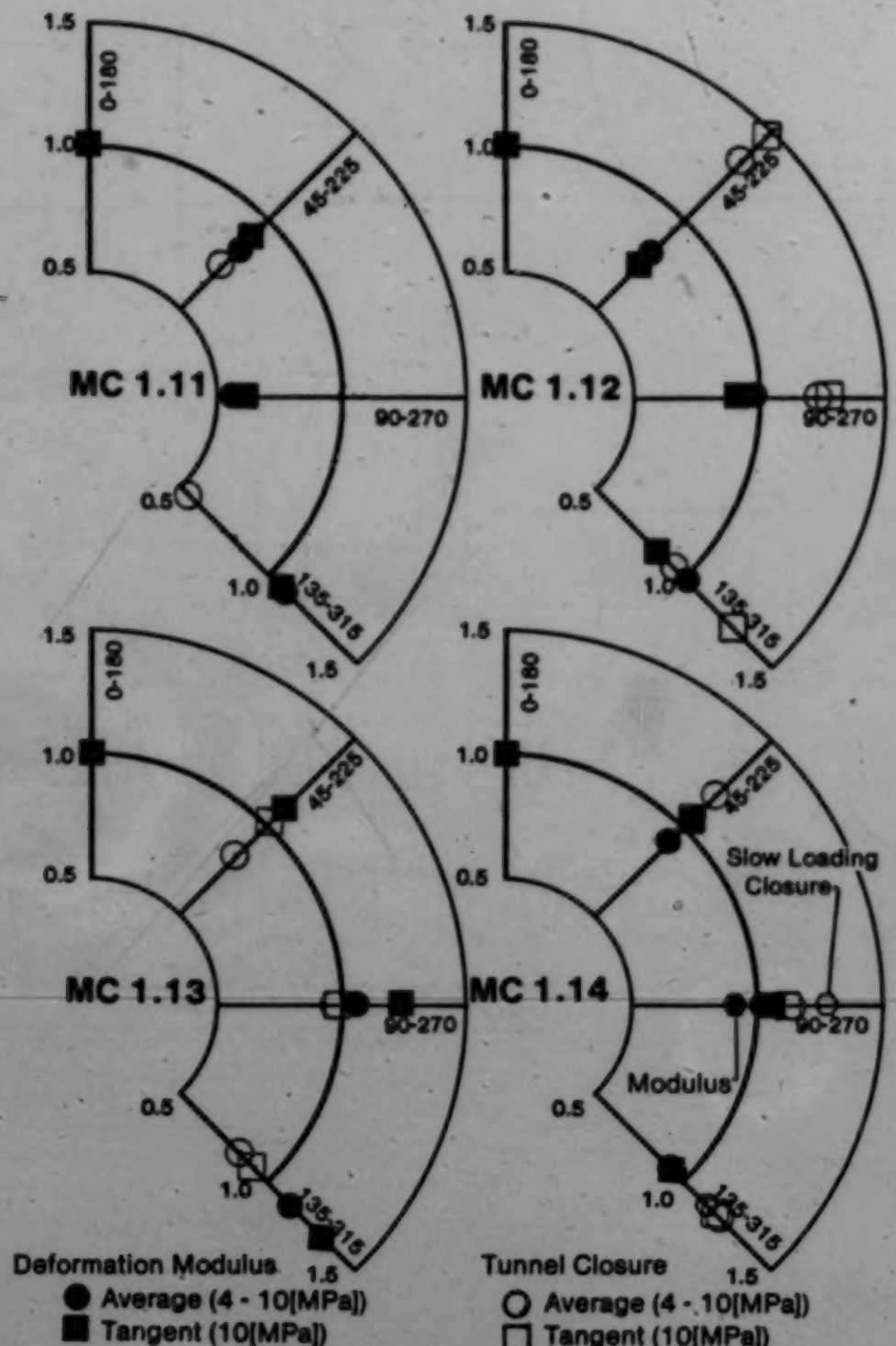

Figure C5-5 Deformation Modulus And Tunnel Closure For Tests MC 1.11 To MC 1.14 Normalized To The 0-180 Diameter

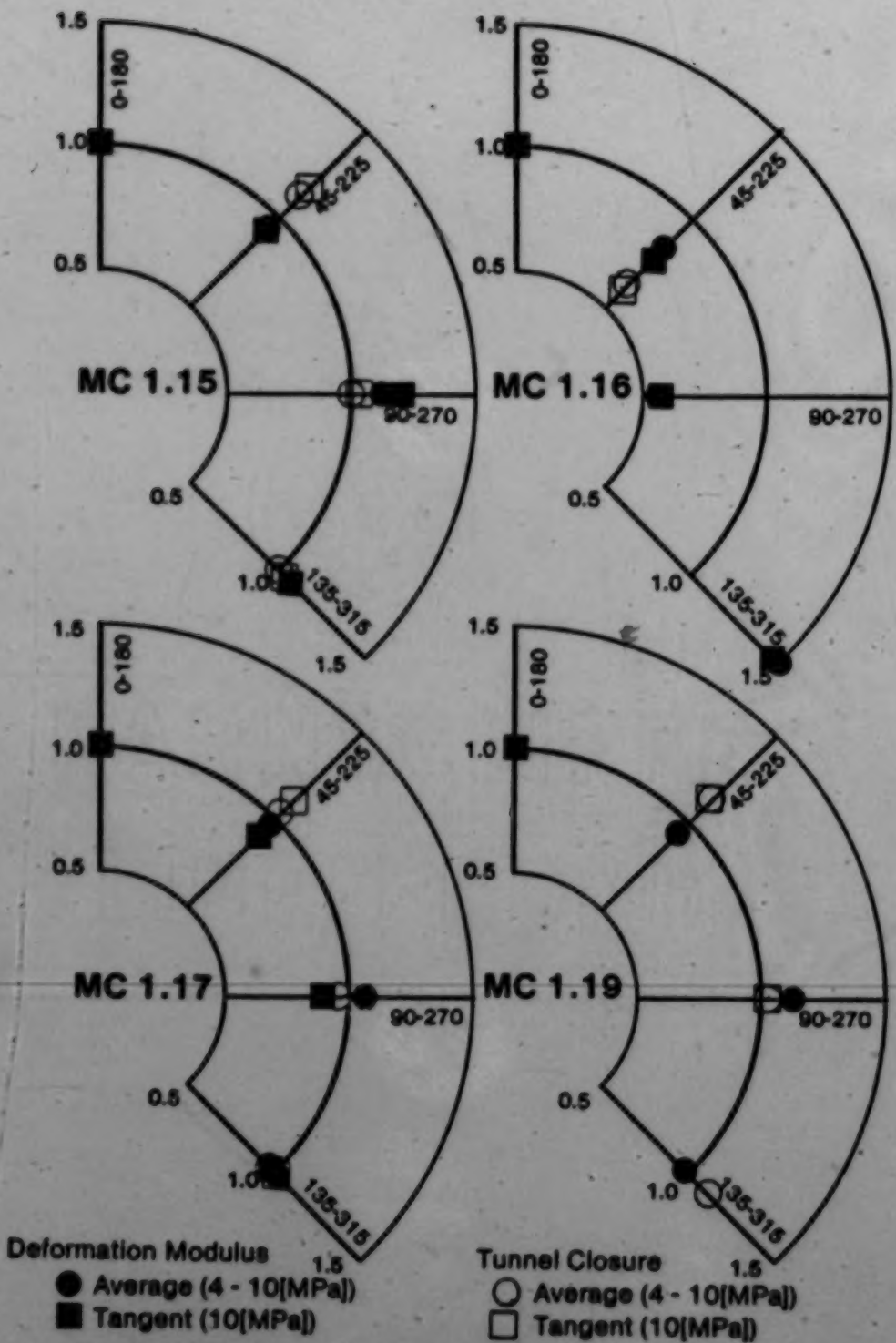

Figure C5-6 Deformation Modulus And Tunnel Closure For Tests M 1.15 To MC 1.19 Normalized To The 0-180 Diameter

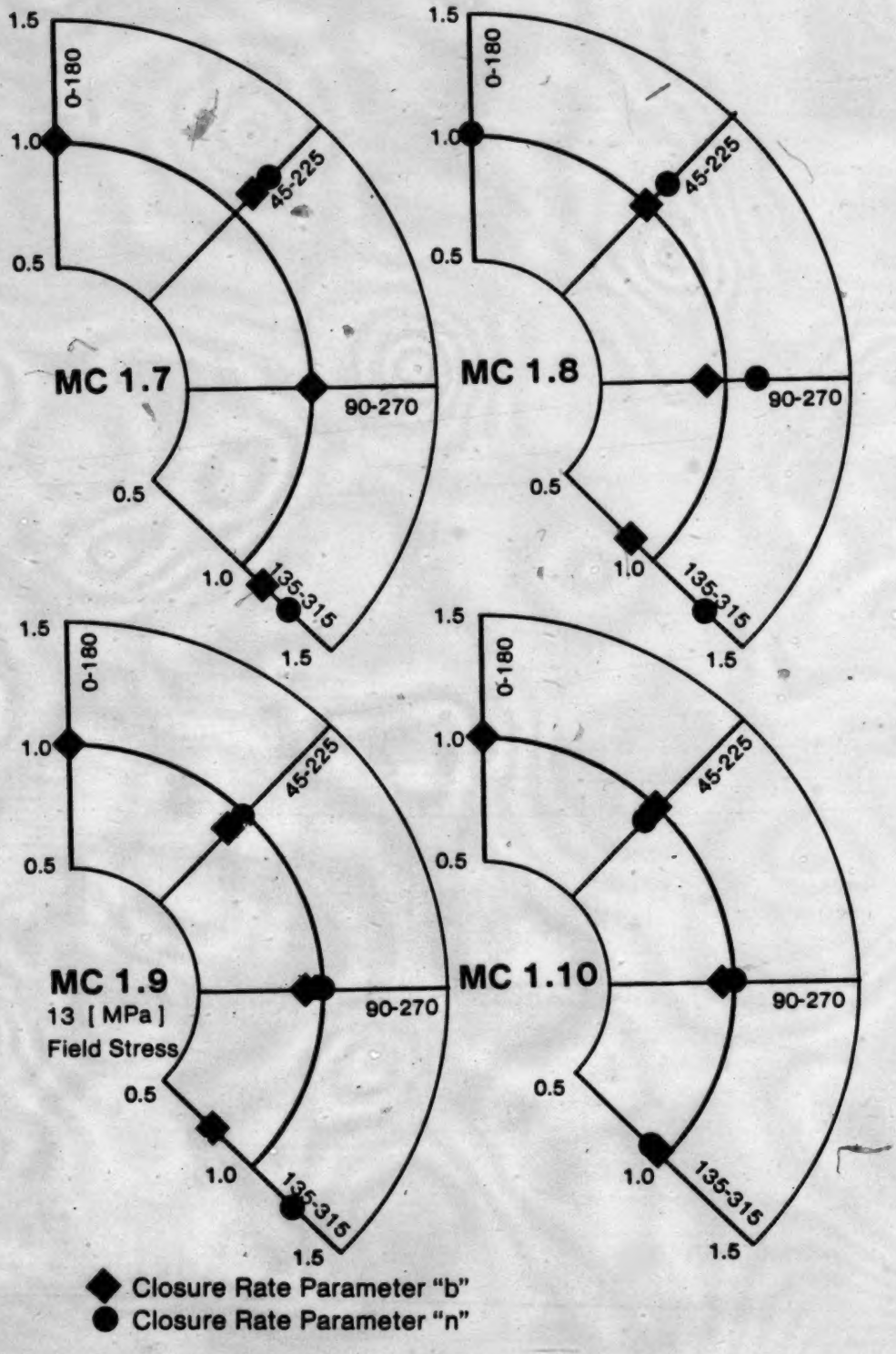

Figure C5-7 Closure Rate Parameters For Tests MC 1.7 To MC 1.10 Normalized To The 0-180 Diameter

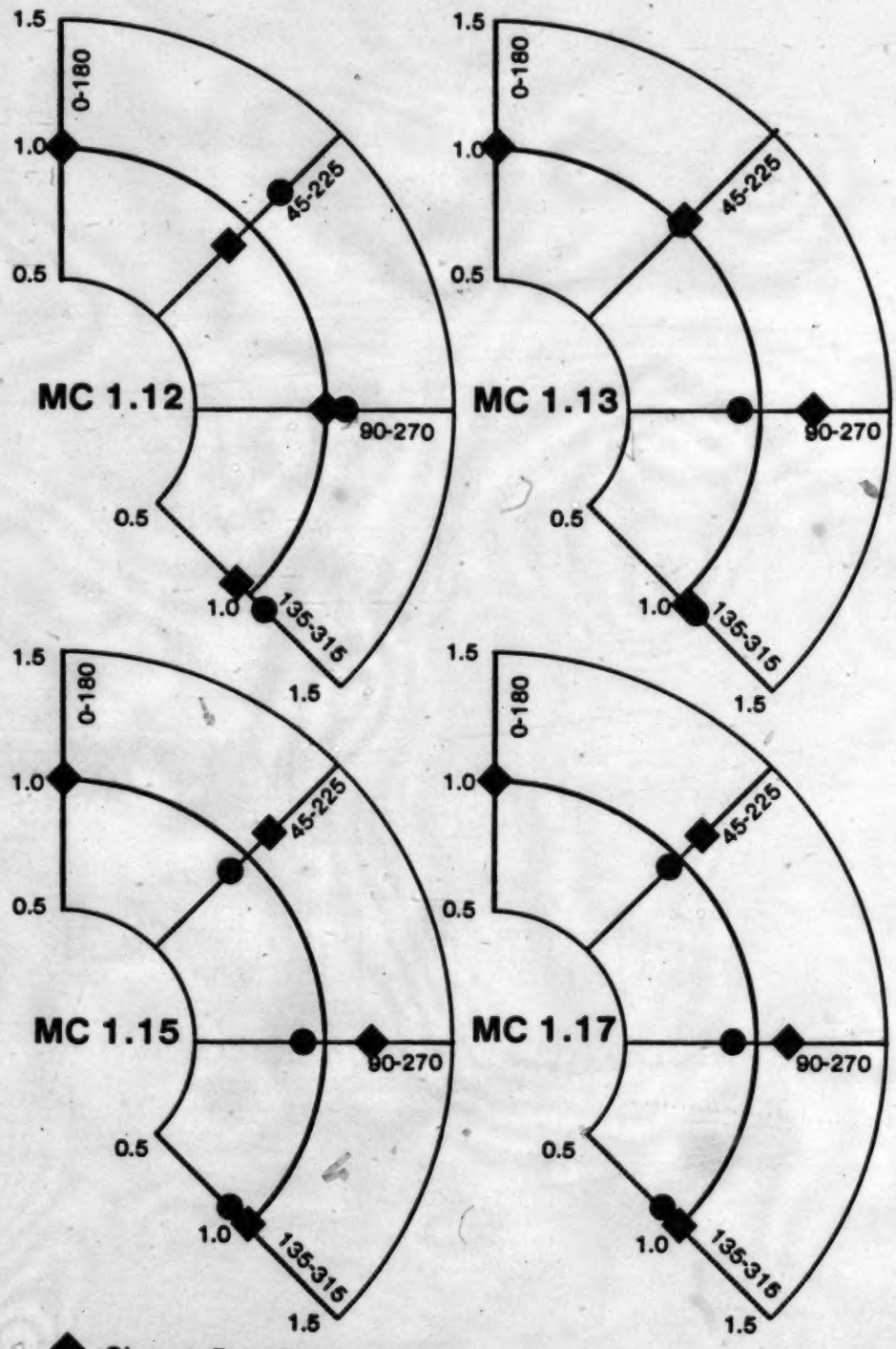

Figure C5-8 Closure Rate Parameters For Tests MC 1.12 To MC 1.17 Normalized To The 0-180 Diameter

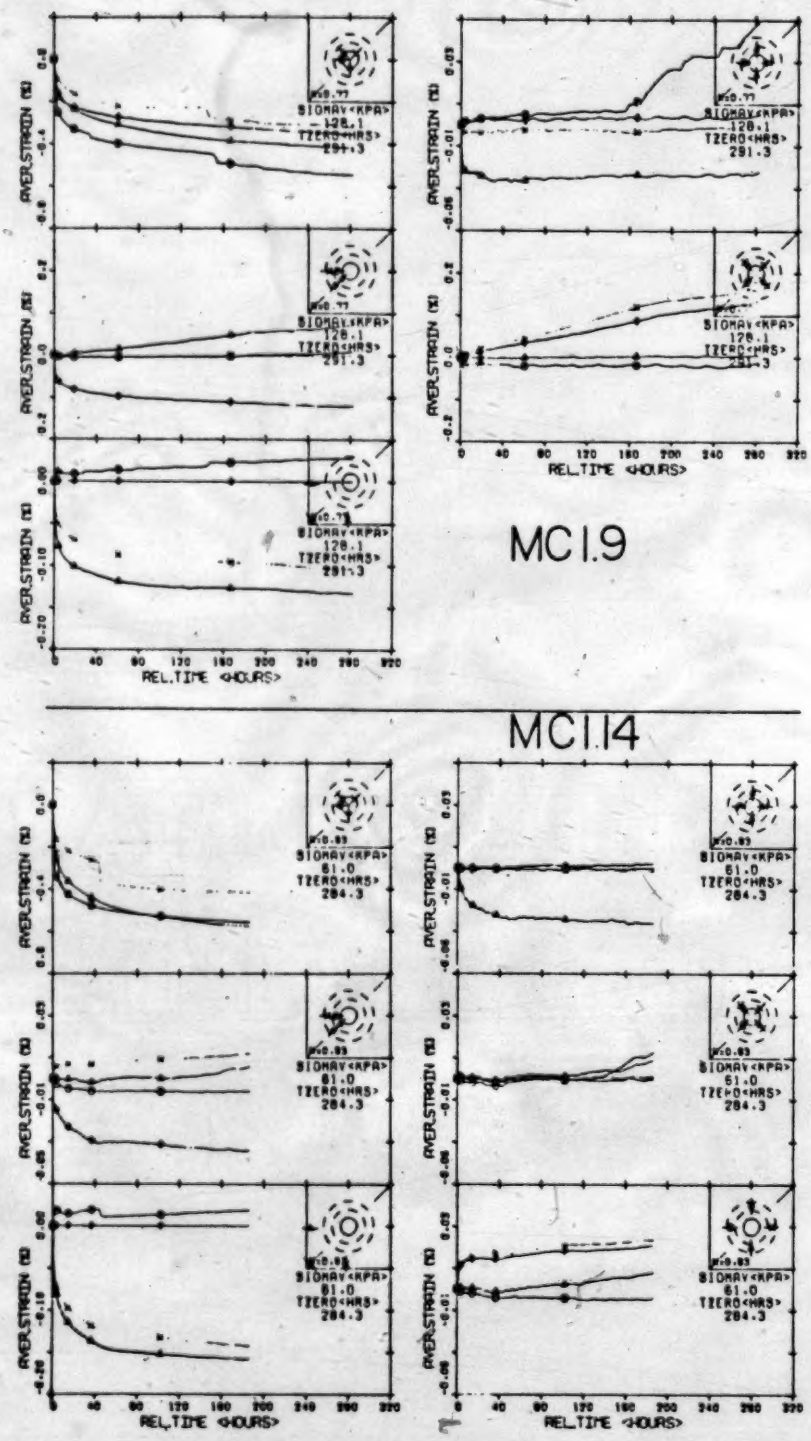

Figure C6-1 Strain Versus Time Curves For Some Locations For Tests MC 1.9 And MC 1.14